



QEX

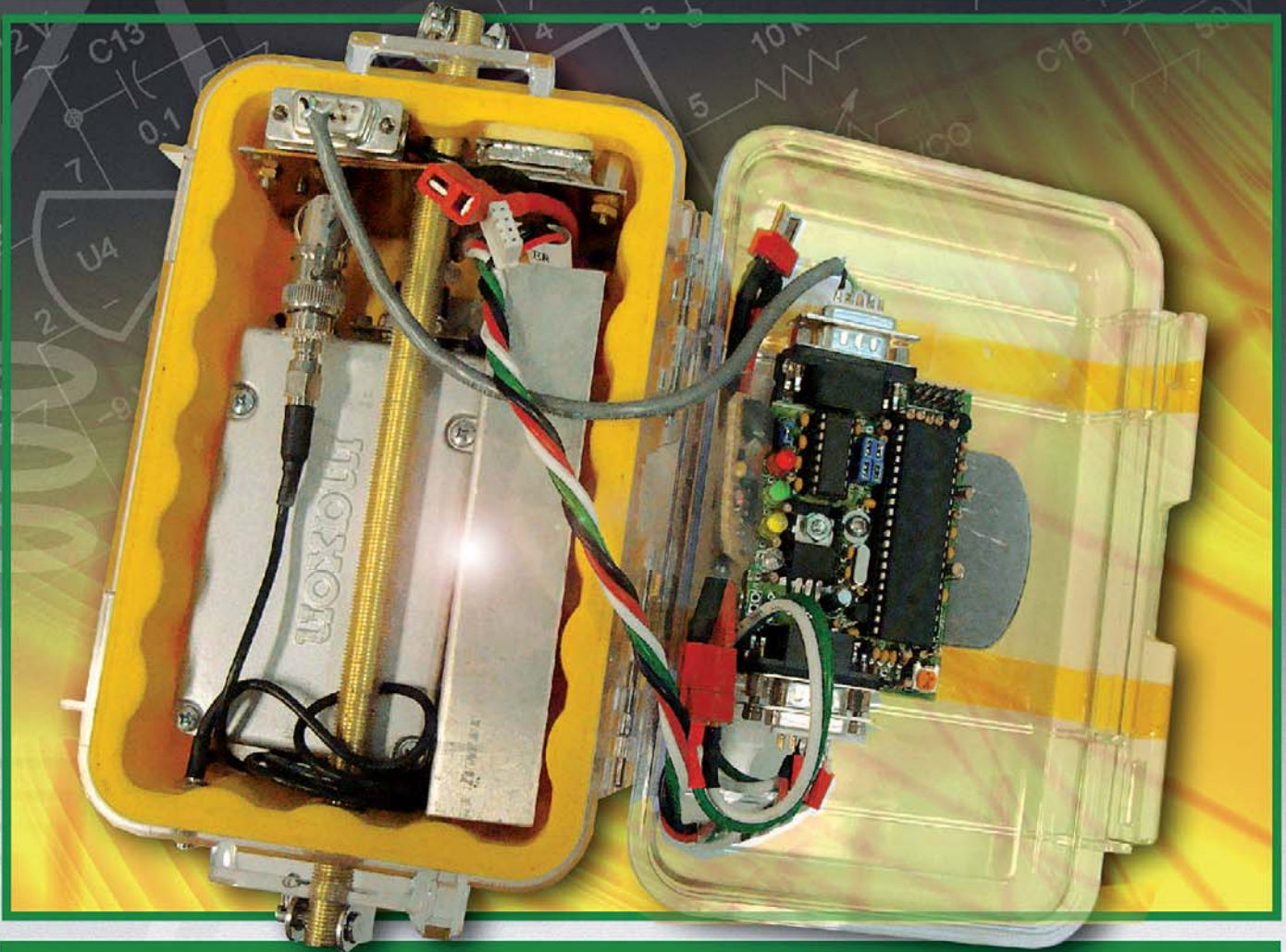
\$5

May/June 2012

www.arrl.org

A Forum for Communications Experimenters

Issue No. 272



KA5GSQ describes the high-altitude balloon sensors he used in a science and engineering program for high school students, which he taught at Embry-Riddle Aeronautical University. Here, we see one of the APRS position trackers that flew on the "balloon train."

KENWOOD

KENWOOD'S NEW HF
TRANSCEIVER AT
DAYTON 2012

KENWOOD

Dates: May 18th - 20th, 2012 Venue: Hara Arena (Dayton, Ohio)



www.kenwoodusa.com
ADS#12212



QEX (ISSN: 0886-8093) is published bimonthly in January, March, May, July, September, and November by the American Radio Relay League, 225 Main Street, Newington, CT 06111-1494. Periodicals postage paid at Hartford, CT and at additional mailing offices.

POSTMASTER: Send address changes to: QEX, 225 Main St, Newington, CT 06111-1494 Issue No 272

Harold Kramer, WJ1B
Publisher

Larry Wolfgang, WR1B
Editor

Lori Weinberg, KB1EIB
Assistant Editor

Zack Lau, W1VT
Ray Mack, W5IFS
Contributing Editors

Production Department

Steve Ford, WB8IMY
Publications Manager

Michelle Bloom, WB1ENT
Production Supervisor

Sue Fagan, KB1OKW
Graphic Design Supervisor

David Pingree, N1NAS
Senior Technical Illustrator

Carol Michaud, KB1QAW
Technical Illustrator

Advertising Information Contact:

Janet L. Rocco, W1JLR
Business Services
860-594-0203 – Direct
800-243-7768 – ARRL
860-594-4285 – Fax

Circulation Department

Cathy Stepina, *QEX Circulation*

Offices

225 Main St, Newington, CT 06111-1494 USA
Telephone: 860-594-0200
Fax: 860-594-0259 (24 hour direct line)
e-mail: qex@arrl.org

Subscription rate for 6 issues:

In the US: ARRL Member \$24, nonmember \$36;

US by First Class Mail: ARRL member \$37, nonmember \$49;

International and Canada by Airmail: ARRL member \$31, nonmember \$43;

Members are asked to include their membership control number or a label from their QST when applying.

In order to ensure prompt delivery, we ask that you periodically check the address information on your mailing label. If you find any inaccuracies, please contact the Circulation Department immediately. Thank you for your assistance.

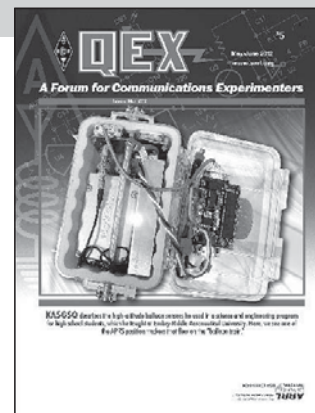


Copyright © 2012 by the American Radio Relay League Inc. For permission to quote or reprint material from QEX or any ARRL publication, send a written request including the issue date (or book title), article, page numbers and a description of where you intend to use the reprinted material. Send the request to the office of the Publications Manager (permission@arrl.org).

May/June 2012

About the Cover

John E. Post, KA5GSQ, taught an intense 4-day science and engineering summer camp program for high school students at Embry-Riddle Aeronautical University. The purpose of the camp was to motivate students to consider pursuing careers in science and engineering, specifically in electrical and computer engineering. It was also an opportunity to introduce the students to some basic Amateur Radio concepts. As part of the program, the students assembled a variety of temperature and pressure sensors, which they launched on a high-altitude balloon. On the cover, we see one of the APRS position-beacon trackers that they attached to the “balloon train.”



In This Issue

Features

3 A Surface Wave Transmission
Glenn Elmore, N6GN, John Watrous, K6ZPB

10 A Simple Sensor Package for High Altitude Ballooning
John E. Post, KA5GSQ

20 More Octave for L-Networks
Maynard, A. Wright, W6PAP

24 A Closer Look at Vertical Antennas With Elevated Ground Systems — Part 2
Rudy Severns, N6LF

34 IMD in FET and Diode Mixers at 70 cm
John B. Stephensen, KD6OZH

40 SDR: Simplified
Ray Mack, W5IFS

46 Upcoming Conferences

45 Letters to the Editor

48 Out of the Box
Ray Mack, W5IFS

Index of Advertisers

American Radio Relay League:..... 45, Cover III, Cover IV
Array Solutions:..... 47
Down East Microwave Inc:..... 9
Kenwood Communications:..... Cover II
National RF, Inc:..... 47
Nemal Electronics International, Inc:..... 47
RF Parts:..... 41, 43
Tucson Amateur Packet Radio:..... 39

The American Radio Relay League



The American Radio Relay League, Inc. is a noncommercial association of radio amateurs, organized for the promotion of interest in Amateur Radio communication and experimentation, for the establishment of networks to provide communications in the event of disasters or other emergencies, for the advancement of the radio art and of the public welfare, for the representation of the radio amateur in legislative matters, and for the maintenance of fraternalism and a high standard of conduct.

ARRL is an incorporated association without capital stock chartered under the laws of the state of Connecticut, and is an exempt organization under Section 501(c)(3) of the Internal Revenue Code of 1986. Its affairs are governed by a Board of Directors, whose voting members are elected every three years by the general membership. The officers are elected or appointed by the Directors. The League is noncommercial, and no one who could gain financially from the shaping of its affairs is eligible for membership on its Board.

"Of, by, and for the radio amateur," ARRL numbers within its ranks the vast majority of active amateurs in the nation and has a proud history of achievement as the standard-bearer in amateur affairs.

A *bona fide* interest in Amateur Radio is the only essential qualification of membership; an Amateur Radio license is not a prerequisite, although full voting membership is granted only to licensed amateurs in the US.

Membership inquiries and general correspondence should be addressed to the administrative headquarters:

ARRL
225 Main Street
Newington, CT 06111 USA
Telephone: 860-594-0200
FAX: 860-594-0259 (24-hour direct line)

Officers

President: KAY C. CRAIGIE, N3KN
570 Brush Mountain Rd, Blacksburg, VA 24060

Chief Executive Officer: DAVID SUMNER, K1ZZ

The purpose of *QEX* is to:

- 1) provide a medium for the exchange of ideas and information among Amateur Radio experimenters,
- 2) document advanced technical work in the Amateur Radio field, and
- 3) support efforts to advance the state of the Amateur Radio art.

All correspondence concerning *QEX* should be addressed to the American Radio Relay League, 225 Main Street, Newington, CT 06111 USA. Envelopes containing manuscripts and letters for publication in *QEX* should be marked Editor, *QEX*.

Both theoretical and practical technical articles are welcomed. Manuscripts should be submitted in word-processor format, if possible. We can redraw any figures as long as their content is clear. Photos should be glossy, color or black-and-white prints of at least the size they are to appear in *QEX* or high-resolution digital images (300 dots per inch or higher at the printed size). Further information for authors can be found on the Web at www.arrl.org/qex/ or by e-mail to qex@arrl.org.

Any opinions expressed in *QEX* are those of the authors, not necessarily those of the Editor or the League. While we strive to ensure all material is technically correct, authors are expected to defend their own assertions. Products mentioned are included for your information only; no endorsement is implied. Readers are cautioned to verify the availability of products before sending money to vendors.

Larry Wolfgang, WR1B

lwolfgang@arrl.org

Empirical Outlook

Smart Phones and Tablets

Many of our readers have been carrying "smart phones" or even some form of "tablet" for some time now, perhaps several years. It seems like every consumer electronics company has one or more offerings in these categories, and each one claims to be so much better (or less expensive) than the competition. Add in the various "e-readers" and it will make your head spin! How do you decide which choices are right for you? I have checked some of them out in the stores, but what can you really learn with such a limited demonstration? What applications might I want to try, and will they be available on the platform I choose?

Certainly we can talk to our friends who are already using iPads or other tablets, and we might be able to borrow their Kindle or other e-reader for a few days. That would be a more practical real world demonstration than we can get in a store. If one of those friends is also a ham, so much the better! It is still a big decision, and no one wants to spend perhaps the price of a new laptop computer just to see if they will like it.

I have been using a basic cell phone for a number of years, and was quite happy just to use it for the convenience of phone calls when I am away from home. My plan did not include text messaging, and I didn't feel the need for that feature. Isn't that why I have e-mail on my computer? Recently my son gave me an Android phone that was on a spare line on his cell phone account. I began to realize that it is convenient to be able to send a quick text (not while driving, of course!), or to check an e-mail account when I was away from my computer. That Android phone was several years old and some features didn't work the way I expected them to, so when Chris told me it was eligible for an upgrade, I decided to take advantage of the opportunity. Of course I wasn't going to be satisfied with the bottom-of-the-line phones that I could get for free!

Now I am searching for Amateur Radio applications to add to my phone, and I am finding that there are many offerings for free or for a small fee. There are license exam practice programs, Morse code trainers, repeater listings, various data bases, common calculations and so much more. I am more intrigued by programs that are directly related to on-the-air operation.

A few weeks ago I met a ham on a local repeater. He was coming into the repeater over an EchoLink connection. It turned out that he was riding a train across Massachusetts, talking to me on a repeater in eastern Connecticut — using an App on his iPhone! On the cover of the May 2012 issue of *QST* we see an AFSK interface that connects an Android phone to an HF radio. PSK31 contacts with a smart phone! The possibilities are endless.

What are some of your favorite applications? Maybe you have found something that far exceeds your expectations, and has become an important part of your Amateur Radio experience. I invite you to share the information about some of your favorite finds. Send me a note, perhaps with links to your favorite application store, and I'll include the information in a future issue.

I imagine that some of our readers have written applications for their phones and tablets, too. What is involved with programming for these devices? Your fellow readers would probably enjoy learning about your experiences, and in picking up some tips for writing their own applications. We often have articles about projects with microcontrollers, including code listings. There have been articles about the programming process as well, but we haven't seen any articles about writing applications for smart phones or tablets yet. The aforementioned May *QST* article is a nice description of the hardware needed to interface the phone to a radio, but has no information about the application, except to tell us where to find and download the program. What can you offer for the other side of that equation? We're waiting to hear from you.

A Surface Wave Transmission Line

This article is the first in a series of QEX articles that involve surface wave transmission line theory and applications for use by radio amateurs. The second article describes a new theory for understanding antennas. The third article describes a very wide band antenna.

Many we've shown this to have a first response of something like "How can a signal hooked to a long wire not radiate?" This particular type of transmission line has not been previously described in the Amateur Radio literature, but it may be mistaken for one that has. Surface wave propagation has been known for a very long time. In fact, in the early days of radio, prior to 1900, theoretical work was done by Sommerfeld to explain beyond the horizon propagation. Then in the 1950s, Georg Goubau introduced a new surface wave transmission line (SWTL) that required only a single conductor.¹ That line, known since as "G-line," required dielectric (insulation) around the wire or else special feathering of the conductor to slow the relative velocity of propagation in order to keep the signal from leaving the wire conductor. Reference books, including *The ARRL VHF Manual*, provided information from Goubau's work and a 1974 *QST* article by George Hatherell, K6LK, further described the use of this unusual mode for amateur radio purposes.^{2,3}

The SWTL being described here does not use the same mode as described for G-Line. Unlike G-line, no insulation or conditioning around the conductor is necessary. In fact, a bare conductor can actually work better than one with insulation, at least while the surface is bright and shiny. Also, there is no slowing of the propagating wave. The wave may travel more than 50% faster than signals in common coax and has been measured to have a relative propagation velocity of unity — it travels right at the speed of light.

For those who are familiar with antennas and have difficulty understanding that this SWTL isn't one, it is perhaps useful to first consider the familiar dipole. A dipole can make a good antenna, particularly when it is an odd number of half wavelengths long. You may have operated a 40 meter dipole on both 40 and on its 3rd harmonic at 15 meters. A dipole can be fed from the middle and



Completed 400 MHz launcher mounted on a "holder." The no. 24 SWTL conductor extends from the center of the horn and can be seen as a faint line in this photograph.

exhibits resonance at the fundamental, 3rd, 5th and higher odd harmonics.⁴ In a sense, a resonant dipole, "knows" how long it is — that is, by connecting only at the center, responses due to total length can be seen. A dipole's response depends upon the length and on something happening at the element ends.

A monopole fed against a ground can be thought of rather like a dipole. Fed from one end, the signal (wave) travels to the far end of an element and is reflected back from the discontinuity there. Since the conductor

ceases at the end, real current is zero and voltage is highest there. As a result of that discontinuity a free wave is radiated into the surrounding space while at the same time a reflected wave returns toward the center.

A dipole simultaneously exhibits properties characteristic of a radiator, a transmission line and a resonator.⁵ A monopole element fed from the end does this as well.

If we put a load at the far end of an element that is able to couple to the signal (wave) and prevent both reflection and radiation, then the resonance disappears and signal energy goes into that load. If you've ever grabbed the end of a driven element of a VHF or UHF Yagi with your hand while watching an SWR meter you have witnessed this effect. The structure operated less like an antenna. Depending upon whether you were transmitting or receiving, signal power to or from a distant location was reduced, resonance was suppressed and some of the transmitted energy was absorbed in your hand. Under these conditions, the driven element became more of a transmission line and less of a radiator. Energy put into the element traveled as a wave along the conductor and was absorbed into a load at the end.

With appropriate coupling and loading, this behavior can occur at all frequencies, not just at frequencies where the unloaded element happens to be resonant. With proper connections, called "launchers" at each end of a conductor, a simple transmission line that exhibits very low attenuation along with very wide bandwidth operation can result. The plot in Figure 1 compares the measured attenuation of 100 feet of a SWTL made from no. 24 AWG copper wire conductor with the attenuation of LMR400 coax. Not only is this SWTL simpler, less expensive

¹Notes appear on page 9.

Table 1 Materials and Sources for Building the Launcher

1. Pacon® Metallic-Colored Four-Ply Poster Board: www.amazon.com/Pacon%C2%AE-Metallic-Colored-Four-Ply-Poster-Carton/dp/B002XJHGDK/f=sr_1_3?ie=UTF8&s=office-cts&qid=1309381399&sr=8-3
2. SMA connector: www.jameco.com/webapp/wcs/stores/servlet/Product_10001_10001_159531_-1
3. 0.005 inch brass shim stock: www.amazon.com/Brass-Shim-Stock-0-005-Thick/dp/B00065UXZG
4. No. 24 Magnet wire: www.frys.com/product/6279330
5. Metal tape: www.amazon.com/Shurtech-Brands-50-47523-01-Metal-Repair/dp/B0050BY230
6. K&S brass tubing stock in various sizes: Available from many local hobby and hardware stores.
7. Styrofoam insulation, 2 inches thick: Available at most home building supply stores.

and lighter than coax, but above a lower frequency limit which is determined by the launcher design, it can also exhibit lower loss than even this excellent coax.

While the preceding discussion may help describe the SWTL for those familiar with antennas, the question “How can a transmission line as simple as this not have been discovered and used before?” may still occur. For those who prefer to examine the SWTL from the point of view of transmission line rather than antenna theory, more detail on the theory, historical background and operation of this SWTL is available.⁶ In the rest of this article we’ll just show you how to make and use it.

Fabrication

The launchers use broad band coaxial transmission line transformers described by Klopfenstein and having a Chebyshev impedance taper that matches a 50 Ω coaxial connection at the narrow end to the 377 Ω impedance at the wide end, where the SWTL conductor attaches.⁷ This transformation has a low frequency limit set by the lowest frequency at which the total transformer length is approximately one half wavelength. Two designs are shown here, one with a 400 MHz lower limit and the other with a 144 MHz lower limit. Both designs should operate from their low frequency cut-off to well above 3 GHz. The outer conductor of these coaxial transformers is a cone made from metalized paper. The inner conductors, which have specially varying diameters to provide the correct impedance profile along the length of the launcher, are made from brass tubing. Table 1 lists the materials needed to build the launchers, with one source.

400 MHz Launcher Fabrication

Cut the metalized paper and the brass shim stock from flat stock using the patterns shown in Figure 2A. Using a cloth and some acetone, clear the gold ink away from the paper in the indicated area prior to folding it into a cone with the metalization on the outside.

With the overlapping tab lined up along the entire inside length, temporarily tape the cone together on the inside with transparent tape or masking tape. Then go back and tape the entire outer seam with metal foil tape. It may help to have two people for this operation.

Similarly, with the brass shim pattern, once cut out, overlap the edges carefully and tack solder it in a few places to hold it in place before going back and completely soldering the seam.

When you are finished building these cones, the brass cone should fit snugly over the narrow end of the metalized paper cone and the brass and cleared metalization should have good electrical contact.

The center conductor is fabricated from K&S Metals brass tubing stock, as shown in Figure 2B. This brass tubing is available in 1/2 inch diameter steps from many hobby and hardware stores. Figure 2B shows at what position along the tapered center the next size begins. Cut the tubing about 1/2 inch longer

than the required length to allow for overlap at each end. Carefully position these, both as to length and straightness, and tack solder them together. Once you have the entire tapered center conductor assembled and are pleased with the lengths and alignment, you can go back and solder each joint completely. Finally, sand or file away any excess solder so that you finish with a smooth step-tapered center conductor.

Cut a Styrofoam stiffener from 2 inch stock. This is available from home supply stores for use as thermal insulation. If possible, cut the circle using a small band saw with the table tilted to provide about a 22° angle, so that it will fit snugly in the finished paper cone about 2/3 of the way toward the open end. Drill an 1/8 inch hole through the center of the stiffener.

For final assembly, shown in Figure 3, first slip the brass cone over the center conductor and then solder the SMA connector center pin into the end of the tube. Set the paper cone on a flat work surface, wide end down, and seat the brass cone over the

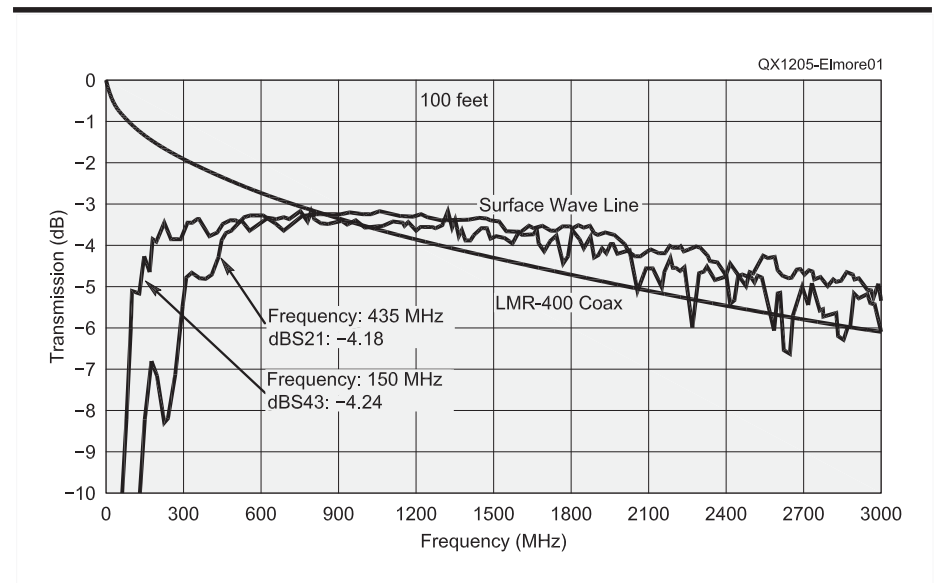


Figure 1 — Measured performance of SWTL compared with measurement of Times Microwave LMR-400 coaxial cable. Plots of 100 feet of no. 24 AWG conductor with a pair of 400 MHz launchers and a pair of 144 MHz launchers are shown. The main difference between these is the cut-off frequency.

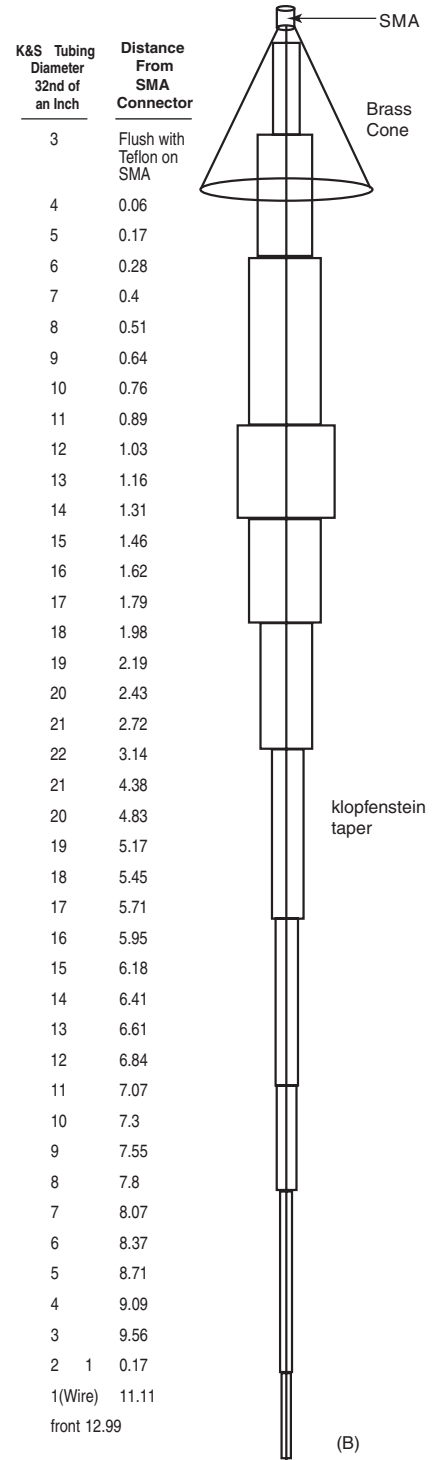
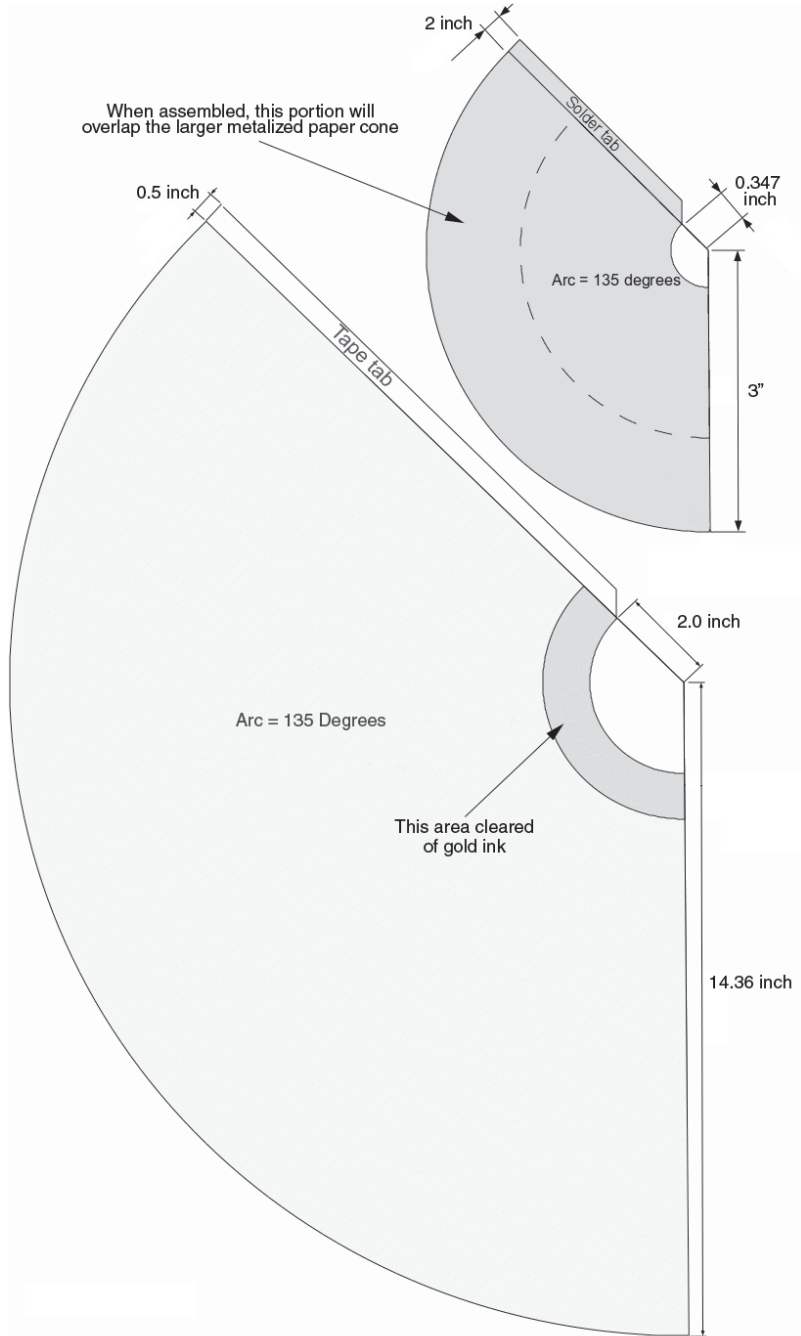
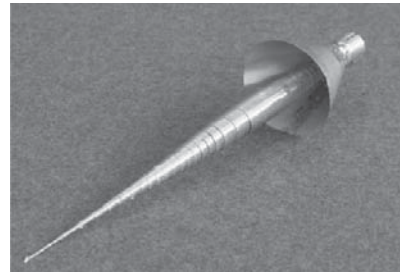
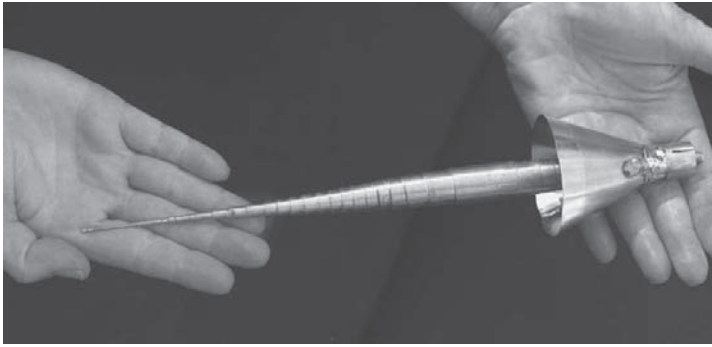


Figure 2 — Part A shows the metalized paper and brass shim stock cone patterns before folding. Part B gives the dimensions of the inner launcher tapered conductor sections made from K&S Metals brass tubing (in 32nds of an inch) versus position from the SMA connector for the 400 MHz launcher.

paper cone while guiding the tapered center conductor through the Styrofoam stiffener. The center hole will enlarge slightly as the center conductor pushes into it. With everything in alignment, you can then solder the SMA connector flange to the brass cone. Use metal tape to fasten the brass cone to the paper cone and your 400 MHz Klopfenstein taper launcher is complete. You only need to solder the no. 24 copper line to the center conductor at the wide end of the tube to use the launcher.

144 MHz Launcher

The 144 MHz version of the launcher is simply a “stretch” version of the 400 MHz version. Both should operate to well beyond 3 GHz, but the 144 MHz version, at a little over 40 inches of overall length, will operate at lower frequencies as well — including the 2 meter and 1¼ meter amateur bands.

Construction is basically the same as already described for the 400 MHz version except that significantly more brass tubing is required for the center conductor, and three sheets of metalized paper are needed to construct the outer cone.

Figure 4 provides a template for the paper cone and Figure 5 is a template for the brass cone. The inner conductor dimensions are listed in Table 2. An SMA connector is used the same way as it was for the 400 MHz launcher.

The target impedance profile for a 20 dB return loss Klopfenstein taper wide band transmission line transformer is shown in Figure 6. This same profile can be scaled in length for different lower frequency limits. When built from stepped diameter tubing sections rather than continuously varying line diameters, the performance is just slightly poorer than this target.

Figure 7 shows the measured transmission attenuation and impedance match of the line, both as return loss and SWR. As shown, it has a corner frequency just below 2 meters but the line is actually usable from below 100 MHz and has a usable upper limit well above 3 GHz. Actual performance is probably somewhat better than shown by the measurement because the calibration of the vector network analyzer used to measure it was compromised due to variations in the 100 foot long test cables and connections that were required for measuring this large structure. After calibration with precision standards, the lines had to be dragged to the ends of the SWTL and were flexed in the process. This reduced the resulting measurement accuracy.

SWTL Line Use

For simple transmission line use, you’ll need to make two of the above launchers, of

Table 2
Step-tapered Center Conductor Dimensions for the 144 MHz Launcher

<i>K&S Tubing OD, (32nds of an inch)</i>	<i>Position from SMA (inches)</i>
3	0
4	0.18
5	0.51
6	0.85
7	1.20
8	1.56
9	1.93
10	2.30
11	2.70
12	3.11
13	3.52
14	3.96
15	4.43
16	4.92
17	5.43
18	6.00
19	6.63
20	7.36
21	8.25
22	9.53
21	13.27
20	14.65
19	15.67
18	16.52
17	17.30
16	18.03
15	18.74
14	19.43
13	20.04
12	20.73
11	21.42
10	22.13
9	22.87
8	23.64
7	24.47
6	25.37
5	26.40
4	27.56
3	28.96
2	30.81
1	33.66

Note: The last tubing section is 1/32nd inch OD and extends to the front of the paper cone, where it is soldered to the no. 24 wire SWTL conductor.

either the 400 MHz or the 144 MHz versions. Once these are built, to use the line, simply reel out the desired length of no. 24 bare copper or enameled magnet wire, tin the ends and solder it into the center conductors of each launcher. Some sag in the line is really not a problem but it is important that the line be kept away from the ground and obstacles, preferably by at least a foot or more, over its entire length. If you use it this way, you should have a low attenuation, very broadband transmission line that can be used just like any other line for connecting a receiver or transmitter to an antenna or any similar transmission line use over the 400 MHz to 3 GHz or 144 MHz to 3 GHz range, as shown by Figure 1.

As you can see in Figures 2B and 3, we soldered a ½ inch copper water pipe coupling

on the back of the brass cone and around the SMA connector to facilitate mounting each launcher. Prior to soldering, we slotted the open end of this fitting so that the entire launcher could be supported from a piece of standard ½ inch copper pipe and an SMA fitted coaxial cable could be run down the center of that same mounting pipe and secured with a small metal hose clamp.

Very long runs of this line may be quite useful in connecting a transceiver to a distant antenna, perhaps one located at the top of a tower or a nearby hill. If very long lines are used, the weight of the line may be partially borne by intervening Styrofoam supports, periodically placed along the span, to keep the wire away from ground and obstacles. The use of insulators that have higher relative

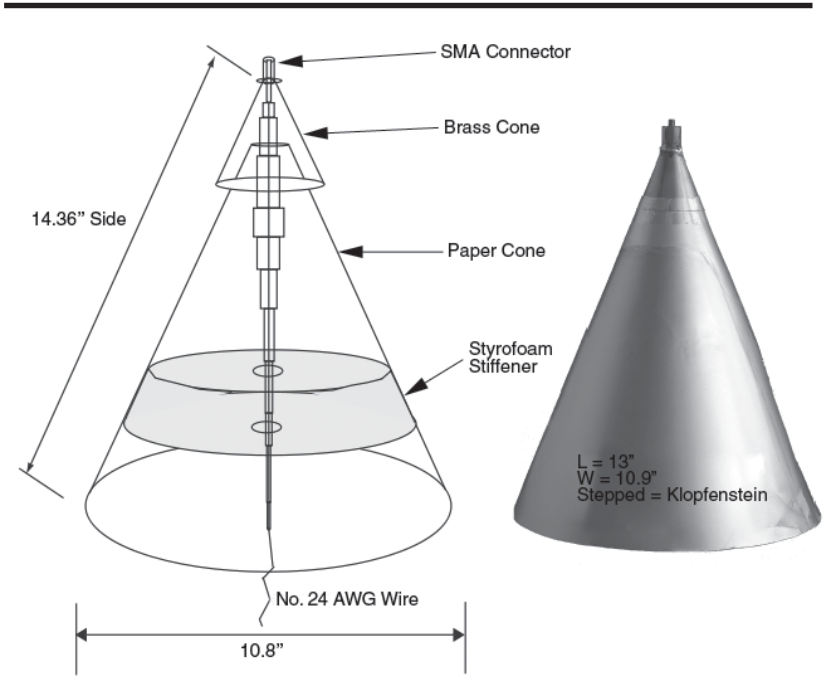
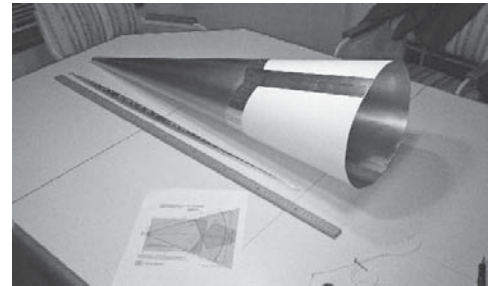


Figure 3 — Assembly of the 400 MHz Launcher.



This photo shows a 144 MHz cone, along with the Klopfenstein taper impedance matching line and the template sheet for the cone.



Here is a completed 144 MHz launcher, mounted to a wooden frame for testing.

**Construction detail for 144MHz Klopfenstein
Outer conductor (horn)**

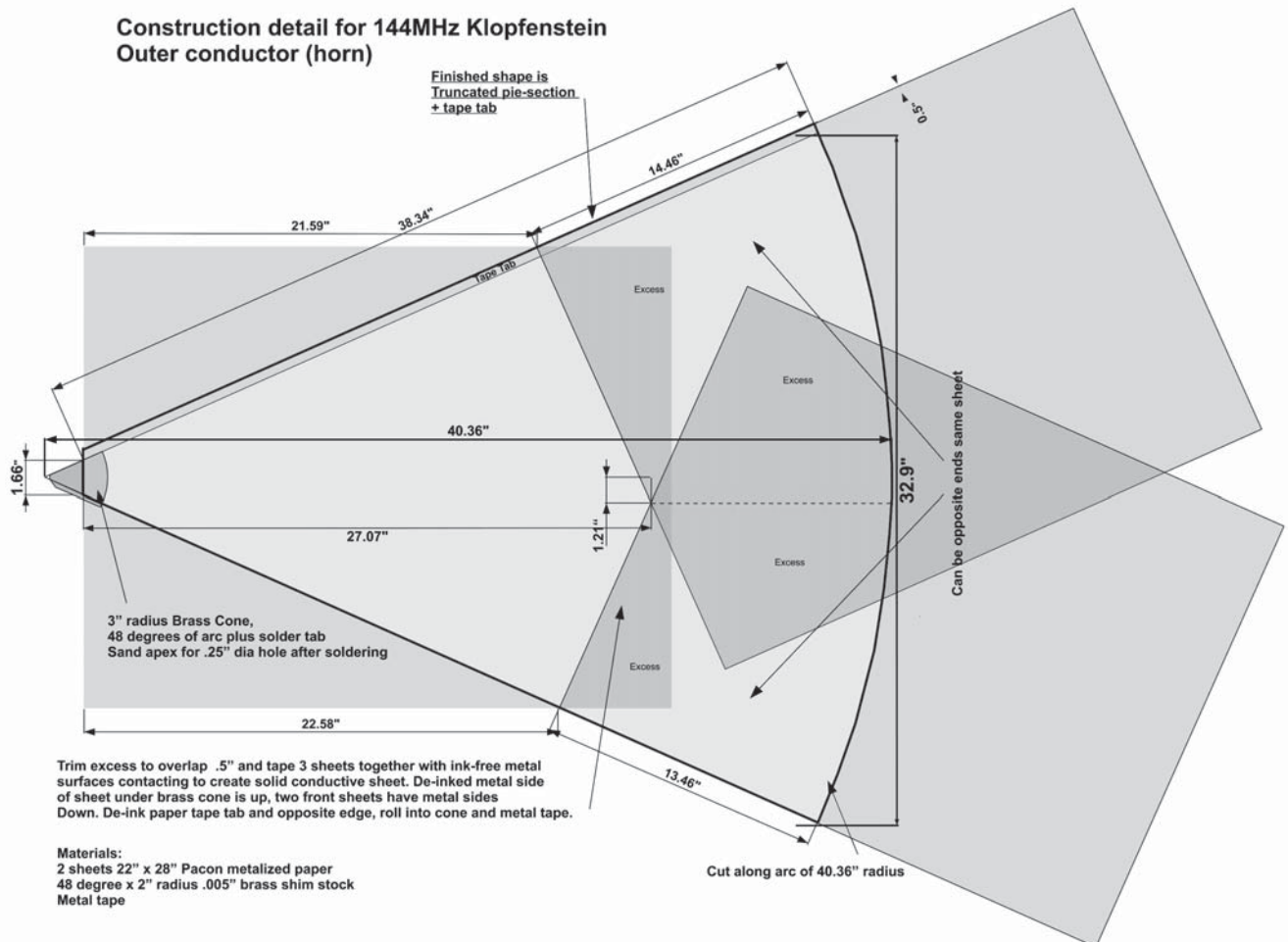


Figure 4 — The paper cone for the 144 MHz version of the launcher requires three 18 x 24 inch sheets of metalized paper.

dielectric constants such as ceramic or glass, however, will tend to unbalance the wave on the line and will cause additional attenuation and reflection so should be avoided.

If you accidentally break the no. 24 conductor, even if you are using enamel covered magnet wire, it isn't necessary to re-solder in order to reattach. A linesman's splice made by twisting one to two inches of each end tightly and closely around the other end will provide a "gimmick" capacitor that will make quite a good connection at 400 MHz and above. Because the characteristic impedance of the line is 377 Ω , it doesn't take much capacitance to make a very adequate RF connection even if there is insulation that prevents a dc connection. At lower frequencies you should make the splice longer or else solder any break, keeping the overall length and diameter of the splice as small as is practical.

It is possible to substitute different wire diameters. Particularly for very long lines that are supported at intermediate points with Styrofoam, you may find you can achieve lower losses by going to significantly larger and heavier wire or conductor diameters. Particularly if you taper gently between different diameters, perhaps by using intermediate diameters for a few inches at the transition, you should be able to achieve very low loss on extremely long runs. Because line attenuation is primarily influenced by the conductivity of the SWTL conductor used and further limited by skin effect, large diameter conductors made from copper will tend to show better performance than small ones made from metals having poorer conductivity. Even so, because of the high characteristic impedance of the line, materials that might not normally be considered for RF use, such as iron or stainless steel, may be used to create a very adequate SWTL. Commercial applications of this SWTL have used 1/4 to 2 inch diameter aluminum power line cables to achieve good performance even at 5 GHz and above. It is common to see attenuation at microwave of around 2 dB/100 feet with these larger conductors. For Amateur Radio applications, it may prove convenient to use a tower or mast guy cable as a feed line as well as a mechanical support. If this is to be done, a different launcher design that doesn't put mechanical strain directly onto the launcher's coaxial cable center pin must be arranged. A launcher that mechanically and electrically clamps to the cable with an RF attachment one quarter wavelength in front of the attachment point is one possibility but is not detailed in this article.

It is also possible to use non-circular cross-section conductors, as long as they are radially symmetric. There has been a report of the use of metalized Mylar ribbon of very great lengths (a kilometer or more)

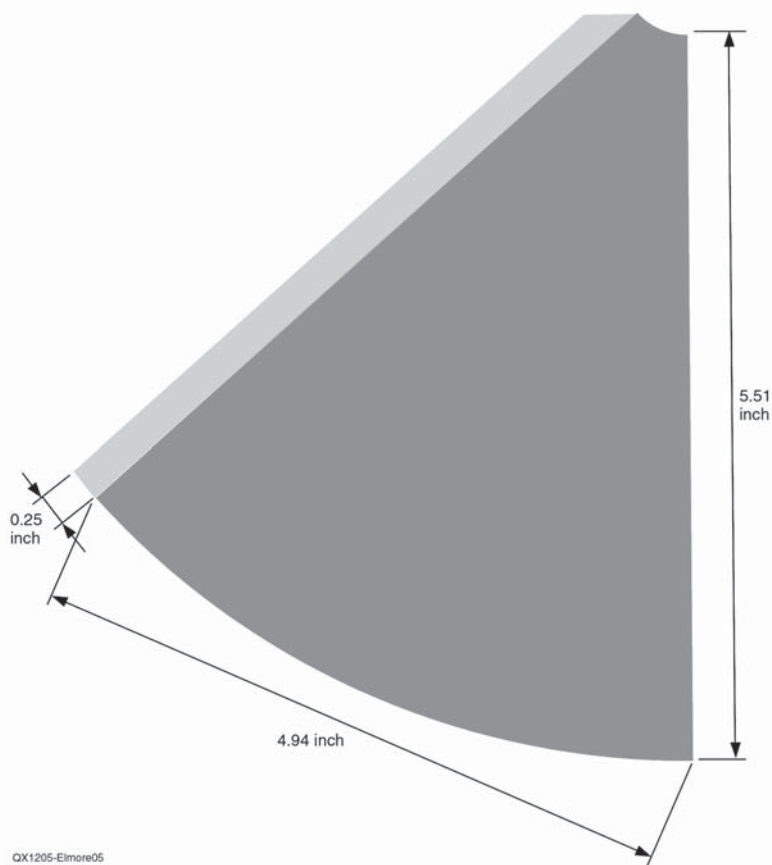


Figure 5 — This is the template for the brass portion of a 144 MHz launcher outer cone. The material can be 0.01 inch thick brass shim stock.

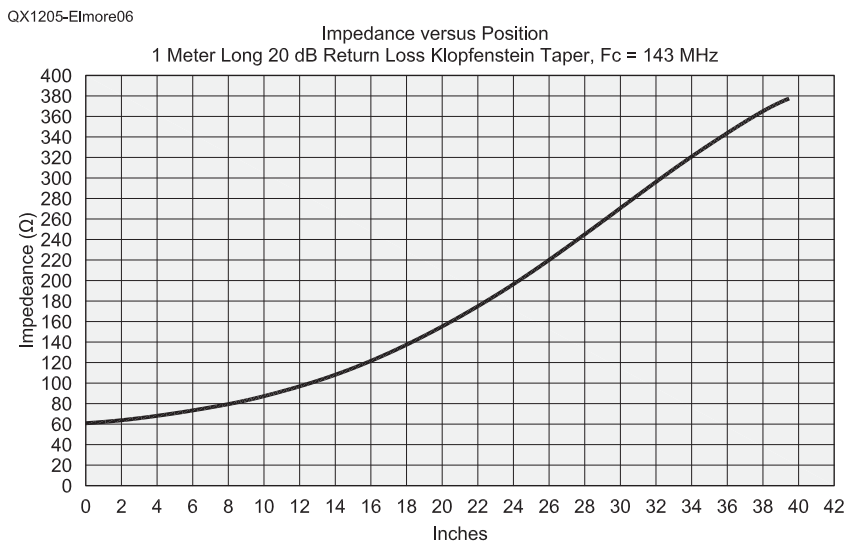


Figure 6 — This graph shows the line Impedance versus position for a 20 dB return loss Klopfenstein taper with a corner frequency of 143 MHz.



In this photo, a pair of 144 MHz Launchers are being measured with 100 feet of no. 24 magnet wire conductor in the driveway at N6GN. The vector network analyzer used for the measurement can be seen to the right, between the two ends.

as a SWTL transmission line conductor.⁸ While this report implied that this was a form of Goubau line, it seems likely that it was actually operating in the same manner as the SWTL lines described here, in a TM00 mode, longitudinal e-field wave guide rather than as the transmission line described by Goubau.

This SWTL should have quite high power handling capacity, particularly with larger diameter conductors. The authors have not tried kilowatt level transmitting, but it is very likely that the SMA connector will be the limiting factor rather than the line itself

Permission to Use

The surface wave transmission line technology described here is patented and requires licensing agreements to build or use. Corridor Systems Inc, the patent holder, is, however, permitting licensed Amateur Radio operators worldwide to build and deploy devices and systems which use it for their personal, non-commercial use, under the terms of their Amateur licenses. Any other use requires licensing from Corridor Systems Inc, 3800 Rolling Oaks Road, Santa Rosa, California 95404, USA.⁹

Glenn Elmore, N6GN, has been a licensed Radio Amateur for the past 50 years, and has held call signs of WV6STS, WA6STS and now N6GN. He has held an Amateur Extra class license since 1972. For most of his working career, Glenn has been an electrical engineer involved with the design of RF and microwave test and measurement equipment, notably scalar, vector network and spectrum analyzers.

Glenn's Amateur Radio interests have included weak signal VHF/microwave operation including meteor scatter; EME, terrestrial DX as well as higher speed Amateur TCP/IP radios and networks. He has recently been active on WSPR, the weak signal reporting network. Glenn is an ARRL Member.

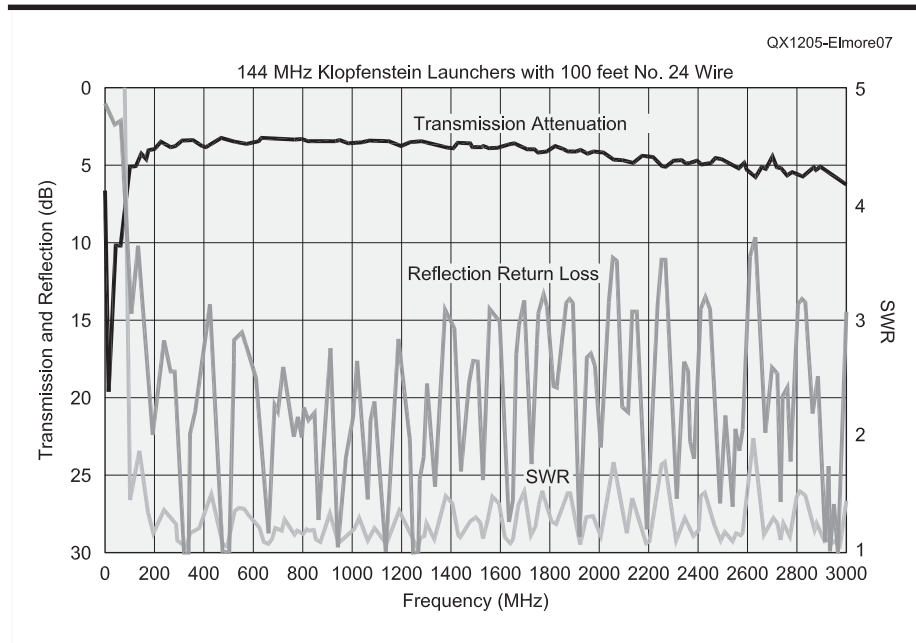


Figure 7 — Here is the measured performance of 100 feet of SWTL line with 144 MHz Launchers.

John Watrous, K6PZB, is an ARRL Member who was first licensed in 1956. Several times he has won the San Francisco VHF Contest in the QRP category. He is active in WSPR and has been working with Glenn Elmore on radio projects for over 20 years. For 34 years he taught people to behave more creatively in an Art Department at Santa Rosa Junior College, where he first used computers in art in 1983. He initiated the college's first on-line class in 1995. Retiring in 1997, John has focused his energy toward brainstorming ideas with Glenn, and building models in his shop. John holds a Masters Degree in sculpture and has always been interested in art and technology.

Notes

- ¹C. E. Sharp and G. Goubau, "A UHF Surface Wave Transmission Line," *Proceedings of the IRE*, Vol 41, pp 107-109, January, 1953.
- ²*The Radio Amateurs VHF Manual*, Eleventh edition, ARRL, 1968, p 175.
- ³George Hatherall, K6LK, "Putting the G-Line to Work," *QST*, June 1974, pp 11-15, 152, 154.
- ⁴R. Dean Straw, N6BV, Ed, *Antenna Book*, 21st edition, ARRL, p 2-3.
- ⁵John Kraus, W8JK, *Antennas*, McGraw-Hill Book Company, 1950, p 2.
- ⁶Glenn Elmore, N6GN, "Introduction to the Propagating Wave on a Single Conductor," www.corridorsystems.com/FullArticle.pdf.
- ⁷R W Klopfenstein, "A Transmission Line Taper of Improved Design," *Proceedings of the IRE*, Jan 1956 p 31.
- ⁸M. Friedman and Richard Fernsler, "Low-Loss RF Transport Over Long Distances," *IEEE Transaction on Microwave Theory and Techniques*, Vol 49, No. 2, Feb 2001.
- ⁹For further information about the surface wave transmission line and Corridor Systems atent, see their website: www.corridorsystems.com



Down East Microwave Inc.

We are your #1 source for 50MHz to 10GHz components, kits and assemblies for all your amateur radio and Satellite projects.

Transverters & Down Converters, Linear power amplifiers, Low Noise preamps, coaxial components, hybrid power modules, relays, GaAsFET, PHEMT's, & FET's, MMIC's, mixers, chip components, and other hard to find items for small signal and low noise applications.

We can interface our transverters with most radios.

Please call, write or see our web site www.downeastmicrowave.com for our Catalog, detailed Product descriptions and interfacing details.

Down East Microwave Inc.
19519 78th Terrace
Live Oak, FL 32060 USA
Tel. (386) 364-5529

A Simple Sensor Package for High Altitude Ballooning

High-altitude ballooning provides a unique opportunity to motivate high school students to pursue careers in science and engineering, as well as introduce them to exciting Amateur Radio applications.

This paper describes a simple sensor system designed for a balloonsat that was assembled and flown by high school students during an intensive four-day summer camp experience. The camp was held on

the campus of Embry-Riddle Aeronautical University in Prescott, Arizona. The purpose of the camp was to motivate students to consider pursuing careers in science and engineering, specifically in electrical and computer engineering. At the end of the camp, the students were given a written survey to complete. Student responses indicated that for the most part the objectives of the camp were achieved. Several students indicated that the camp increased their interest in science and engineering topics, while one

student stated a direct interest in studying electrical engineering upon graduation from high school.

Figure 1 shows the high-altitude balloon system shortly after launch. The system consists of a balloon, a parachute, and a string of payloads commonly referred to as the “balloon train.”¹ The balloon is typically a 1200 to 1500 gram natural rubber meteorological

¹Notes appear on page 19.

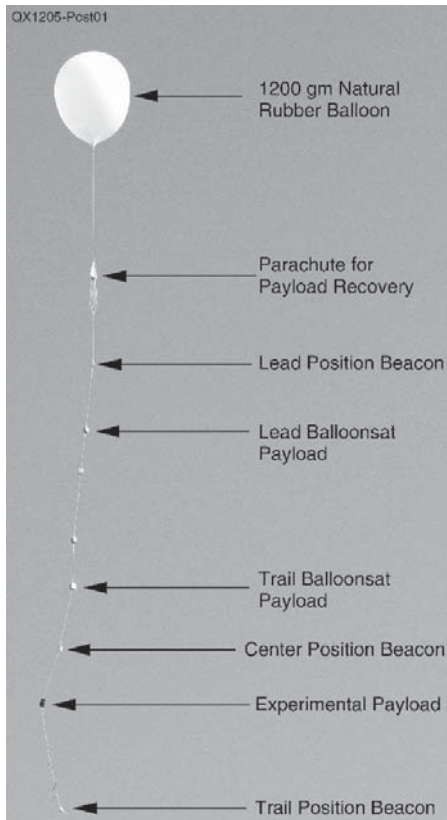


Figure 1 — This photo shows the high-altitude balloon system shortly after launch. You can see the trail of payloads that are known as the “balloon train.”

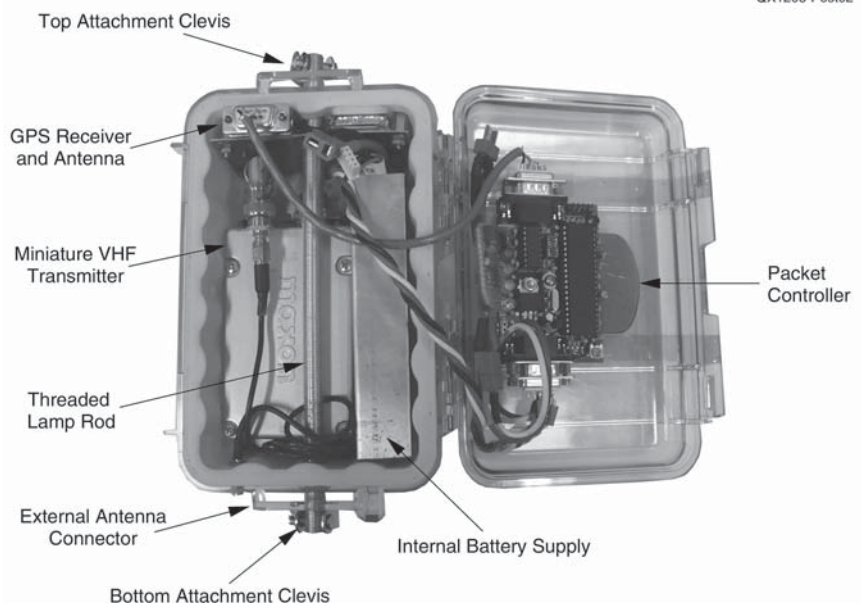


Figure 2 — This photo shows a typical GPS/APRS position beacon with the case open and major components labeled.

or “weather” balloon that inflates to a diameter of 18 to 22 feet, and bursts at a diameter of approximately 22 to 27 feet.² The balloon train consists of individual payloads or “balloonsats,” which are attached end-to-end using 10 to 15 foot lengths of high-strength nylon cord. The first and last payloads in the balloon train are usually position beacons containing a GPS receiver that determines position from the GPS satellite constella-

tion and a packet transmitter that broadcasts that position using the Automatic Packet Reporting System (APRS). The balloon train includes multiple position beacons in order to improve the likelihood of recovering the payloads if an unanticipated structural or electrical failure occurs during flight. Figure 2 is a close up view of a position beacon constructed for operation in the 70 cm Amateur Radio band.

The purpose of the sensor system is to record sensor data taken during the ascent and descent of a balloonsat payload during a high-altitude balloon flight. The data recorded during the flight includes the temperature inside the payload, the external ambient temperature, the ambient atmospheric pressure, as well as the voltage of the internal Lithium-ion Polymer (LiPo) battery supply. The balloonsat payloads also contained still and video cameras that obtained breath-taking images from the edge of space. After recovery of the balloonsat payloads, the students were able to download and analyze the data in order to better understand the characteristics of the near-space environment.

This article details the design and operation of the sensor package developed for the balloonsat payloads. Additionally, the article will discuss application of the APRS digital communications protocol in order to track the payload during flight, and facilitate payload recovery after landing. Finally, the article will review a selection of the sensor data and still images obtained during the flight of ERAU-06, which occurred the morning of June 29, 2011.

Sensor System Overview

Figure 3 presents an overview of the sensor and data recording system. As shown in the figure, four sensors measure atmospheric pressure, internal and external temperature, and battery voltage during the flight. The output of each sensor drives an op amp subtractor to remove the dc offset voltage and rescale the sensor readings so that they are within the 0 to 3.3 V data logger input range. The data logger digitizes the four analog voltages at a sampling rate of 1 Hz and writes the data in table format onto a micro-SD card installed on the data logger board.

Sensor System Sub-Circuit Details

Data logger: The data logger used for the sensor system is a Logomatic v2, obtained from Sparkfun Electronics.³ See Figure 4. The Logomatic v2 digitizes analog voltages between 0 and 3.3 V with a resolution of 10 bits, which is equivalent to $2^{10} = 1024$ possible integer values (0 to 1023). This results in a resolution of $1/1023 \text{ bits} \times 3.3 \text{ V} = 3.22 \text{ mV per bit}$. The Logomatic writes data to a microSD card installed on the circuit board. Additionally, the Logomatic includes a type B mini-USB connector, so the microSD card mounts on the desktop of a PC just like a standard flash drive. Once the drive mounts on the desktop it is straightforward to edit, copy or delete the data files from the PC desktop. Table 1 lists the configuration file used to initialize the data logger for this

QX1205-Post03

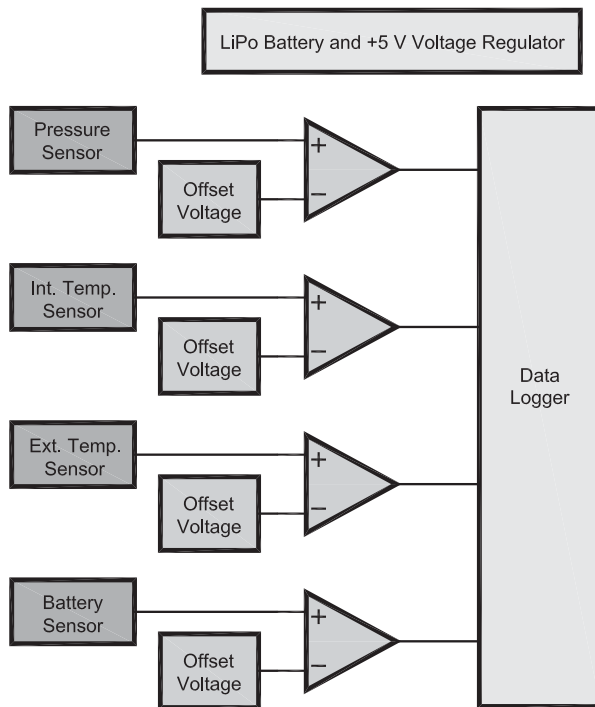


Figure 3 — Here is the block diagram of the sensor system, depicting the analog signal processing that occurs prior to digitization and recording of sensor data by the data logger.

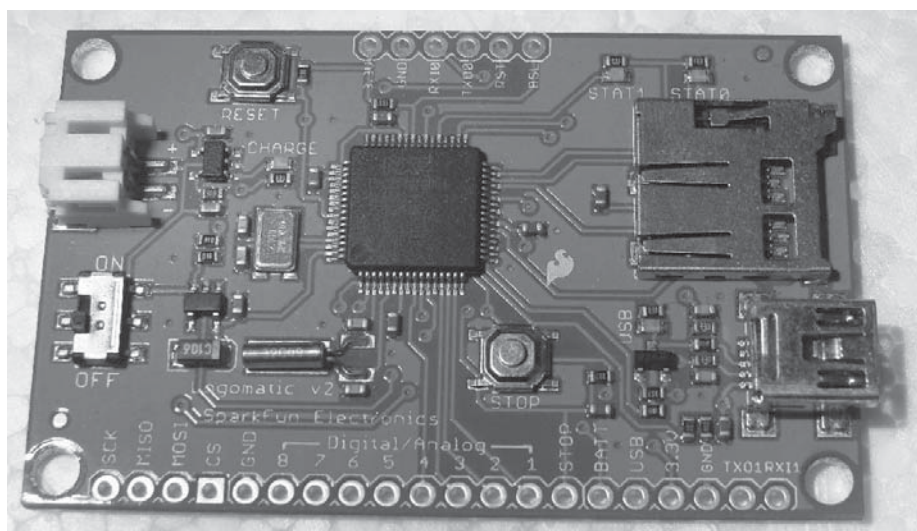


Figure 4 — This photo shows the Logomatic v2 purchased from www.sparkfun.com.

Table 1

Datalogger Configuration File.

This file configures the datalogger for analog-to-digital conversion (MODE=2), in text format (ASCII=Y), at 1 sample/sec (Frequency=01), with four channels active (AD0.3=Y, etc.) and four channels disabled (AD1.3=N, etc.). The other commands do not apply to ADC logging.

```

MODE = 2
ASCII = Y
Baud = 4
Frequency = 01
Trigger Character = $
Text Frame = 100
AD1.3 = N
AD0.3 = Y
AD0.2 = Y
AD0.1 = Y
AD1.2 = N
AD0.4 = Y
AD1.7 = N
AD1.6 = N
Safety On = Y
    
```

application, along with a description of the more important control commands.

Analog Signal Processing: Analog signal processing of the output of each sensor is necessary in order to maximize the resolution of the recorded data. This design uses op amp difference amplifiers to level shift and scale the output of each sensor so that the output remains inside of the 0 to 3.3 V range of the data logger. See Figure 5. Since the input voltage to the data logger must remain positive, a single-supply quad op amp such as the LM324 is satisfactory.⁴ The LM224 was selected for this application because it is capable of operating at temperatures as low as -40°C. The four independent op amps on the LM224 provide the ability to level-shift and scale the outputs from four different sensors.

Pressure Sensor: Atmospheric pressure is determined with a Honeywell ASDXACX015PAAA5 0 to 15 PSI absolute pressure sensor.⁵ This sensor has a maximum sensor output of 4.58 V at 15 PSI, with a sensitivity of 0.267 V/PSI. The ambient pressure at the launch location (5000 feet) is approximately 12.23 PSI. This reduces the maximum expected sensor output voltage to $4.58 - 0.267 \times (15 - 12.23) = 3.85$ V. The minimum zero pressure offset voltage for the sensor is 0.42 V. Adding this value to the sensor voltage at the anticipated maximum altitude of 100,000 feet (0.162 PSI) gives the minimum sensor voltage of $0.42 + 0.162 \times 0.267 = 0.463$ V. Thus, in order to maximize the resolution of the recorded data, the output

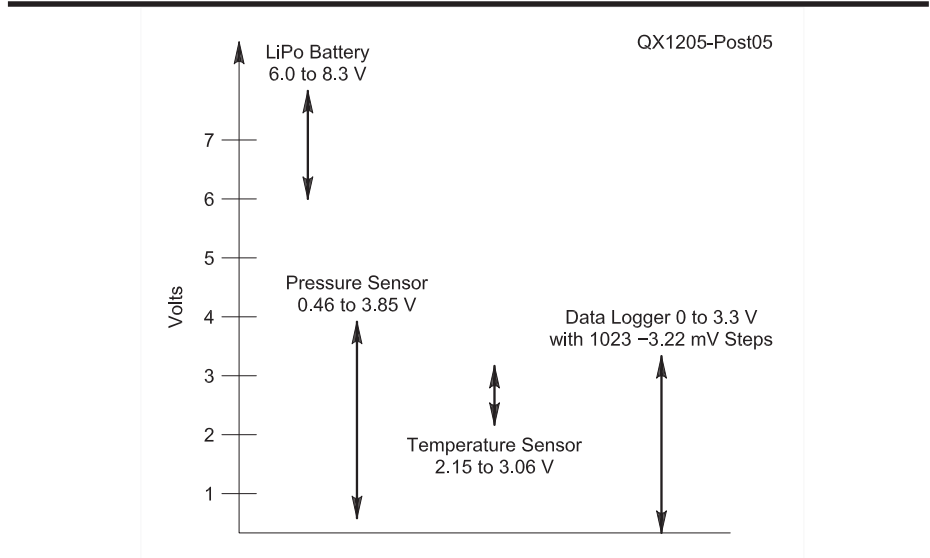


Figure 5 — This graph shows the relationship between sensor output voltages and data logger input voltages. This illustrates the need to level shift and scale each sensor voltage in order to maximize the resolution of the recorded measurements.

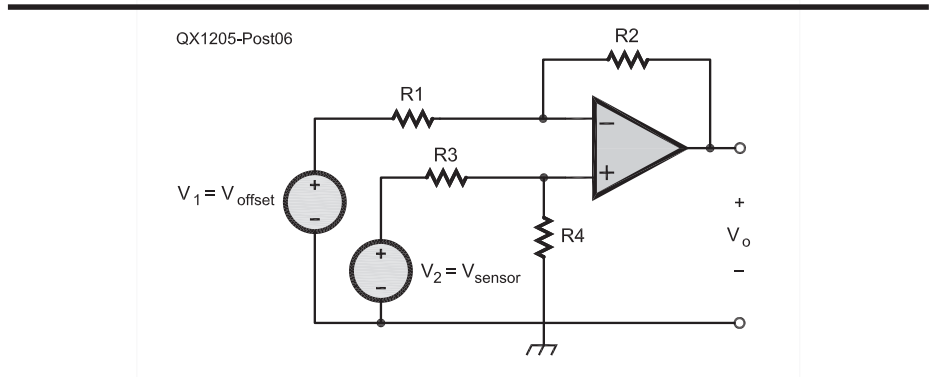


Figure 6 — This is a schematic diagram of an op amp difference amplifier. This circuit amplifies the difference between the two input signals v_{sensor} and v_{offset} in order to level-shift and scale the sensor output voltage

of the pressure sensor must be level shifted by 0.463 V and amplified by $3.3 / (3.85 - 0.463) = 0.974$ by the analog signal processing circuit prior to digitization.

Temperature Sensor: Internal and external temperatures are determined using the LM135 and LM335 precision temperature sensors.⁶ The LM335 operates from -40°C to 100°C, so it is suitable for obtaining internal temperatures, whereas the LM135 operates from -55°C to 150°C so it is suitable for obtaining external temperatures. Each device has a sensitivity of +10 mV/°C with maximum and minimum output voltages of 3.04 V and 2.92 V at 25°C. Assuming a maximum launch temperature of 80°F, or 27°C, the maximum output voltage is $3.03 + (27 - 25) \times 0.01 = 3.05$ V. Assuming a minimum temperature at altitude of -50°C gives a minimum output voltage of $2.92 - (25 - (-50)) \times 0.01 = 2.17$ V. Thus, the output of

the temperature sensors must be level shifted by 2.17 V and amplified by $3.3 / (3.05 - 2.17) = 3.75$ by the analog signal processing circuit prior to digitization.

Power Supply and Voltage Regulator: A lightweight, rechargeable 7.4 V LiPo battery provides sufficient capacity to power the sensor package for approximately five hours.⁷ Note that LiPo batteries require a recharging system specifically designed for this type of battery. (Do not recharge them with chargers designed for NiCd or NiMH batteries.) Additionally, an MC78L00A 5 V regulator establishes a constant voltage supply for the op amp difference amplifiers as well as providing a stable reference from which to establish the necessary offset voltages⁸.

Battery Monitor: The data logger records the voltage of the LiPo battery during the flight in order to monitor the reduc-

tion in battery voltage at colder temperatures. The battery voltage varies from a maximum of about 8.3 V when the battery is fully charged to approximately 6 V, at which the MC78L00A 5 V voltage regulator drops out. Level shifting by 5 V gives a maximum voltage of $8.3 - 5 = 3.3$ V and a minimum voltage of $6 - 5 = 1$ V. In this case, no additional scaling was necessary, since this is a satisfactory resolution for this application.

Op Amp Difference Amplifier Design

Figure 6 gives the schematic diagram of a general difference amplifier.⁹ This circuit amplifies the difference between two input voltages, so it is useful for performing the analog signal processing necessary to interface the output of each sensor to one input

channel of the data logger. The mathematical relationship between the output voltage, v_o , as a function of the input voltages v_1 and v_2 and the resistors $R_1 - R_4$ is given by Equation 1.

$$v_o = \frac{R_2 \left(1 + \frac{R_1}{R_2} \right)}{R_1 \left(1 + \frac{R_3}{R_4} \right)} \times v_2 - \frac{R_2}{R_1} \times v_1 \quad [\text{Eq 1}]$$

Under the constraint that $\frac{R_1}{R_2} = \frac{R_3}{R_4}$, then Equation 1 becomes:

$$v_o = \frac{R_2}{R_1} (v_2 - v_1) \quad [\text{Eq 2}]$$

If the offset voltage is applied to v_1 , the sensor output voltage is applied to v_2 , and the ratio R_2 / R_1 selected properly, the difference amplifier is able to accomplish the level shifting and scaling necessary to interface each sensor to the data logger. Inverting Equation 2 yields Equation 3, which allows recovery of the original sensor voltage v_2 from the digitized voltage v_o .

$$v_2 = \frac{R_1}{R_2} v_o + v_1 \quad [\text{Eq 3}]$$

As discussed in the next section, R_1 is actually a Thevenin equivalent resistance that may not be readily available as a standard resistor value for R_2 . Thus, a more general result requires inverting Equation 1 to solve for the sensor voltage v_2 , given with Equation 4.

$$v_2 = \left(\frac{R_1}{R_2} v_o + v_1 \right) \left(\frac{1 + \frac{R_3}{R_4}}{1 + \frac{R_1}{R_2}} \right) \quad [\text{Eq 4}]$$

Design of Offset Voltage Sources

Voltage sources are required to provide the proper offset voltage (v_1 in Figure 6) for each sensor, as discussed earlier. For this design a simple voltage divider was applied to reduce the +5 V provided by the voltage regulator. See the top circuit in Figure 7. Comparing the Thevenin equivalent circuit of the voltage divider (bottom circuit of Figure 7) with the series combination of the voltage source v_1 and the resistance R_1 in Figure 6 demonstrates that

$$v_1 = 5 \frac{R_B}{R_B + R_A} \quad [\text{Eq 5}]$$

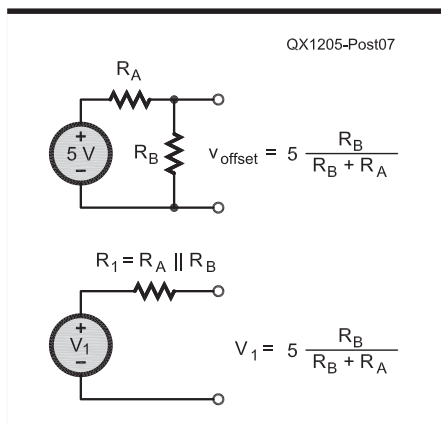


Figure 7 — At the top is the schematic diagram of the offset voltage source, with its Thevenin equivalent circuit on the bottom. Comparing the Thevenin equivalent circuit with v_1 and R_1 in Figure 6 shows the effects of Equations 5 and 6, which are also shown on the right side of this diagram.

Table 2

List of standard resistor values R_A , R_B , R_2 , R_3 , and R_4 for design of op amp analog signal processors along with the resulting voltage gain, A_v , and offset voltage, v_1 , produced for each choice.

Case	R_A (k Ω)	R_B (k Ω)	$R_A R_B = R_1$ (k Ω)	R_3 (k Ω)	$R_2 = R_4$ (k Ω)	$A_v = R_4 / R_3$ (V/V)	$v_1 = V_{offset}$ (V)
Pressure	47	3	2.82	2.7	2.4	0.889	0.3
Temperature	18	12	7.2	7.5	22	2.93	2.0
Voltage	10	10	5	10	10	1	5

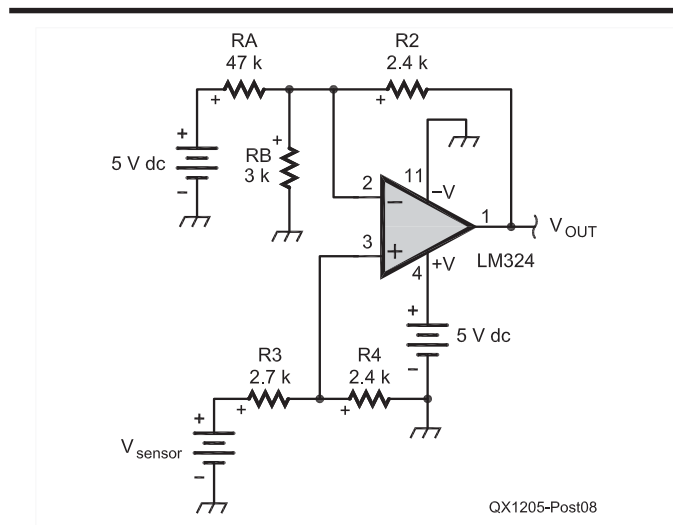


Figure 8 — This schematic shows the final design of the difference amplifier that processes voltage from the pressure sensor.

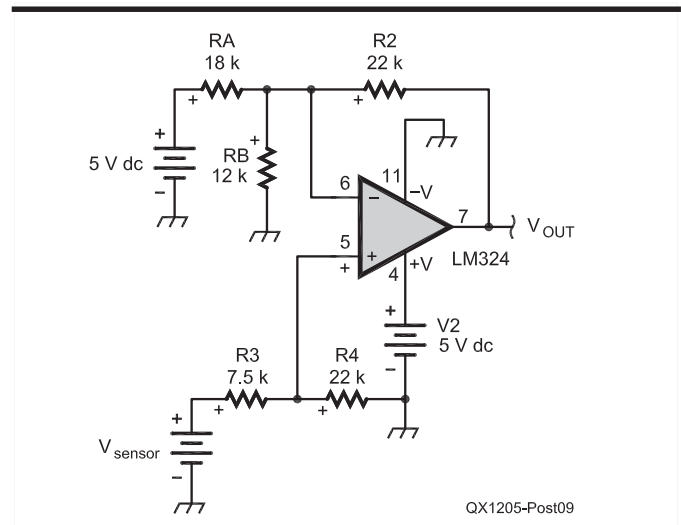


Figure 9 — Here is the final design of the difference amplifier that processes voltage from the temperature sensor.

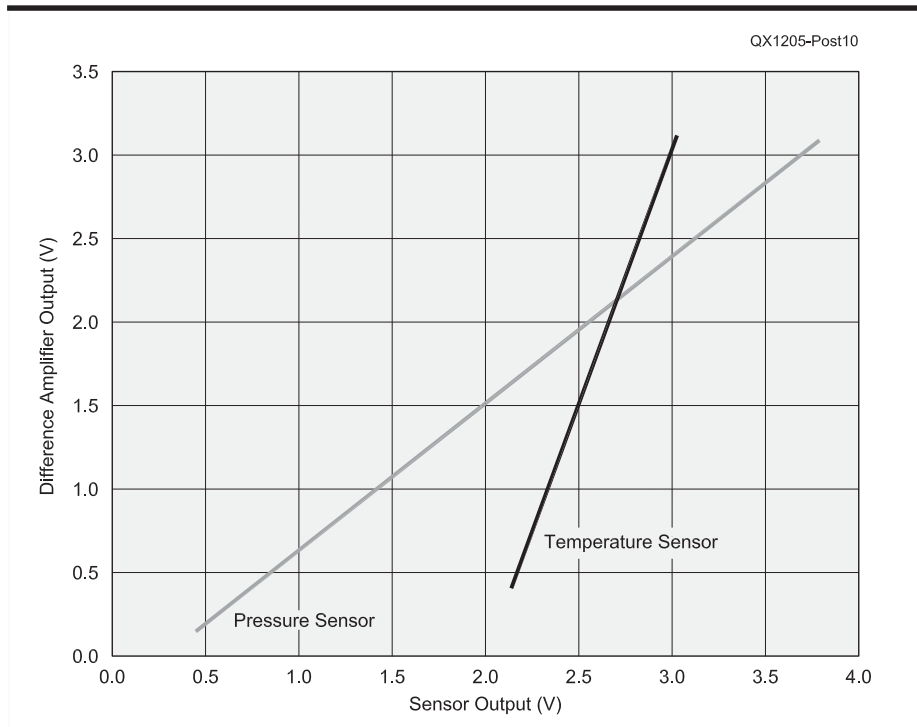


Figure 10 — This graph is a plot of the output voltages from the simulation of the difference amplifier circuits shown in Figures 6 and 7. This plot shows that the output of the difference amplifier remains between 0 to 3.30 V as the output of the pressure sensor ranges from 0.463 V to 3.85 V and the output of the temperature sensor ranges from 2.15 V to 3.06 V.

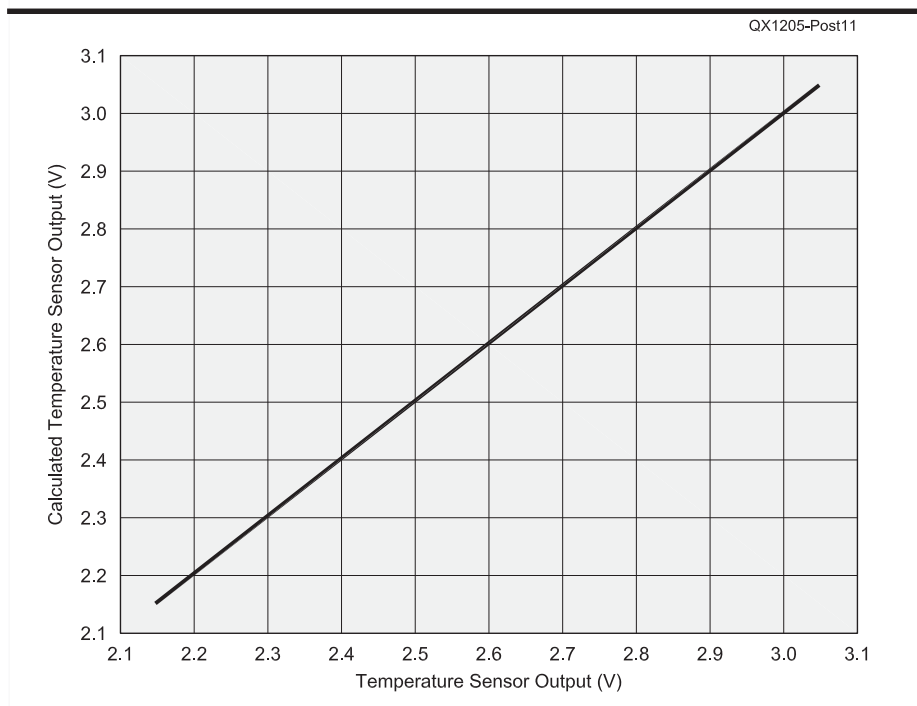


Figure 11 — Here is the output of the temperature sensor versus the calculated temperature sensor output obtained by applying Equation 4 to the output voltage produced by the simulation of the difference amplifier circuit. The figure demonstrates the exact correspondence of the calculated result to the original sensor output voltage.

and

$$R_1 = R_A \parallel R_B \quad [\text{Eq 6}]$$

Since only standard resistor values were available, it is not possible to obtain the exact offset voltages and gains for each sensor derived previously. This situation is reflected in Table 2, which shows the offset voltage, v_1 , and scaling factor for the temperature, pressure, and voltage sensor as functions of the resistors R_A , R_B , R_2 , R_3 and R_4 . Referring to this table, columns 2 and 3 give the values for resistors R_A and R_B , column 4 shows the equivalent value of $R_A \parallel R_B$, while column 5 shows the nearest standard resistor value to the adjacent value shown in column 4. Continuing to refer to the table, column 6 gives the standard value for resistor R_2 , which equals resistor R_4 , while columns 7 and 8 give the scaling factor and offset voltage that result from these design choices. It is important to note that even though the constraint $R_1/R_2 = R_3/R_4$ no longer applies, the sensor voltage is still recoverable uniquely through application of Equation 4. A slight loss of resolution does occur because the amplitude scaling factors of 0.889 and 2.93 V/V shown in Table 2 are somewhat smaller than the ideal scaling factors of 0.974 and 3.75 derived in the previous section.

Difference Amplifier Simulation

Figure 8 shows the difference amplifier circuit of Figure 6, using resistor values from the first row in Table 2 for processing the output of the pressure sensor. Figure 9 shows the difference amplifier circuit, Figure 6, using resistor values from the second row in Table 2 for processing the output of the temperature sensor. Figure 10 shows the difference amplifier output voltage obtained by *PSpice* circuit simulations of Figs. 8 and 9 when the appropriate sensor output voltage range is applied to each circuit.¹⁰ Maximum resolution is obtained when the amplifier output ranges between 0 and 3.3 V as the sensor output voltage ranges between its minimum and maximum values. Review of Figure 10 demonstrates that the goal of performing analog signal processing on the sensor output voltages so that they remain within the 0 –3.3 V input range of the data logger was achieved.

As a final check of the design of the analog signal processing circuit, Equation 4 was applied to recover the temperature sensor voltage from the simulated difference amplifier output, in order to verify that Equation 4 is correct. Figure 11 gives this result and shows an exact correspondence between the sensor voltage with the voltage recovered after applying Equation 4. An identical

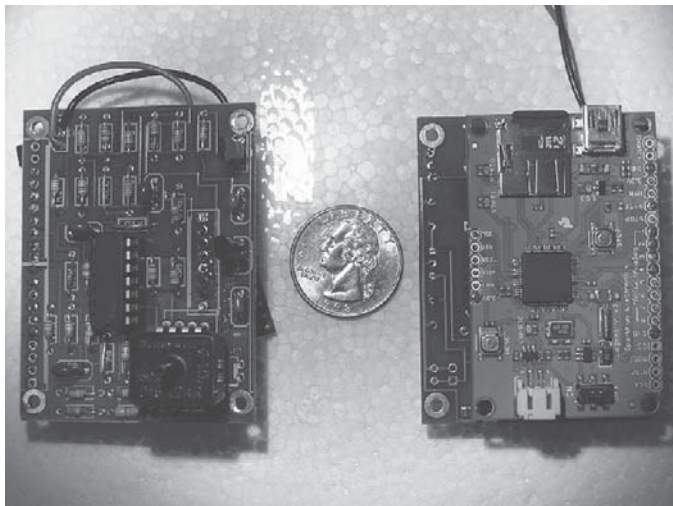


Figure 12 — Here is a photo of the front (left side) and back (right side) of the sensor system circuit board. The photo of the back of the board shows how the Logomatic v2 board was mounted as a daughterboard using the sensor system circuit board as the motherboard.



Figure 13 — Students assembled the sensor system circuit boards under the watchful eye of a veteran instructor.



Figure 14 — Balloonsat payloads were constructed by folding $\frac{3}{8}$ inch thick foam-core board into a cube shape approximately 6 inches on a side. The cubes were covered with adhesive-backed aluminum tape and the interior filled with automotive-type foam to provide insulation from both thermal and mechanical shocks.

procedure was followed to verify that the pressure sensor voltage was also properly recovered.

Circuit and Balloonsat Construction

A custom printed circuit board was designed and manufactured for the sensor system.¹¹ The left side of Figure 12 shows the analog signal processing circuitry installed on the front side of the printed circuit board. The right side of Figure 12 shows that the back side of the printed circuit board served as a motherboard to which the Logomatic v2 was installed as a daughterboard using low-profile connection sockets and terminal pins. This approach allowed for separate verification of the sensor system and data logger prior to mating them together and testing the entire assembly. This was important because most of the students who assembled the circuits had little or no prior experience in electronic circuit construction. Thus, it was important to verify circuit functionality frequently during the construction phase. Figure 13 is a photograph taken during the construction phase of the project.

Figure 14 is a photo that was taken looking down at the top of a balloonsat payload. The balloonsats were constructed by cutting a cross-shaped pattern out of $\frac{3}{8}$ inch thick foam-core board, which was then folded up to form a cube approximately 6 inches on each side. The joints of the cube were hot glued together and the entire cube covered in adhesive-backed aluminum tape in order to provide a rigid structure. The interior of the cube was filled with pieces of $\frac{1}{2}$ inch thick automotive-type foam to provide both for thermal insulation as well as to cushion the components against mechanical shock. Voids were left in the foam packaging to provide space for the sensor system, batteries, a small electric heater, and either a video or still camera.

Preflight Environmental Testing

In order to simulate the extreme conditions encountered by the balloonsat in the near-space environment, as well as verify the functionality of the sensor system, thermal and vacuum tests were conducted prior to the flight. Figure 15 shows the balloonsats stacked in the vacuum chamber ready for testing. Once the door is closed and the chamber is sealed a vacuum pump is started, which evacuates the air from the chamber simulating a “flight” up to an altitude of 100,000 feet. Next the vacuum pump is switched off and a small valve opened to allow the air pressure to return to the ambient state in order to open the door and retrieve the balloonsats.

Next, the balloonsats were placed in a



Figure 15 — Balloonsat payloads were placed in a vacuum chamber from which the air was evacuated to simulate a flight to 100,000 feet.



Figure 16 — Balloonsat payloads were placed in a thermal chamber, which was cooled to approximately -40°C to simulate the temperatures encountered during flight through the troposphere.

thermal chamber in order to simulate the sub-zero temperatures encountered during flight in the troposphere. See Figure 16. Thermal tests were important to verify that the small onboard electric heater had sufficient capacity to maintain the balloonsat's internal temperature such that the LiPo battery voltage did not drop below the minimum voltage necessary to power the sensor system.

During the approximately 1 hour long environmental tests, the sensor system and data logger were enabled in order to record the temperatures and pressures that the balloonsat encountered, as well as to monitor

the voltage of the onboard LiPo battery during testing.

Balloon Tracking and Recovery using Position Beacons

The balloon train includes one or more APRS position beacons, in order to facilitate tracking of the balloon during flight and recovery of the balloonsat payloads after landing. Figure 2 shows one of the trackers. The position beacons are enabled prior to launch to verify their functionality using portable or mobile receivers tuned to the appropriate APRS frequency. Next, the bea-



Figure 17 — Four students act as “handlers” to stabilize the balloon during inflation. The balloon is tethered to 15 pounds of weights to give an approximate indication of the amount of lift the balloon provides.

cons are inserted into the balloon train along with the other balloonsat payloads, attached to a properly inflated meteorological balloon, and then released for flight. Figure 1 shows the whole system ascending.

In the APRS digital communications protocol digital repeaters (digipeaters) receive and rebroadcast APRS packets, while Internet gateway stations (iGates) transfer the packets to the Internet. Once the balloon has ascended to an altitude so that position beacon broadcasts are received by an iGate, the balloon's position and altitude are available to anyone by entering the callsign of the appropriate beacon at <http://aprs.fi>. Additionally, APRS packets are digipeated as long as the altitude of the balloon allows for digipeater reception.

Prior to launch the approximate landing location for the balloonsat payload is predicted based on forecast winds aloft and an

estimate of the balloon burst altitude. Based on this position estimate, one or more mobile recovery teams equipped with GPS enabled APRS receivers are stationed on high terrain in the recovery area as the balloonsat payloads return to the surface under parachute. This is necessary because the final position beacon broadcasts prior to landing are normally terrain masked from the digipeater and are not retransmitted. The goal of the recovery team is to position themselves so that they receive the final position beacon transmissions before landing. This will minimize the search area if the position beacons are disabled by a hard landing or rough terrain or inclement weather prohibits immediate recovery of the payloads before beacon power is exhausted.

Once the payload has landed the recovery teams follow distance and direction information provided by a GPS enabled APRS portable receiver to the final location transmitted by the position beacon. The best-case scenario is that one or more position beacons are still in operation at the landing location and the recovery team is within range to receive these packets containing the actual location of the payload. Payload recovery is easy in this case since the recovery team can literally walk or drive to within a few meters of the actual location of the payloads.

The situation quickly becomes more complicated and recovery of the payload is problematic if one or more of the following occurs: Failure to capture the final position beacon packets by the recovery team, failure of the beacons during flight or after landing, landing in rough terrain or inclement weather, inaccurate forecast of surface winds or winds aloft, separation of one or more of the balloonsats from the balloon train during flight, and many other difficulties that space constraints preclude listing.

Sample Flight Images and Data

Wednesday morning, June 29, 2011 a high altitude balloon designated ERAU-06 (Embry-Riddle Aeronautical University-06) was launched from the Embry-Riddle campus in Prescott, AZ, shortly after 8:30 AM local time. The balloon payload consisted of the four student-constructed balloonsats, along with three position beacons that periodically transmitted position information using APRS. Figure 17 shows the balloon during inflation while Figure 18 shows an image taken at an altitude of approximately 1000 feet by an onboard camera carried by one of the balloonsats shortly after launch. Figure 19 shows an image of the cloud layer recorded by a camera as the balloon ascends through the stratosphere. Figure 20 shows an image taken by a camera immediately following the “post burst chaos” that ensues

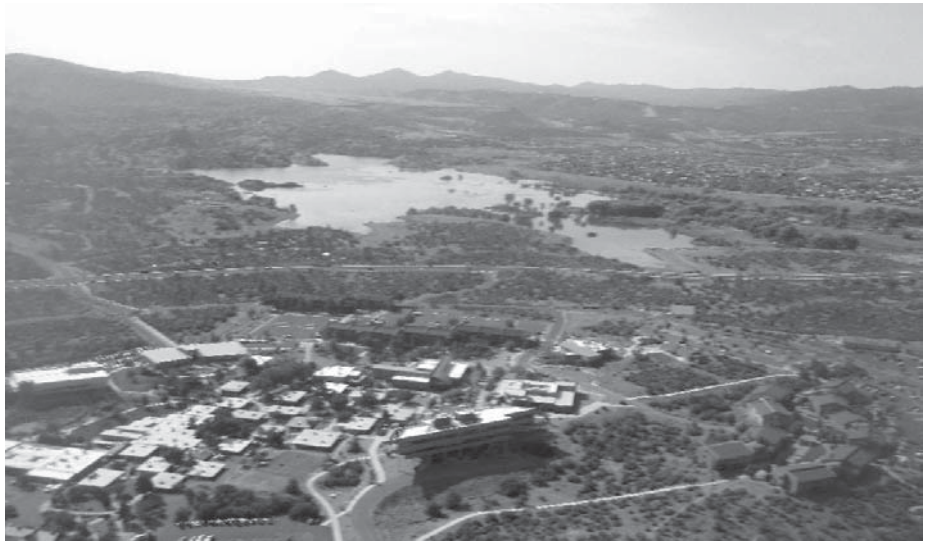


Figure 18 — This is one of the first images captured after launch. It shows a panoramic view of the Embry-Riddle Prescott campus as well as Willow Lake just east of campus.



Figure 19 — Here is a photo taken from high in the stratosphere of clouds over northern Arizona.

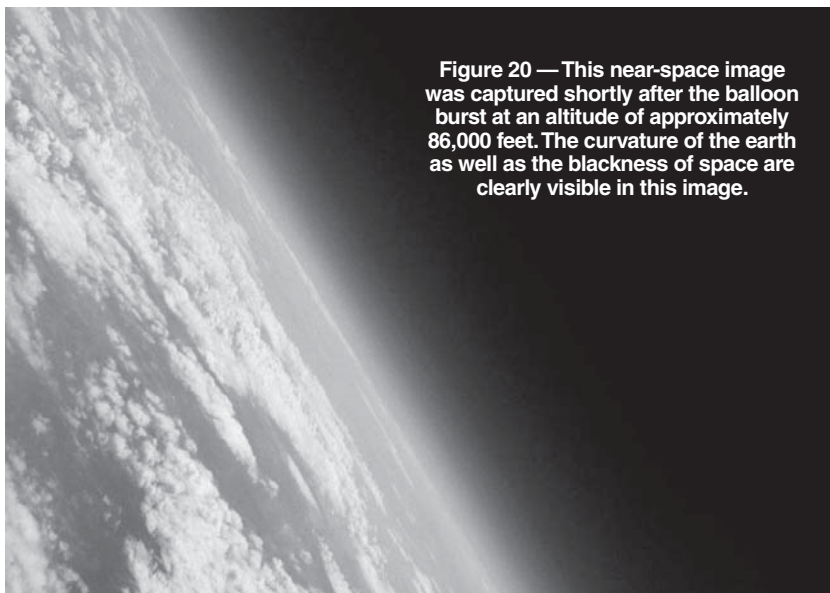


Figure 20 — This near-space image was captured shortly after the balloon burst at an altitude of approximately 86,000 feet. The curvature of the earth as well as the blackness of space are clearly visible in this image.



Figure 21 — During landing the balloon train became entangled in a dead tree. None of the balloonsat payloads sustained much noticeable damage, however.

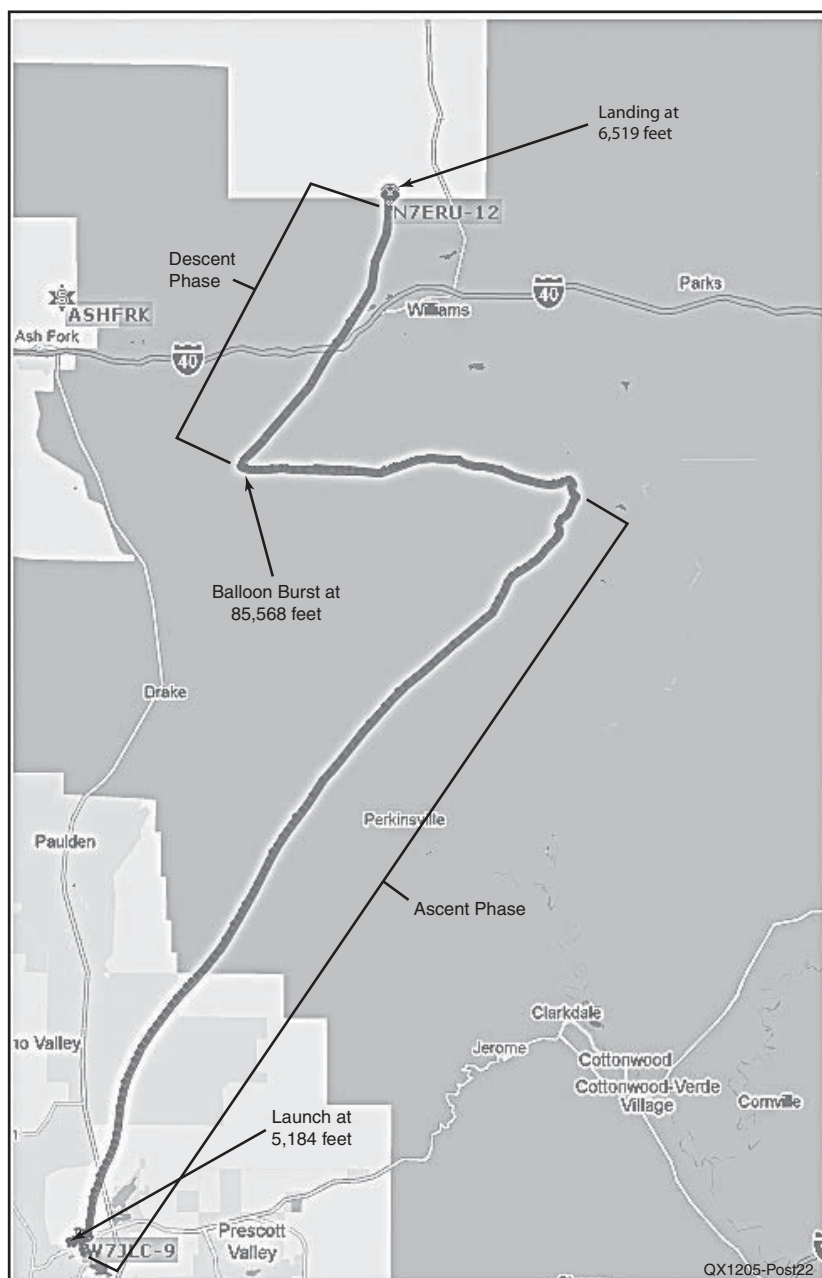


Figure 22 — This two-dimensional depiction of the flight of ERAU-06 on June 29 2011 was generated by plotting GPS data on a Google Earth map. You may view this flight by searching for “N7ERU-12” on 29 June 2011 at <http://aprs.fi>. (See Note 12.) This map shows the launch point near Prescott, Arizona, the burst elevation near 85,568 feet, as well as the landing location approximately five miles north of Williams, Arizona.

after the balloon bursts.

The balloonsat payloads and position beacons were recovered intact near the final position location, as shown in Figure 21. The sensor systems and cameras were powered down after recording data and images for approximately 4½ hours. All sensor systems and cameras appeared to operate normally and over 1 MB of data, hundreds of still images, and several hours of video images were recovered from the flight.

Figure 22 shows a two-dimensional depiction of the flight created by plotting GPS flight data on a Google map.¹² The GPS flight data shows that the balloon ascended through the troposphere in a generally northeasterly direction until easterly winds were encountered in the stratosphere, which directed the balloon almost due west. Once the balloon burst it again drifted in a generally northeasterly direction while parachuting through the troposphere until landing on national forest land approximately 5 miles north of Williams, Arizona.

Figure 23 is an example of the data generated by one balloonsat’s sensor systems before, during, and after the flight. The top panel depicts the battery voltage versus time. The flat spot at the beginning of the curve is due to the voltage of a freshly-charged LiPo battery exceeding the maximum of 8.3 V the system was designed to measure. Once the battery voltage falls below 8.3 V, the curve shows a gradual reduction in voltage as the battery discharges.

The middle panel in Figure 23 depicts the internal and external temperatures recorded before, during, and after the flight. Upon power up the two temperatures are almost identical, but the internal temperature quickly shows a steady increase in temperature due to the small electric heater inside the balloonsat container. About 45 minutes after power up, launch occurs and the external temperature decreases steadily to a minimum of about -40°C as the balloonsat ascends through the troposphere. The thermal mass of the balloonsat package, along with the heat produced by the internal heater, delays the decline of the internal temperature and limits its minimum value to approximately 0°C. Once the balloonsat encounters the stratosphere, ambient temperatures begin to *increase* with increasing altitude until they reach a maximum temperature of approximately 0°C.

Approximately 2½ hours after sensor system power up the balloon bursts and the process is reversed. As the balloonsat parachutes down through the stratosphere temperatures plunge from 0°C to -40°C at the top of the troposphere. After this, temperatures rise steadily while the balloonsat parachutes through the troposphere to the

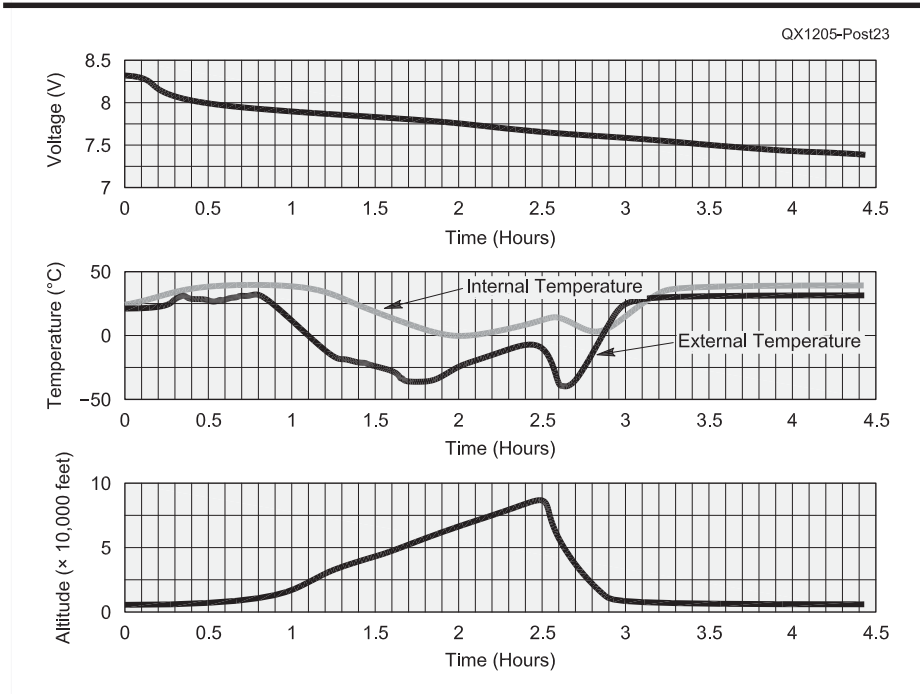


Figure 23 — These three graphs represent data recovered from one of the balloonsats during the flight of ERAU-06 on 29 June 2011. The top panel depicts battery voltage versus flight time. The middle panel shows internal and external temperature versus flight time. The bottom panel shows altitude computed from air pressure readings versus flight time. Results from the other three balloonsats were similar to those presented in this figure.

surface of the Earth. After landing, the internal heater, along with the afternoon Arizona sun, overcomes the thermal mass of the balloonsat payload and increases the internal temperature well above the maximum value of approximately 38°C the system was designed to record. This limitation produces the flat spot on the internal temperature curve that is clearly visible after landing.

The bottom panel in Figure 23 shows the altitudes recorded before, during, and after the flight. The launch site elevation was approximately 5000 feet, so this value was used to calibrate the altitudes computed from the measurements that followed. The altitude curve clearly depicts balloon launch at approximately 48 minutes after sensor system power up. After that the balloon ascends at a relatively constant rate of approximately 900 ft/min until burst at a measured altitude of approximately 90,000 feet, about 2½ hours after power-up (compared with a maximum altitude of 85,568 feet reported by the position beacon). The curve then depicts the decrease in altitude as the balloonsat returns by parachute at an average descent rate of 2000 ft/min. The balloonsat payloads landed on the Earth's surface at a measured altitude of approximately 6300 feet (compared with an altitude of 6519 feet reported

by the position beacon). In this case, the altitude measurements taken at burst and landing were within 5% or better of the GPS positions, which seems satisfactory for such a simple system. The results from the other three balloonsats were similar to those presented here.

Conclusion and Future Opportunities

The data returned from the flight of ERAU-06 validated the sensor system design methodology. Given the modest size and weight requirements for the balloonsat payloads, a low-power, light-weight sensor system with a very small form factor was required. The approach described in this article successfully met these constraints.

Finally, many opportunities exist for further expansion of the sensor system. One of the most interesting possibilities is to incorporate a low-power packet-radio transmitter that would broadcast sensor system measurements periodically during flight. This would provide students with real-time snapshots of the atmospheric conditions and system status during the flight. Successfully introducing a more complex system will require rethinking how to go about the construction and testing phases in order to keep the project within the capability of high school students, the

patience of the instructors, as well as within the time constraints of the program.

Acknowledgement

The author gratefully acknowledges many helpful discussions with Mr. Jack Crabtree, W7JLC, concerning the topics covered in this article. Jack is the founder of two high-altitude balloon groups, Edge of Space Sciences (EOSS) in Denver, Colorado and Arizona Near Space Research (ANSR).

John E. Post, KA5GSQ, is an assistant professor of electrical and computer engineering with Embry-Riddle Aeronautical University in Prescott, AZ. He holds an Amateur Extra class license and has BS, MS, and PhD degrees in electrical engineering.

Notes

¹For information about the parachute recovery system used, see: www.the-rocketman.com/recovery.html.

²Scientific Sales is one source for weather balloons. See www.scientificsales.com/8244-Weather-Balloon-1200-Grams-Natural-p/8244.htm.

³Sparkfun Electronics has many electronics experimentation projects. For the datalogger board, see: www.sparkfun.com/products/10216.

⁴The data sheet for the LM324 series of op amps is available on the National Semiconductor website. www.national.com/mpf/LM/LM324.html#Overview.

⁵Information about the Honeywell pressure sensor is available at: http://sensing.honeywell.com/index.php/ci_id/45330/la_id/1/document/1/re_id/0.

⁶You can find information about the Texas Instruments temperature sensors at: www.ti.com/lit/ds/symlink/lm135.pdf.

⁷Lithium ion polymer batteries provide a very lightweight power source for the balloonsat electronics. For one source of battery packs, see www.electrify.com/batteries/batteries-lipo.html.

⁸You can find more information about the voltage regulator used with the sensor electronics package at: www.onsemi.com/pub_link/Collateral/MC78L00A-D.PDF.

⁹Charles K. Alexander and Matthew N.O. Sadiku, *Fundamentals of Electric Circuits*, 4th Edition, McGraw Hill, Boston, Massachusetts, 2009.

¹⁰You can download a student version of PSpice at www.electronics-lab.com/downloads/schematic/013/.

¹¹ExpressPCB is a convenient way for electronics experimenters to design and purchase circuit boards. See www.expresspcb.com.

¹²See <http://aprs.fi/?call=N7ERU-12>. There are tracks available on the map for N7ERU-11, N7ERU-12 and N7ERU-13, which are all APRS beacons used on balloon flights. Along the right side of the screen, select the 2011 tab, then select the 2011/6 date and that will bring you to the track for the June 29th balloon flight.



More *Octave* for L-Networks

In this installment of our Octave lessons, we continue to learn about impedance matching with L-Networks.

Orientation of L-Networks

In “*Octave for L-Networks*” we used GNU *Octave* to design L-networks for impedance matching.^{1,2} We discovered that the rule requiring the series arm of the L-network to interface the lower of the two impedances to be matched applies strictly only to the matching of resistive terminations.^{3,4} We found that if the impedance that interfaces the parallel arm of the L-network is complex, then the network may, in at least some cases and with revised series and parallel elements, be reversed successfully.

But how significant is this departure from the rule? If it takes the addition of a large reactive component to achieve a minor change in the ratio of resistances involved in the usual rule, then it probably isn’t worthwhile to pursue it. If, though, a relatively small reactive component of impedance allows the reversal of the L-network over at least a moderate range of ratios of resistive impedance components, then we might find it useful to think about the matter.

Conditions for Reversing an L-Network

Let’s start by considering what needs to happen to allow an impedance match when the resistance ratios are “wrong.” For the moment, we’ll assume that we want to achieve a resistive match on the

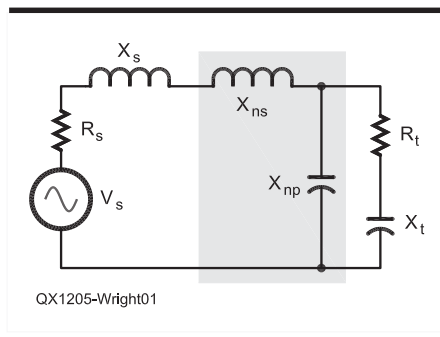


Figure 1 — This schematic diagram shows the use of an L-Network to match the source impedance to the load impedance.

source side of the circuit in Figure 1. From Equation 4 of “*Octave for L-Networks*,” we know that the requirement for matching with linear, passive, reactive elements in the L-network is:

$$0 \leq r t^2 + x t^2 - r s \times r t \quad [\text{Eq 1}]$$

where the variables in Equation 1 are elements of the circuit of Figure 1.⁵ We’d like to find a way to discriminate between reversible impedance ratios and irreversible ratios, so we’ll begin by converting Equation 1 to an equality:

$$0 = r t^2 + x t^2 - r s \times r t \quad [\text{Eq 2}]$$

Next, we’ll divide through by $r t^2$ and rearrange terms:

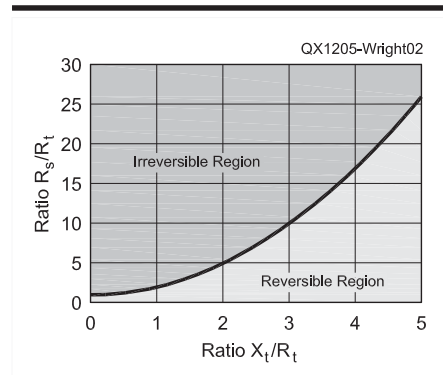


Figure 2 — This graph illustrates the reversibility of an L-Network.

Table 1

Octave Code

```
#!/usr/bin/octave
xt_o_rt = linspace(0, 5, 100);
rs_o_rt = 1 .+ xt_o_rt .^ 2;
plot(xt_o_rt, rs_o_rt, 'o');
grid("on")
xlabel("RATIO xt / rt")
ylabel("RATIO rs / rt")
title("REVERSIBILITY OF L-NETWORK")
text(1.5, 17, "IRREVERSIBLE REGION")
text(3.0, 4.0, "REVERSIBLE REGION")
pause;
exit;
```

¹Notes appear on page 23.

Table 2*Octave Code*

```
#!/usr/bin/octave
#
printf("\n\n      OCTAVE L-NETWORK DESIGN SCRIPT");
rt = input("\n\n  ENTER TERMINATING RESISTANCE: ");
xt = input("    ENTER TERMINATING REACTANCE: ");
rs = input("    ENTER SOURCE RESISTANCE: ");
xs = input("    ENTER SOURCE REACTANCE: ");
a = rs - rt;
b = 2 * rs * xt;
c = rs * rt ^ 2 + rs * xt ^ 2;
reversed = 0;
if ((b ^ 2 - 4 * a * c) < 0)
    reversed = 1;
    rtemp = rt;
    rt = rs;
    rs = rtemp;
    xtemp = xt;
    xt = xs;
    xs = xtemp;
    a = rs - rt;
    b = 2 * rs * xt;
    c = rs * rt ^ 2 + rs * xt ^ 2;
endif
if (rt == rs)
    printf("\n  L-NETWORK NOT SUITABLE FOR MATCHING\
    IDENTICAL SOURCE AND LOAD RESISTANCES.  \n\n");
    exit;
else
    xnp = (-b + sqrt(b ^ 2 - 4 * a * c)) / (2 * a);
    zn = (1j * xnp * (rt + 1j * xt)) / (1j * xnp + rt + 1j * xt);
    xns = -imag(zn);
    if(reversed == 0)
        printf("\n\n          *** FIRST OPTION: SERIES LEG TOWARD SOURCE ***");
    else
        printf("\n\n          *** FIRST OPTION: SERIES LEG TOWARD LOAD ***");
    endif
    printf("\n  SERIES ELEMENT REACTANCE = %g", (xns + xs));
    printf("  PARALLEL ELEMENT REACTANCE = %g\n", xnp);
    xnp = (-b - sqrt(b ^ 2 - 4 * a * c)) / (2 * a);
    zn = (1j * xnp * (rt + 1j * xt)) / (1j * xnp + rt + 1j * xt);
    xns = -imag(zn);
    if(reversed == 0)
        printf("\n\n          *** SECOND OPTION: SERIES LEG TOWARD SOURCE ***");
    else
        printf("\n\n          *** SECOND OPTION: SERIES LEG TOWARD LOAD ***");
    endif
    printf("\n  SERIES ELEMENT REACTANCE = %g", (xns + xs));
    printf("  PARALLEL ELEMENT REACTANCE = %g", xnp);
    printf("\n\n");
endif
if (rs / rt <= (1 + (xt / rt) ^ 2))
    a = rt - rs;
    b = 2 * rt * xs;
    c = rt * rs ^ 2 + rt * xs ^ 2;
    if ((b ^ 2 - 4 * a * c) >= 0)
        xnp = (-b + sqrt(b ^ 2 - 4 * a * c)) / (2 * a);
        zn = (1j * xnp * (rs + 1j * xs)) / (1j * xnp + rs + 1j * xs);
        xns = -imag(zn);
        printf("          *** THIRD OPTION: SERIES LEG TOWARD LOAD ***");
        printf("\n  SERIES ELEMENT REACTANCE = %g", -(xns + xt));
        printf("  PARALLEL ELEMENT REACTANCE = %g\n", -xnp);
        xnp = (-b - sqrt(b ^ 2 - 4 * a * c)) / (2 * a);
        zn = (1j * xnp * (rs + 1j * xs)) / (1j * xnp + rs + 1j * xs);
        xns = -imag(zn);
        printf("\n\n          *** FOURTH OPTION: SERIES LEG TOWARD LOAD ***");
        printf("\n  SERIES ELEMENT REACTANCE = %g", -(xns + xt));
        printf("  PARALLEL ELEMENT REACTANCE = %g\n", -xnp);
        printf("\n\n");
    endif
endif
endif
```

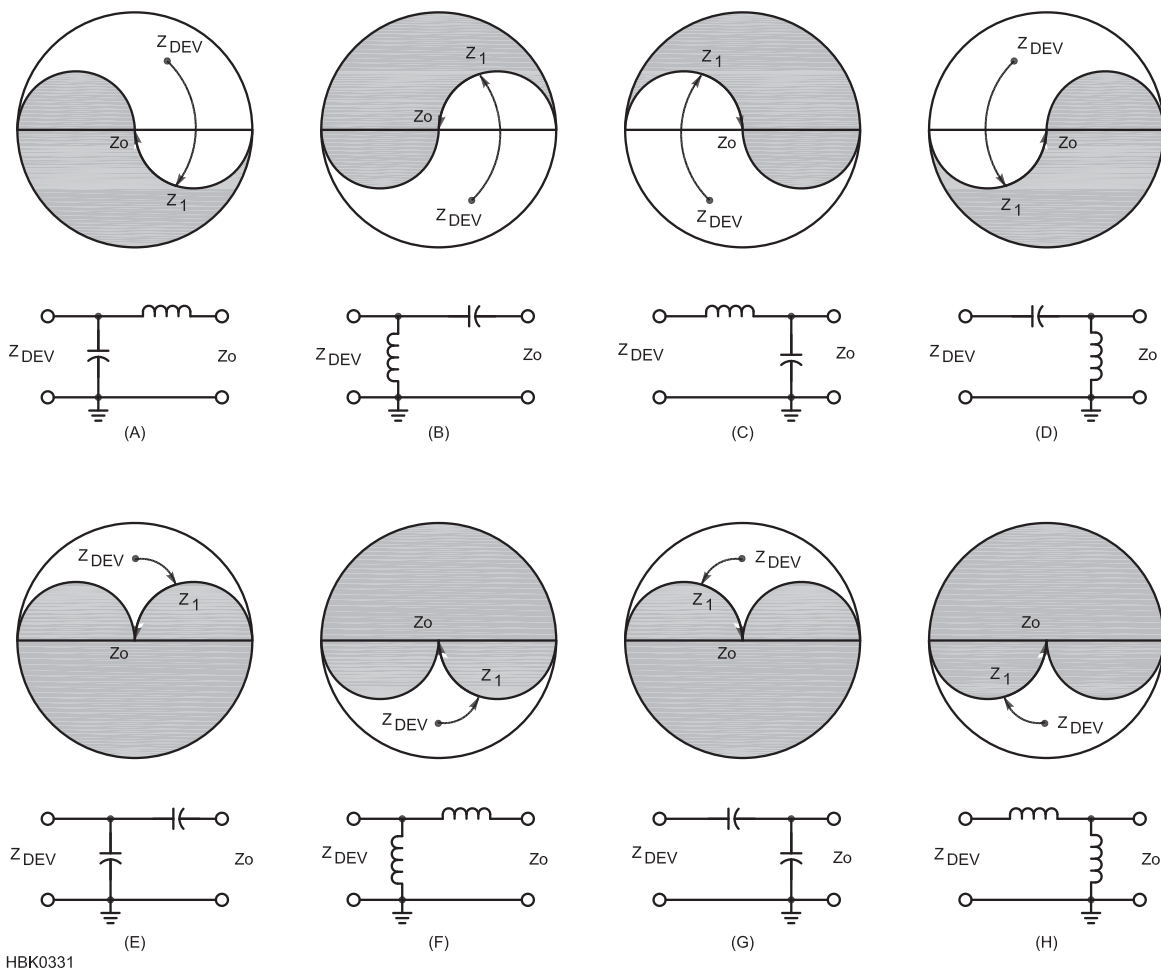



Figure 3 — This chart is Figure 5.57 in the 2012 edition of *The ARRL Handbook*. L-Networks will match a complex impedance (shown here as Z_{DEV} , the output impedance of a device) to Z_0 , a resistive source or load. Impedances in the shaded portion of the simplified Smith Chart cannot be matched by the network. Z_1 represents the impedance that is transformed from Z_{DEV} by the series element.

$$rs / rt = 1 + (xt / rt)^2 \quad [\text{Eq 3}]$$

We now have the boundary between reversible and irreversible ratios rs/rt expressed as a function of the ratio of the reactive to real components of the terminating impedance as shown in Figure 1. We'll calculate this over an arbitrary range using the *Octave* code in Table 1. The result is plotted in Figure 2.

We can see that at the left end of the curve, as xt drops to zero, the value of rs/rt drops to 1, as we would expect, because this supplies the condition that $rs < rt$ when both impedances to be matched are real.⁶

Note that, as the reactive to real ratio of the terminating impedance rises, the permissible ratio of resistive components rises as just one more than its square. This means that a moderately reactive load, say a short antenna, will allow for reversal of the L-network, should the need arise, over a significant range of impedance ratios. Since xt is squared in Equation 3, it doesn't matter in Figure 2 whether xt is posi-

tive (inductive) or negative (capacitive).

We might have drawn a horizontal line across Figure 2 at $rs/rt = 1$, but we omitted it for clarity. Such a line would specify a range of values for which the L-network is not the proper matching device. A series reactance alone will suffice to match two impedances whose real parts are equal. We might alternatively think of such a match as being accomplished by an L-network whose parallel reactance is infinite in value. In the *Octave* code in "Octave for L-Networks," we ignored the case of $rs = rt$ for simplicity.

In addition, the region below $rs/rt = 1$ isn't of much interest to us, at present, as it represents a region of impedance ratios that we already know are all usable, because they all feature a resistive component of impedance on the series side of the L-network that is lower than that on the parallel side.

What if both impedances to be matched are complex? Note from Figure 1 that rs is in series with xs , which is in series with

xns . If xs is other than zero, a match can be implemented by offsetting that value in xns . The ratios and regions of Figure 2 are thus completely general and apply whether or not both source and terminating impedances are complex.

Testing the Method

Let's consider a short antenna with an input impedance of $25 - j85 \Omega$. We'd like to match this to a 50Ω transmission line. Can we use the L-network in either direction, choosing the direction to optimize the Q of the elements, or to favor a particular geometry? The ratio xt/rt in this case equals 3.4. Using either Equation 3 or Figure 2, we find that the permitted resistance ratio rs / rt is 12.6. Since the ratio in our case is only 2.0, we will certainly be able to reverse the network if we choose to do so. If we use the *Octave* code in "Octave for L-Networks" to calculate the L-network reactances for this

case, we'll see that we can successfully orient the L-network in either direction.

More Configurations

While looking at various examples, we notice that the two configurations returned by the *Octave* code in “*Octave* for L-Networks” for a low-resistance, high-reactance load often omit the series L, parallel C, configuration that we might favor for low-pass filtering of harmonics. Does this mean that we will often run into impedances we can't match if we build a tuner using that geometry?

Let's think a bit about our example in “*Octave* for L-Networks.” We used a $230\ \Omega$ resistive source and a load of $16 - j96\ \Omega$. If we want to plot the load impedance on a Smith Chart relative to the source, we would use a normalized impedance of $(16 - j96) / 230 = 0.0696 - j0.4174\ \Omega$. If we plot that point on a Smith Chart and then examine the array of simplified Smith Charts in Figure 5.57 of the *2012 ARRL Handbook*,³ we'll find that the two solutions yielded by our *Octave* code for the example L-network fit Figures 5.57(B) and (F). [Figure 3 here is a reproduction of the Handbook Figure, for the convenience of our readers. — *Ed.*] For both of those Figures, our normalized impedance falls within the unshaded “permissible” region of each simplified Smith Chart. The small L-networks associated with those drawings correspond to the reactances calculated by the code in “*Octave* for L-Networks.”

Note, though, that Figures 5.57(C) and (H) also put our normalized impedance in an area that is usable. There are thus four possible solutions for an L-network to match our impedances. The L-network geometry associated with Figure 5.57(C) features a series L and a parallel C, just what we want. Figures 5.57(C) and (H) represent networks that are reversed with respect to Figure 1 of this article. That is, the series leg of the L-network is adjacent to the load in each of those two networks. How do we solve for the reactances we need to implement those Figures?

We might proceed as we did in “*Octave* for L-Networks” and set up a series of Equations to solve for xns and xnp . This ought to be possible, but with the parallel element of the L-network toward the source, the Equations feature a term $xns \times xnp$, complicating matters a bit. We'll try something else.

If we compare Figures 5.57(B) and (C), we see that in (B), the parallel inductor first rotates the impedance counterclockwise around a circle tangent to the point 0, 0 on the Smith Chart. In (C), the parallel capacitor first rotates the impedance clockwise around a circle tangent to the point 0, infinity.

We notice a sort of mirror-image symmetry between the two, which won't be exact depending on the location of the starting normalized impedance on the Smith Chart. The second “legs” of the impedance transformation also resemble each other in the same manner, moving the impedances in opposite directions around circles situated on opposite sides of the Smith Chart and terminating at Z0, 0 in each case.

This suggests that we might duplicate the impedance transformation of 5.57(B) using (C) by reversing the network and reversing the signs of both reactances. We'll try this by running the code in “*Octave* for L-Networks” in reverse, using the source as the load and vice versa using the following inputs:

$$\begin{aligned}rs &= 16\ \Omega \\xs &= -96\ \Omega \\rt &= 230\ \Omega \\xt &= 0\ \Omega\end{aligned}$$

The result is a network corresponding to that shown in 5.57(D) with a series reactance of $-j154.515\ \Omega$ and a parallel reactance of $+j62.8899\ \Omega$. We'll reverse the polarities of the network elements and use it as is, with the source and load as they were specified originally. An input impedance calculation shows us that we have produced a third L-network that matches our two impedances. We can then do the same with the second solution to the Quadratic Equation and produce a network that corresponds to Figure 5.57(H).

We've modified the code from Table 1 of “*Octave* for L-Networks” to test for reversibility and to then calculate the reactances of the two additional networks when possible and that code is listed in Table 2 in this article.⁸ We've also added a trap to print a diagnostic message when the code is used to try to match two impedances that have the same resistive component. An L-Network is not required for such a match, just a series reactance, and attempting to calculate an L-network for that match will result in a divide by zero error as the *Octave* code attempts to make the parallel leg an infinitely high reactance.

In addition, we've added statements to the output to indicate the orientation of the L-network (series leg toward source or load) as we can now design networks that use either or both configurations.

As in earlier articles in this series, we've omitted comments embedded in the code for brevity.

Conclusions

We might not very often need to determine the exact boundary between “reversibility” and “irreversibility” of an L-network, but Fig-

ure 2 gives us assurance that such networks may often be oriented in either direction over a wide range of possible source and load impedances.

The code in Table 2 supplements that from Table 1 in “*Octave* for L-Networks” to include additional network designs that take advantage of the “reversed” direction of the L-network. The resulting code provides a general design method for L-networks that will handle real or complex source and load impedances without restriction as to ratio.

Maynard Wright, W6PAP, was first licensed in 1957 as WN6PAP. He holds an FCC General Radiotelephone Operator's License with Ship Radar Endorsement, is a Registered Professional Electrical Engineer in California, and is a Life Senior Member of IEEE. Maynard has been involved in the telecommunications industry for over 48 years. He has served as technical editor of several telecommunications standards and holds several patents. He is a Past Chairman of the Sacramento Section of IEEE. Maynard is Secretary/Treasurer and Past President of the North Hills Radio Club in Sacramento, California.

Notes

¹ Maynard Wright, W6PAP, “*Octave* for L-Networks,” *QEX*, Mar/Apr, 2011, pp 44-46.

² You can download the latest version of the GNU *Octave* files at www.octave.org.

³ H. Ward Silver, N0AX, Ed, *The ARRL Antenna Book*, 22nd, The American Radio Relay League, 2011, pp 24-4 and 24-5.

⁴ H. Ward Silver, N0AX, Ed, *The ARRL Handbook for Radio Communications*, 2012, The American Radio Relay League, Inc. 2011, Sections 5.6.1 and 20.4.2.

⁵ In “*Octave* for L-Networks,” we used a “less than” symbol rather than “less than or equal to” in Equation 4, which is the source of Equation 1 here. The use of “less than” wasn't exact, but it eliminated the need to consider the case where $rs = rt$, a case that cannot be matched by an L-network using finite element values. Here we're considering the possibilities for matching impedances over a range of complex values and we'll treat the $rs = rt$ case separately.

⁶ Note that the line between regions in Figure 2 is included in the “reversible” region except at the point $xt/rt = 0$, $rs/rt = 1$. At that point, the source and load resistances are equal and the L-network is not the right matching vehicle for reasons explained in the text and in Note 5.

⁷ The paths we're considering here are from our normalized point $0.0696 - j0.4174$ on the Smith Chart and not the example paths shown in Figure 5.57 of *The ARRL Handbook*.

⁸ The *Octave* code files for this article are available for downloading from the ARRL *QEX* files website. go to www.arrl.org/qex files and look for the file **5x12_Wright.zip**.



A Closer Look at Vertical Antennas With Elevated Ground Systems—Part 2

N6LF shares his results from further HF vertical antenna experiments.

[Part 2 concludes this article, which began in the Mar/Apr 2012 issue of *QEX*. — Ed.]

Multiband Verticals

For a single band antenna we can avoid the problems of long radials by simply using radials that are short enough or by increasing the number of radials, but what about the case of multiband antennas where you typically have four $\lambda/4$ radials for each band? For example, if you have 40 m $\lambda/4$ radials, these will be $\lambda/2$ on 20 m, $3/4 \lambda$ on 15 m, and so on. In light of the information we found for G_a as a function of L in Part 1, is that a problem? I don't have the space here to explore it in detail with modeling, but I have looked at multiband elevated verticals experimentally. The information was in Part 5 of my *QEX* series, "Experimental Determination of Ground System Performance for HF Verticals." Part 5 was in the July/August 2009 issue of *QEX*, pp 15-17. That series of articles is available for viewing on my website: (www.antennasbyn6lf.com). The experimental work indicated that as long as there are a large number of radials (whether they are the same length or of different lengths) you don't have a problem but if you try to use only a few long radials you will have problems. Read the article for the details.

Potentials on the Radials

As Laport stated, elevated ground systems can have very high voltages between the wires and ground. Figure 27 shows examples of the voltage from a radial wire to ground for ideal 4, 12 and 32 $\lambda_0/4$ radial systems.

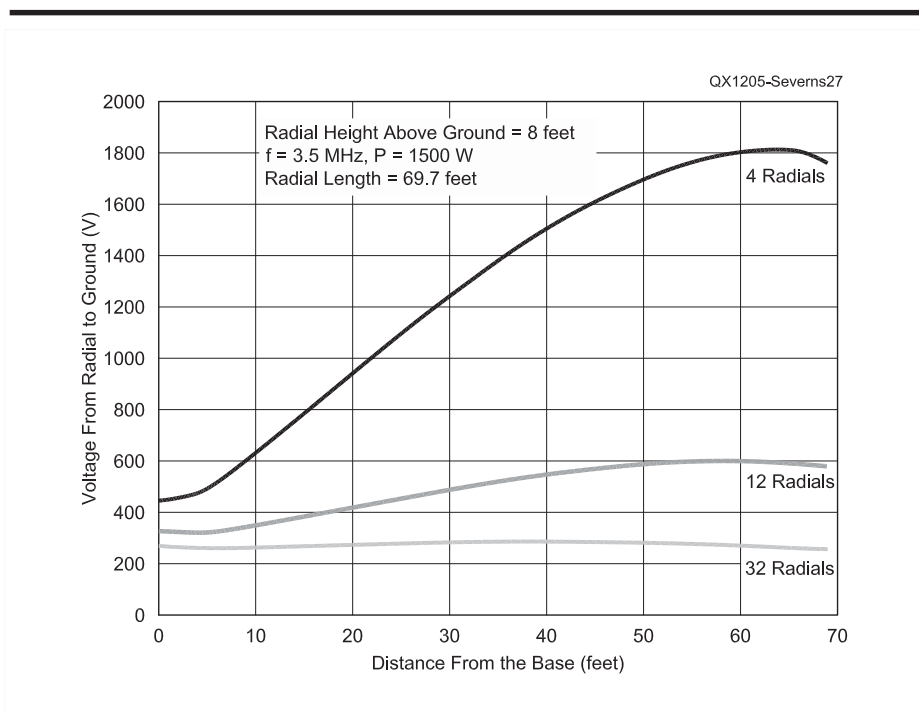


Figure 27 — Examples of the voltage from a radial wire to ground with different numbers of radials. The input power to the vertical is 1500 W, the operating frequency is 3.5 MHz and the radial system is elevated 8 feet above ground.

I think this Figure makes it clear why you want to keep the radials out of reach! Note that as more radials are added the potential difference between the radials and ground drops significantly and becomes more uniform as we go away from the base of the antenna. This is a reflection of the reduction in E-field amplitude with more numerous radials, as was shown in Figures 24, 25 and 26 in Part 1 of this article (Mar/Apr 2012

QEX). Even with a large number of radials that voltage is still high. This voltage will vary with the square root of the power level so that going down from 1500 W to 100 W, a change of 15:1 (0.067), the voltage only drops by 0.26! Be careful!

Feed Point Impedances

The behavior of the feed point impedance over the band (3.5 to 3.8 MHz for these

examples) as we vary H, L, J, N and soil characteristics is an important factor. The point I want to make in this section is how widely the input impedance of ground-plane antenna can vary as we change one or more of the variables. There is no one number for Z_{in} ! We will also look at variations in SWR bandwidth.

A graph of the feed point impedance ($Z_{in} = R_{in} + j X_{in}$) from 3.5 to 3.8 MHz for different numbers of radials is shown in Figure 28. Note that in Figures 28 to 31, $H = L$ and is adjusted so that the model is resonant at 3.65 MHz for each variation of parameters. As the parameters N, J and soil characteristics are changed, the values for H and L vary somewhat. From Figure 28 we can see that N has a strong effect on the feed point impedance (Z_{in}) although that effect diminishes as N increases. As shown in Figure 29, we can convert the information in Figure 28 to SWR. In this case the Z_0 impedance for the SWR calculation is taken to be R_{in} at resonance (3.65 MHz) for each value of N.

Figure 29 shows that the 2:1 SWR bandwidth increases somewhat as N is increased but by N = 16 we are approaching the point of vanishing returns for bandwidth.

Figure 30 shows the effect of height above ground of the radial fan (J) on Z_{in} for N = 4. It's pretty clear that the value for J has a strong effect on Z_{in} . The effect of different soil characteristics for a given value of J (8 feet in this example) is shown in Figure 31.

The information in Figures 28 to 31 represents only a few possible combinations, but the graphs make the point that the feed point impedance of an elevated radial vertical is a strong function of all the variables, so that each installation is unique.

We can also see the behavior of Z_{in} over the band for different combinations of H and L that are resonant at 3.65 MHz. Some examples are given in Figure 32 and the associated graphs for SWR, are given in Figures 33 and 34. N = 4 and the H&L combinations are shown on the graphs.

The combination H = 73.25 feet and L = 43.11 feet has the very nice property that $Z_{in} = 50 \Omega$ at 3.65 MHz. As shown in Figure 33, this results in a relatively wide 2:1 SWR bandwidth compared to the other combinations.

The greater match bandwidth is not just because $Z_{in} = 50 \Omega$ at resonance. The combination also has intrinsically more bandwidth as shown in Figure 33, where the Z_0 at resonance is set to R_{in} at resonance for each combination of H and L separately.

The idea of increasing the feed point impedance at resonance to 50Ω by making the vertical taller and the radial fan radius smaller has actually been around for many

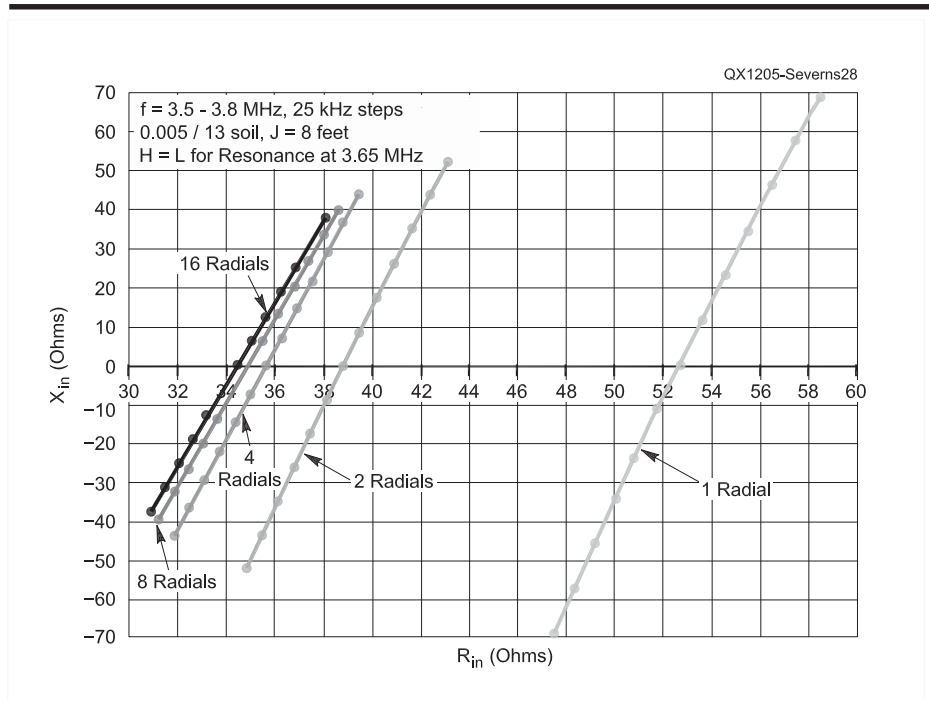


Figure 28 — X_{in} versus R_{in} ($Z_{in} = R_{in} + j X_{in}$) where frequency varies from 3.5 MHz (lower left ends of the curves) to 3.8 MHz (upper right ends of the curves) for different values of N. Frequency is stepped in 25 kHz intervals.

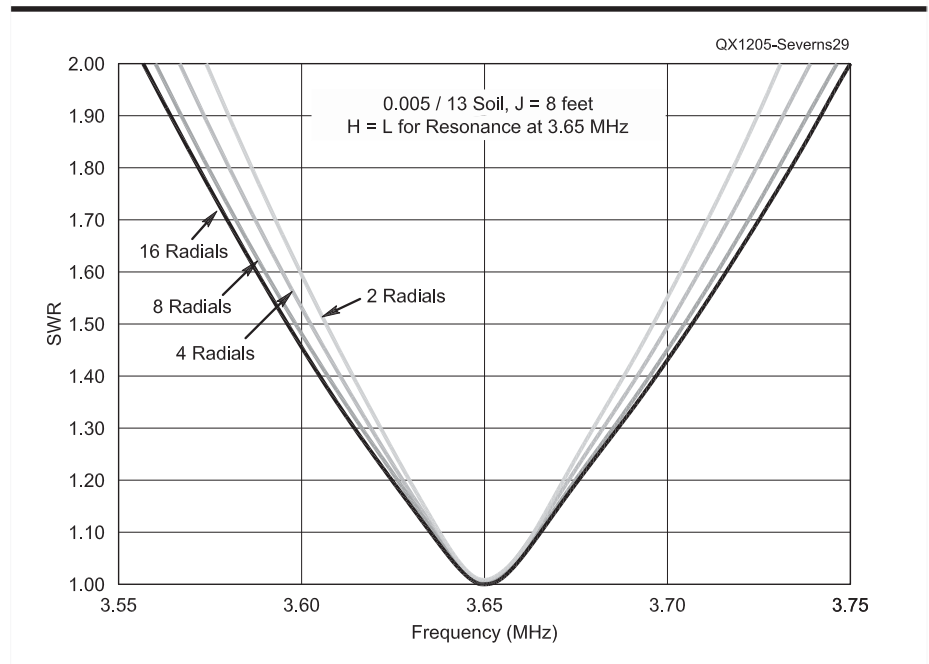


Figure 29 — Feed point SWR as a function of N.

years: R_{in} at resonance can be increased by sloping the radials downwards from the base. In effect you are making the vertical taller and reducing the radial fan radius, which is what we did in the above example.

Figure 9 (in Part 1) showed how L_r varied for different values of N and H. For H = 69 feet, L_r decreased rapidly as more radials were added. We can play this game to find designs

where $Z_{in} = 50 \Omega$ at resonance. Figure 35 is a graph where L is varied from 15 feet to 100 feet for two values of H (72 feet and 77.6 feet). Note that H in the range of 72 feet \Leftrightarrow 77.6 feet represents the limit that allows $R_{in} = 50 \Omega$. Longer or shorter values for H do not have a point where $R_{in} = 50 \Omega$ for L = 15 feet \Leftrightarrow 100 feet. The combination of H = 72 feet, L = 25 feet, N = 16 and J = 8 feet

over average ground will give us $Z_{in} = 50 \Omega$ at 3.65 MHz. Figure 36 shows the comparison for SWR between two combinations where $N = 4$ and $N = 16$. This illustrates one of the advantages of using more radials.

For $H = 72$ feet and $N = 16$, L is only 25 feet that represents a drastic reduction in the radius of the radial fan. In exchange for an increase in height on the order of 6 feet, we have a good match over a wide portion of the band and a small diameter radial fan. Instead of increasing the height we could have just added a couple of short top-loading wires. This is very nice but it's not entirely for free. When compared to the normal four radial system ($H = 67$ feet, $L = 67.7$ feet), G_a for the $H = 72$ feet, $L = 25$ feet combination is lower by about 0.25 dB. You sacrifice a small amount of gain. Whether that is acceptable for the improvement in matching is an individual decision.

In a private communication with Dick Weber, K5IU, he made a suggestion that overcomes the reduction in gain associated with small radial length: use longer radials. This will result in $X_{in} \neq 0$ but you can tune out the reactance with a series impedance. He has also pointed out that if X_{in} is inductive (+) then you can tune out the reactance with a series capacitor at the feed point. Looking back at Figure 35, we see that this trick will work for $H > 72$ feet. (That is for this particular case, where $N = 16$, $J = 8$ feet over average ground!). If we chose $H = 75$ feet, $L = 70$ feet, $N = 16$ and adjust the series capacitor at the feed point as we move across the band, we get the result shown in Table 1. Note that X_{in} is given in the Table, but C_s (the added series capacitor) tunes it out.

What we see is a vertical that can have a very low SWR across the entire 75/80 m band. It isn't necessary that C_s be adjusted at every point. Three or four values of C_s switched with relays would probably still provide acceptable SWR over the entire band. For the case where $H = 72$ feet, $L = 25$ feet and $N = 16$, $G_a = -5.52$ dB. When we change to $H = 75$ feet, $L = 70$ feet and $N = 16$, $G_a = -5.03$ dB. That's an improvement of +0.5 dB in signal strength.

There is another option to make $Z_{in} = 50 + j0 \Omega$ at resonance. Instead of making the antenna taller (or top-loading it) and the radials shorter, you can simply shift the feed point up into the vertical to a point where $R_{in} = 50 \Omega$. This is just a matter of moving the base insulator up into the antenna. You won't get quite as much match bandwidth as with the taller vertical but it will be close and you can use longer radials that give a better G_a . Whether this trick is mechanically feasible depends on the particular implementation.

All the examples to this point have assumed that the excitation at the base of the

Table 1
 Z_{in} and SWR from 3.5 to 4.0 MHz for $H = 75$ Feet, $L = 70$ Feet and $n = 16$

Frequency (MHz)	$R_{in} (\Omega)$	$X_{in} (\Omega)$	$C_s (pF)$	SWR
3.50	43.7	69.6	654	1.14
3.65	49.4	113.7	384	1.01
3.80	56.0	159.4	263	1.12
4.0	66.6	223.6	178	1.33

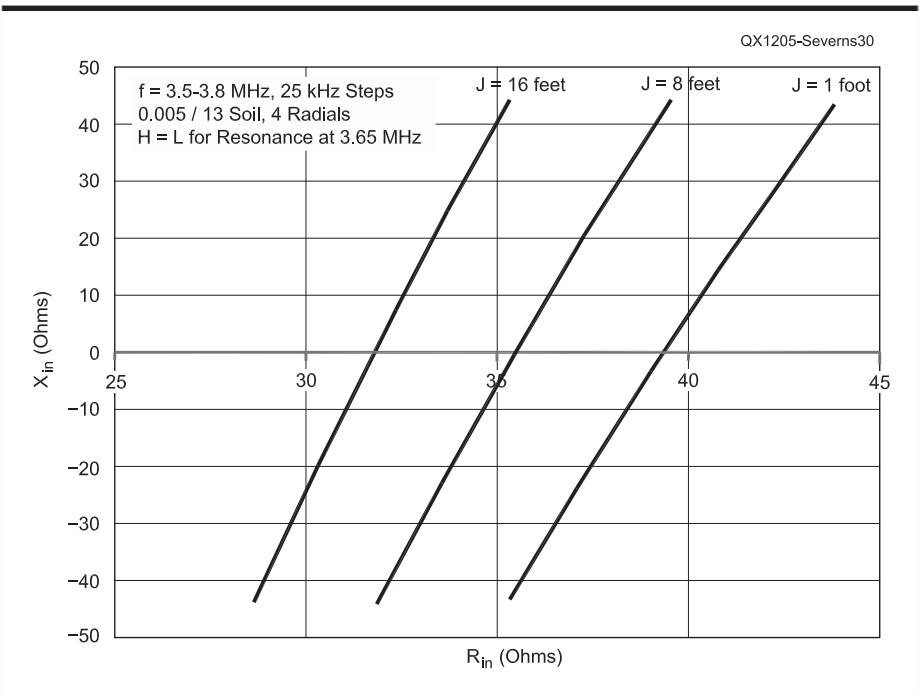


Figure 30 — The effect of height above ground on Z_{in} .

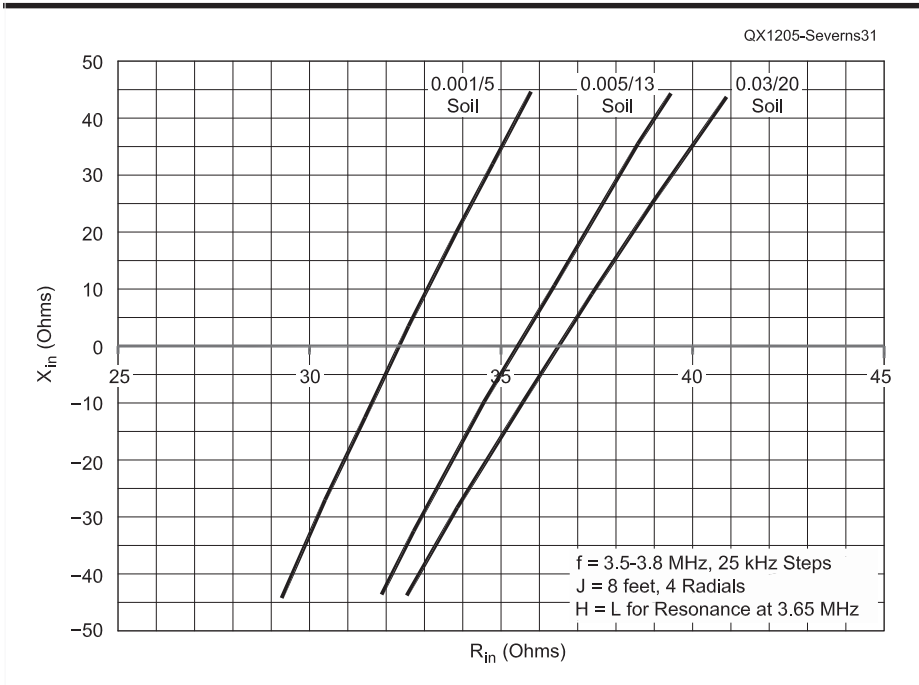


Figure 31 — The effect of different soil characteristics on Z_{in} .

vertical was isolated from ground: a choke (balun) was used in series with the feed line. If a choke is not used and the coaxial feed line is simply connected to the antenna and run down to ground, usually with the shield connected to the radials and the center conductor to the vertical, there will be additional ground currents that increase loss. In a 4-radial elevated system, G_a typically falls -0.25 to -0.5 dB or even more for lossy soils if a choke is not used. If 12 to 16 radials are used, the increased loss is much smaller, usually only a few tenths of a dB. You might argue that when N is large a choke is not needed but I think it is better to be cautious and use a choke even in that case.

Earlier we saw how the radial length (L) affected the efficiency (G_a) of the antenna. We also saw that the effect was reduced when more radials were used. It is useful to look at Z_{in} as both N and L are varied, especially around values of L near $\lambda_0/4$. Figure 37 shows the effect of varying L on X_{in} .

Figure 37 is particularly interesting in that it shows how sensitive the X_{in} component of Z_{in} is to radial length when only a few radials are used. The R_{in} component is not nearly as sensitive. This becomes important when we look at current asymmetries in the radials. Adding more radials reduces the sensitivity of Z_{in} to radial length and also the susceptibility to radial current asymmetry. Dick Weber, K5IU (see Note 43) generated a graph very similar to Figure 37 by assuming the radials were open circuit transmission lines and plotting the impedance at the feed point as more radials were added in parallel. I have more on radials as transmission lines in the next section.

Effect of Asymmetries in the Radial Fan

Is there significant current division asymmetry among the radials of typical

installations and, if there is, do we need to be concerned about it? To answer the first part of this question, Dick Weber, K5IU, made a series of measurements on representative 80 m and 160 m verticals with two and four elevated radials. Dick's work was published in "Optimum Elevated Radial Vertical Antennas," in the Spring 1997 edition of *Communication Quarterly*. (See Note 9 in Part 1 of this article.) I have summarized some of his data in Table 2 but I strongly recommend reading his complete article.

Data tables are helpful but sometimes a graph of the data has more impact. Figure 38 compares the radial current divi-

sion for Weber's 80 m vertical with four radials. Figure 38 shows two things: the radial current division between the radials is far from equal and the division ratios change as we move across the band. Unfortunately, this is typical of elevated ground systems with only a few radials, as shown in Table 2.

Weber explains this behavior by pointing out that a horizontal radial above ground is actually a section of single wire transmission line open-circuited at the far end so that in the region where $L \approx \lambda_0/4$ it acts like a series resonant circuit. Figure 39 shows an equivalent circuit.

Individually the radials may have differ-

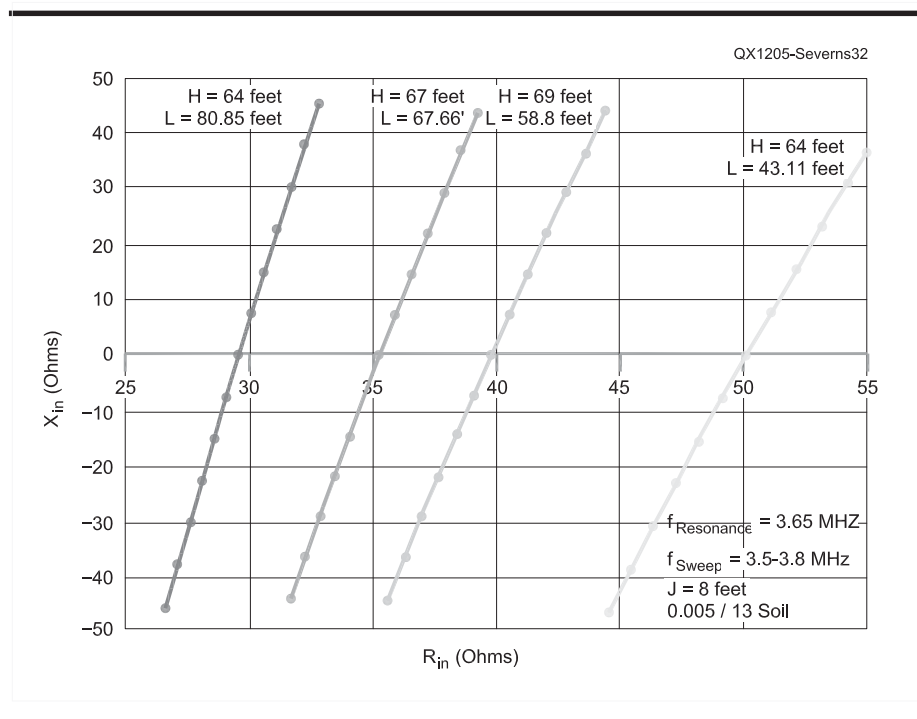


Figure 32 — Z_{in} variation for different combinations of H and L that are resonant at 3.65 MHz.

Table 2

Radial Current Comparisons from K5IU Measurements

(See Note 9 in Part 1 of this article for a reference to the source of this data.)

Antenna #	Station ID	Frequency (MHz)	Relative Current Radial 1	Relative Current Radial 2	Relative Current Radial 3	Relative Current Radial 4
1	K5IU	3.528	1.00	0.52	0.27	0.27
1	K5IU	3.816	0.96	1.00	0.51	0.51
1	WX0B	1.805	1.00	0.01	----	----
1	WX0B	1.885	1.00	0.05	----	----
2	WX0B	1.805	1.00	0.80	----	----
2	WX0B	1.885	1.00	0.10	----	----
1, 0.125 λ radials, w/inductor	WX0B	1.805	1.00	0.83	----	----
1, 0.125 λ radials, w/inductor	WX0B	1.885	1.00	0.76	----	----
1	W7XU	1.805	1.00	0.00	0.00	0.00
1st trim	W7XU	1.805	0.03	1.00	0.10	0.07
Last trim	W7XU	1.805	1.00	0.00	0.00	0.00
Last trim	W7XU	1.900	0.03	1	0.10	0.07

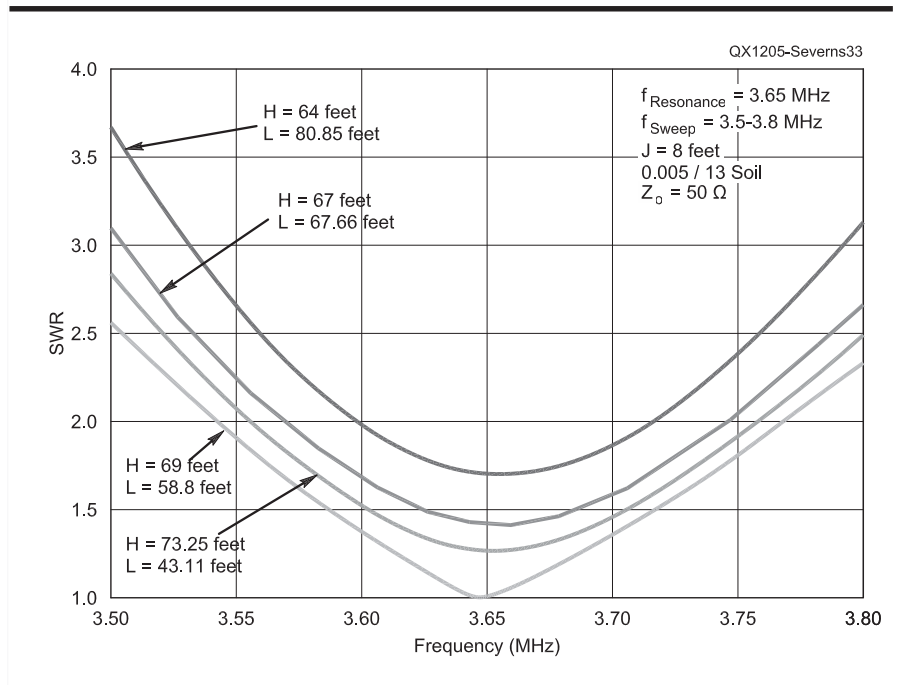


Figure 33 — SWR for various combinations of resonant H and L. $Z_0 = 50 \Omega$ for all curves.

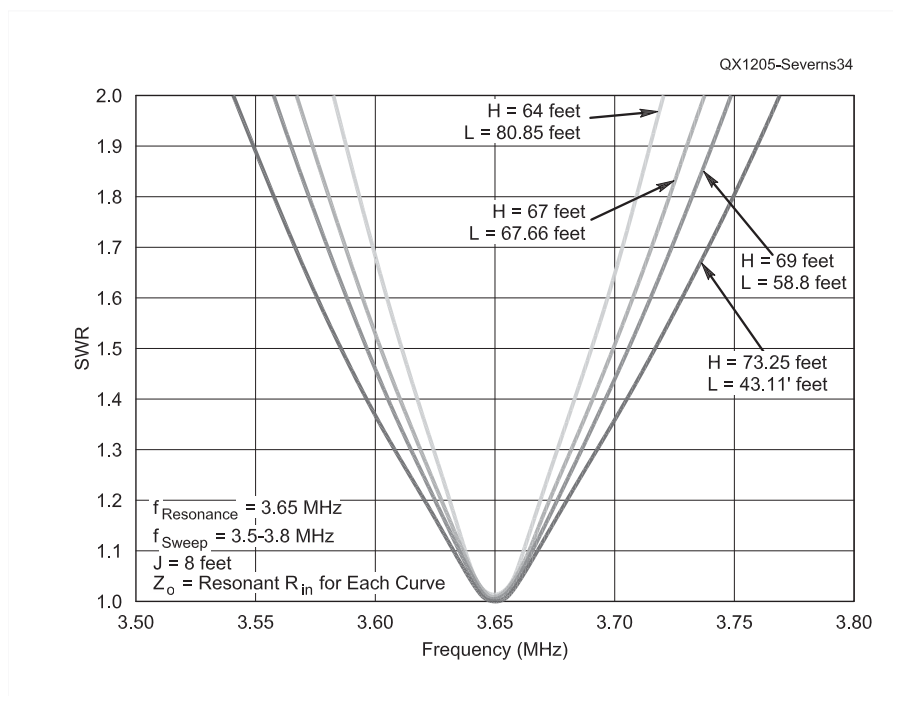


Figure 34 — SWR with Z_0 equal to R_{in} at resonance for the particular combination of H and L.

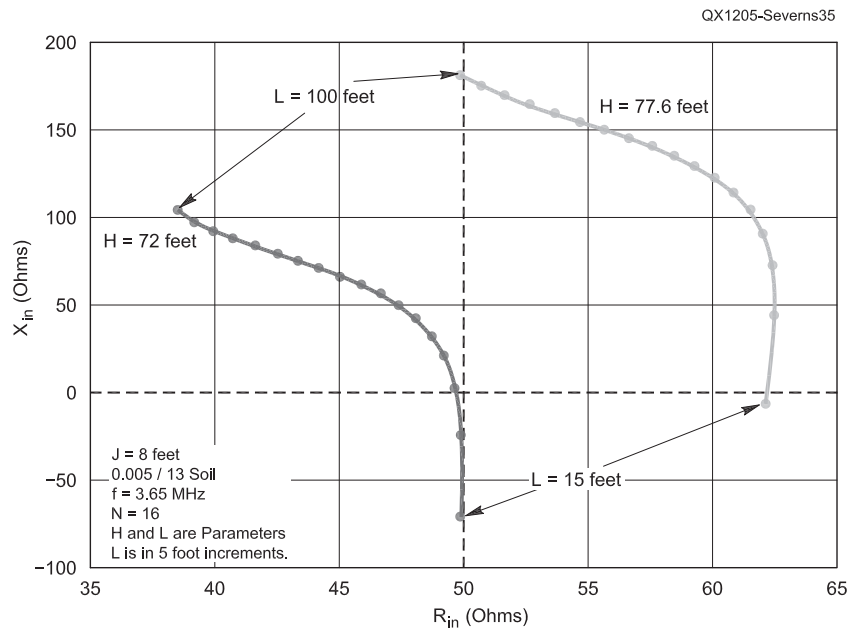


Figure 35 — Z_{in} as a function of radial length (L) for $H = 72$ feet and 77.6 feet with $N = 16$.

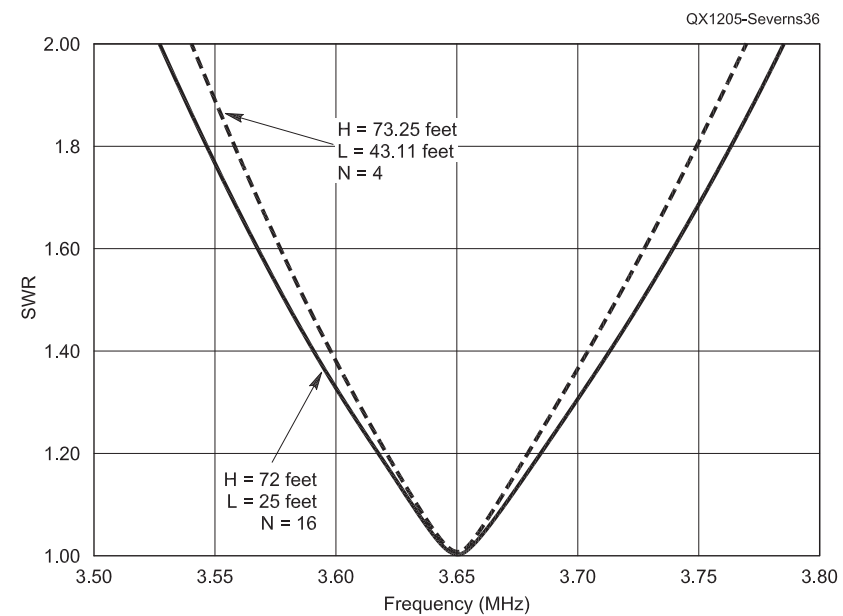


Figure 36 — SWR over 3.5 to 3.8 MHz for two different combinations of H and L .

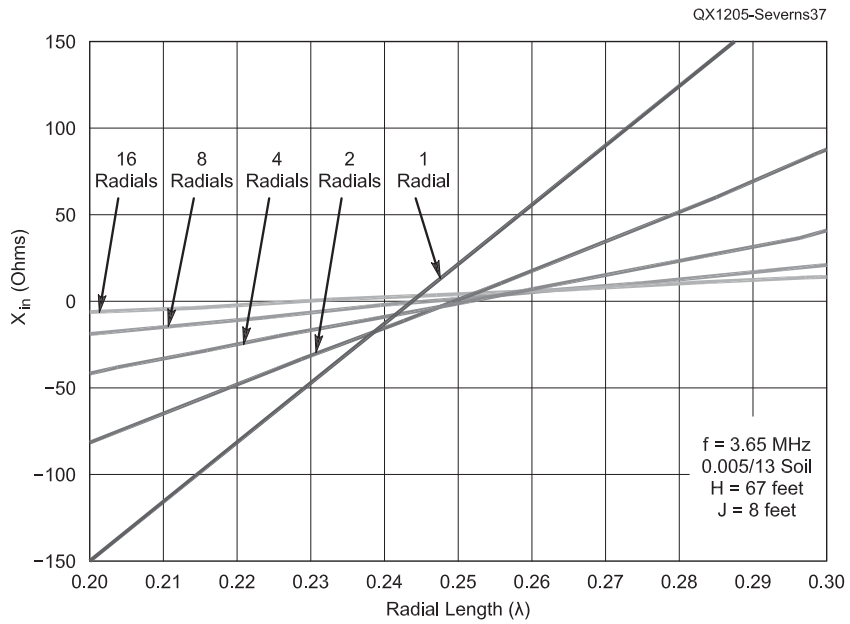


Figure 37 — Effect of changing L in the neighborhood of $\lambda/4$ as a function of radial number.

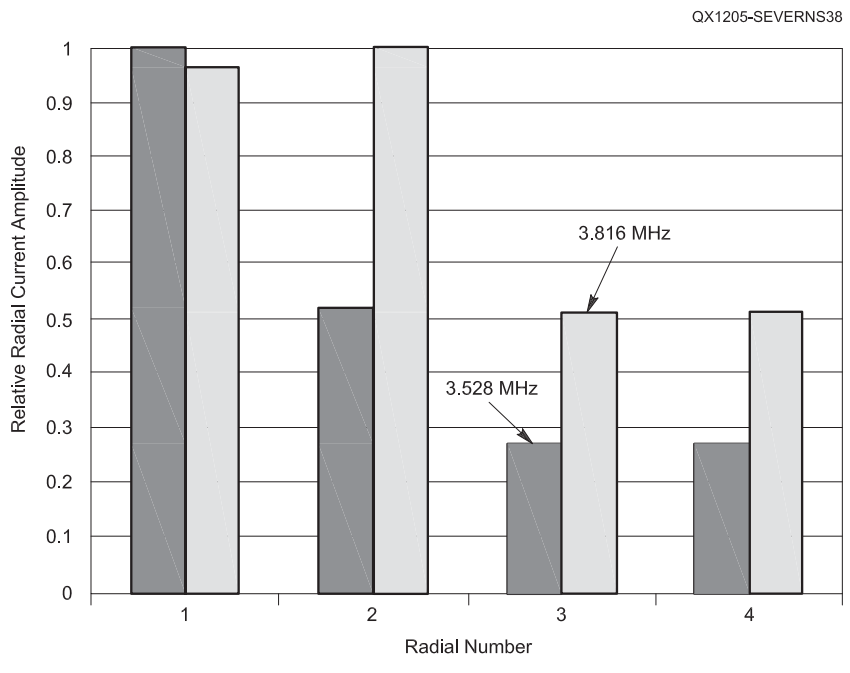


Figure 38 — Current division between the four radials at 3.528 and 3.816 MHz for the 80 m vertical at K5IU.

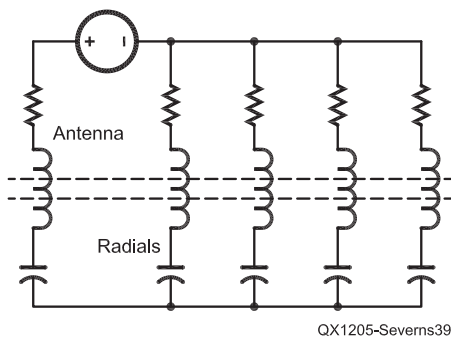


Figure 39 — Equivalent circuit for a vertical with elevated radials.

ing resonant frequencies due to length variations, varying ground characteristics under a particular radial, nearby conductors, and other factors. (See Note 12 in Part 1, Doty, Frey and Mills, "Efficient Ground Systems for Vertical Antennas," *QST*, Feb 1983, p 20.) At a given frequency, a particular radial may be close to series resonance, which means it has a low input impedance and may therefore take the majority of the current. This is a reasonable idea but the basic model in Figure 39 doesn't take into account the coupling between the individual radials or between the radials and the vertical. It would be more correct to add mutual coupling between all the inductive elements of Figure 39 as shown by the dashed lines. In the case of four radials, the radials are at right angles to each other and to the vertical so that the mutual coupling is small (but not zero). When you go to eight radials, for example, the angle between the radials goes from 90° to 45°. That greatly increases coupling between the radials.

All this is very interesting but so what? Does current-division asymmetry in the radials cause any problems we should worry about? One way to look into this is to model a system with only one radial, which might be a worst case. Several of the examples in Table 2 show almost all the radial current to be in one radial. Figure 40 shows a comparison in the azimuth radiation patterns between one and four radials with $J = 8$ feet and $f = 7.2$ MHz, at an elevation angle of 22°. Note that I have changed from 80 m to 40 m for the following examples simply because this work was already on hand. With four radials, the pattern is symmetric within 0.1 dB but with only one radial the pattern is distorted with a F/B ratio of 4.6 dB. In addition, the average gain for one radial is about 0.5 dB lower than G_a with four radials. There is substantial signal reduction (almost 5 dB!) in the direction away from the single radial. Over poor soil, G_a is even lower and the F/B can be 6 dB or more.

Does having all the current in one radial

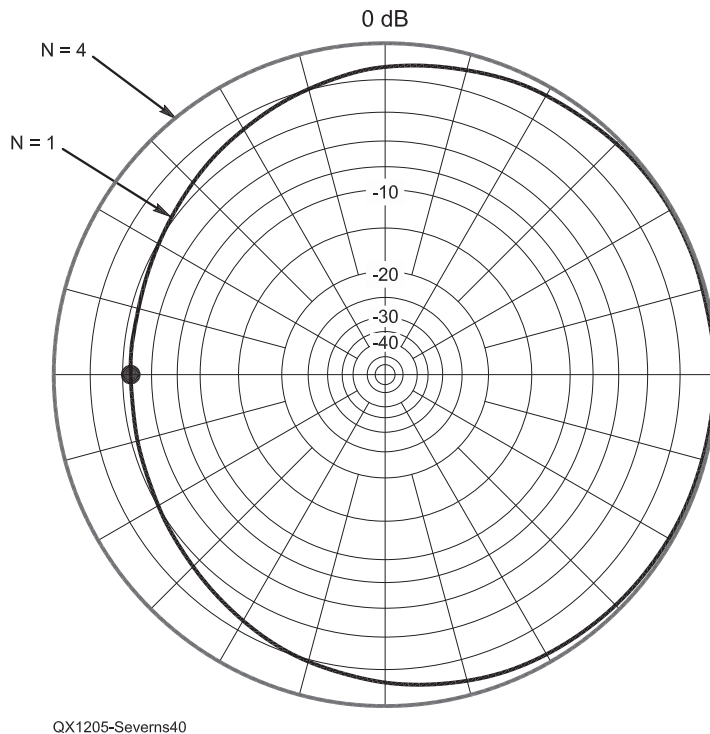


Figure 40 — Azimuth radiation pattern comparison between one and four elevated radials. $J = 8$ feet, $f = 7.2$ MHz over average ground. The elevation angle for these plots is 22°.

actually represent the worst case or can we have even more pattern distortion and/or lower G_a in some other cases? NEC modeling can be used to investigate this question. We'll start with a 40 m $\lambda/4$ vertical with four radials (see Figure 4 in Part 1). Radials 1 and 2 form an opposing pair with a length = L. Radials 3 and 4 are a second opposing pair with length = M. First we'll model the antenna with all the radials the same length ($L = M$) and then with radials that differ in length ($L \neq M$).

The feed point impedances for three different radial length configurations are compared in Figure 41 as the frequency is varied from 7.0 to 7.3 MHz. The plot on the left is for the case where all the radials are identical ($L = M = 34.1$ feet). The looping plot on the right is for the case where $L = 35.6$ feet and $M = 33.1$ feet. This represents a length error of $\pm 2.9\%$. The middle plot is for $L = 34.6$ feet and $M = 33.6$ feet. That is a length error of $\pm 1.4\%$. Clearly even modest radial length asymmetry can have a dramatic effect on the feed point impedance and resonant frequency. The resonant frequency is the point at which $X_{in} = 0$.

Feed point impedance is not the only problem associated with asymmetric radial lengths. Figure 42 compares radiation patterns between symmetric and asymmetric systems at 7.25 MHz. The amount of pattern distortion varies across the band from a frac-

tion of a dB at 7.0 MHz to 3 dB at 7.25 MHz. Besides the distortion, the gain in all directions is smaller for the asymmetric case. Computing the average gains for the symmetric and asymmetric cases, there is about a 1.6 dB difference. What this tells us is that asymmetric radials can lead to significantly higher ground losses!

Pattern distortion and increased ground loss with asymmetric radials occurs because the radial currents with asymmetric radial lengths are very different from the symmetric case. An example is given in Figure 43.

The graph bars represent the current amplitudes at the base of the vertical and each of the radials immediately adjacent to the base of the vertical. The grey bars are for symmetric radial lengths ($L = M = 34.1$ feet) and the black bars are for asymmetric radials ($L = 35.1$ feet and $M = 33.1$ feet). In the symmetric case, each of the radials has a current of 0.25 A, which sums to 1 A, the excitation current at the base of the vertical. The radial currents are also in phase with the base current.

With asymmetric radials the picture is very different: the current amplitudes are different between radial pair 1 and 2 and pair 3 and 4, and the sum of the current amplitudes is *not* 1 A (the base current amplitude), it is much larger! This would seem to violate Kirchhoff's current law that requires the sum of the currents at a node to be zero. In this

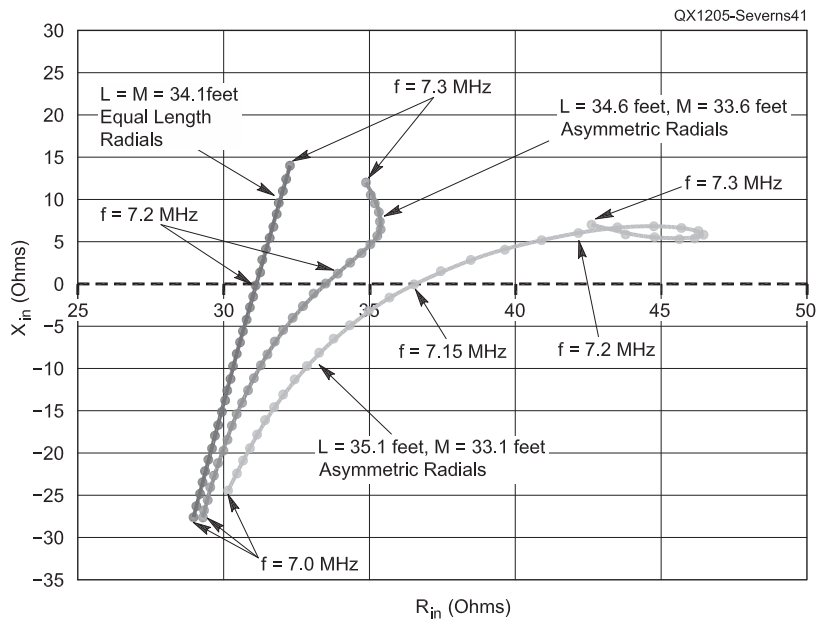


Figure 41 — A comparison of the input impedances ($Z_{in} = R_{in} + jX_{in}$) from 7.0 to 7.3 MHz at the feed point of the vertical, for symmetric and asymmetric radial lengths. The frequency is stepped in 10 kHz increments.

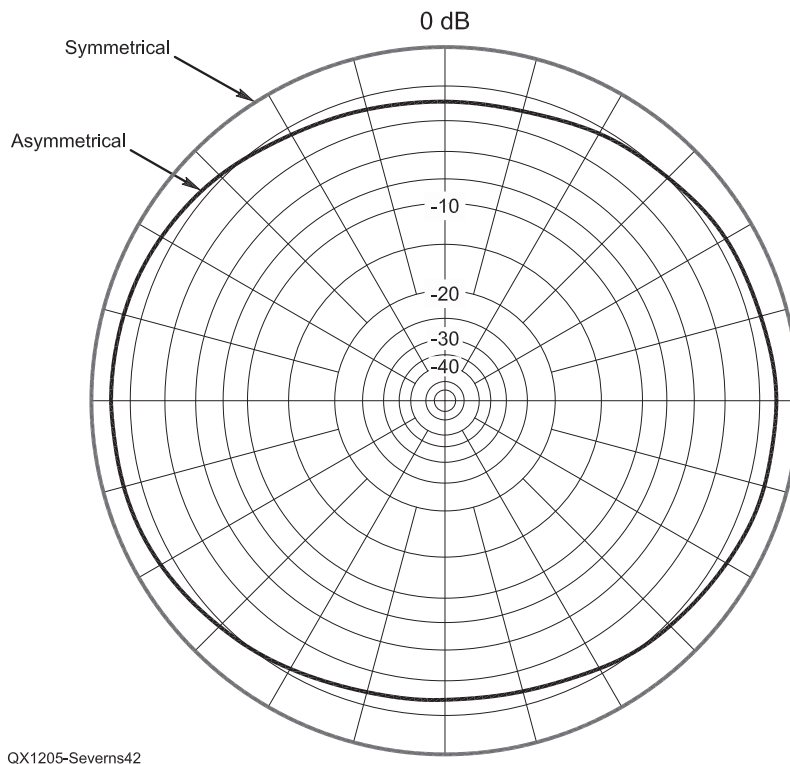


Figure 42 — Radiation pattern comparison between symmetric ($L = M = 34.1$ feet) and asymmetric ($L = 35.1$ feet and $M = 33.1$ feet) radials at 7.25 MHz.

case the radial currents in the two pairs of radials are not in phase with each other or the vertical base current. The current in radials 1 and 2 is shifted by -62° from the base current and the current in radials 3 and 4 is shifted by $+89^\circ$. The base and radial currents sum *vectorially* to 0 however. That satisfies Kirchhoff's law! These large asymmetric currents go a long way towards explaining the increased ground loss and pattern distortion. Note that the current asymmetry shown in Figure 43 is for $f = 7.25$ MHz. As the frequency is changed the pattern for the asymmetric currents in Figure 43 will change in a way similar to Weber's data shown in Figure 38.

If we take the example of $L = 35.6$ feet and $M = 33.1$ feet and add a wire from the junction of the radials to a ground stake, the G_a drops *another* -0.5 dB and the radial current asymmetry increases.

These examples represent only two particular cases. Obviously there are an infinite variety of radial fan distortions including radial lengths, azimuthal asymmetry, droop of the radials, and on and on. As we increase the number of radials what we see is a rapid decrease in the sensitivity to asymmetric radial lengths. A primary effect of additional elevated radials (>4) is to reduce the sensitivity to radial asymmetry, nearby conductors, variations in ground conductivity or objects under the radial fan, and, as shown in Figure 27, more numerous radials reduce the potentials on the radials.

How can we tell if there is a problem in an existing radial fan? One way is to measure the current amplitudes in the individual radials close to the base of the vertical. (See Part 1 of my series, "Experimental Determination of Ground System Performance on HF Verticals; Test Setup and Instrumentation," in the Jan/Feb 2011 issue of *QEX*.) If the current amplitudes are significantly different between the radials and/or if the sum of the current amplitudes in the radials is greater than the base current, then you have a problem. Current amplitude measurements can be made with an RF ammeter. More accurate measurements that also show the phase can be made using current transformers and an oscilloscope or a vector network analyzer.

Final Comments

This discussion has shown that a vertical with an elevated ground system has many subtleties and many potentially useful variations, but it has also shown that you cannot simply throw up a vertical with a few radials dangling in various directions and expect it to work properly. You have to take some care. Are there a few simple rules that will keep us out of trouble?

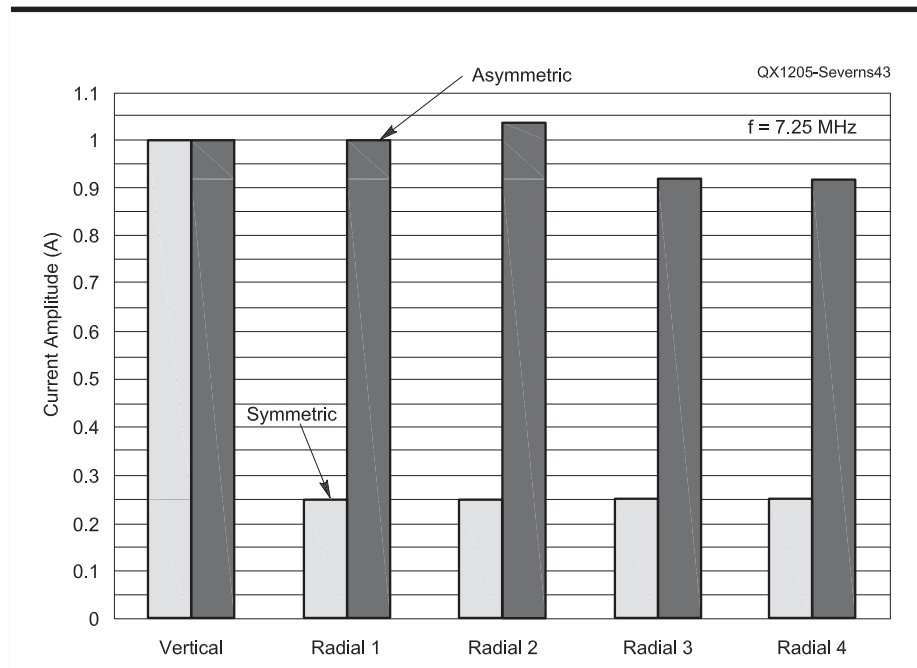


Figure 43 — Comparison of currents between symmetric and asymmetric radials.

Here's my advice:

- 1) Use at least 10 to 12 radials.
- 2) Make an effort to have the radial system as symmetric as possible.
- 3) Keep the radial system as far as possible from other conductive objects.
- 4) While it is certainly possible to use almost any height for the vertical, I suggest you start with $H = \lambda_0/4$ and trim the radials for resonance. This makes H a little tall, but it shortens your radials (especially if you're using 10 to 12) and raises the feed point impedance a bit.
- 5) Use a balun or common mode choke on the feed line at the base of the vertical. To be effective, the balun should have a shunt impedance of >2 k Ω .
- 6) If you have a special problem situation by all means model some trial solutions first. That will save you a lot of time over cut-and-try in the field. If you can't afford NEC4 software, the free NEC2 software will still be very helpful. (See www.4nec2.com.)

This article has covered a lot of ground looking in detail at the behavior of verticals with elevated ground systems. Despite the length of this article, it really just scratches the surface of the subject. There are many other topics that deserve attention. For example: a more detailed look at counterpoises, or, in an array, the interaction between the radial systems associated with the individual verticals, the effect of non-level terrain, and so on. I particularly recommend the articles by Al Christman, K3LC, that address many of these issues. (See Notes 18 through 33 in Part 1.) While I hope the work reported here

is helpful, there's still lots more to be done before we can claim to really understand this class of antennas.

Acknowledgement

Much of the modeling data for the graphs was derived using *MultiNEC*, an *Excel* program developed by Dan Maguire, AC6LA, that interfaces with NEC modeling programs allowing multiple runs for parameter studies. This is truly a wonderful program. Unfortunately it is currently being revised and not available as of this writing. I also want to thank my reviewers Al Christman, K3LC, George Cutsogeorge, W2VJN, Mark Perrin, N7MQ, Ward Silver, NØAX, Dean Straw, N6BV, and Dick Weber, K5IU. They gave freely of their time going through my drafts, making many important suggestions and corrections.

Rudy Severns, N6LF, is a retired electrical engineer (UCLA '66). He holds an Amateur Extra class license and was first licensed in 1954 as WN7WAG. He is a life fellow of the IEEE and a life member of the ARRL. His current Amateur Radio interests are antennas, particularly HF vertical arrays and interactions between towers and arrays. He also enjoys 600 m operation as part of the group under the WD2XSH experimental license. Some of his publications about antennas are posted on his website at www.antennasbyn6lf.com.

IMD in FET and Diode Mixers at 70 cm

The author describes the construction and test results of some UHF mixers that he built.

In order to test wideband Orthogonal frequency-division multiplexing (OFDM) communication on the 70 cm Amateur band, I had to construct at least two field programmable gate array (FPGA) based transceivers.^{1,2} FET resistive mixers work well at HF and seemed attractive at UHF. Some types should also be less sensitive to mixer terminations and this is important at UHF, because it's harder to provide a purely resistive termination at all ports. Since I had 7 helical filters left over from an AMSAT project, and it's inexpensive to add more area to a circuit board, I decided to build transceivers with two different FET mixers. After initial testing, I made a circuit board with a diode mixer for comparison. IMD was measured for transmit and receive paths and the results are summarized here.

The first mixer is a single-balanced design using two FETs used as resistive switches to ground. The second mixer uses four FETs in series with the signal. The third design is a high-level diode-ring mixer. All were tested with a +16 dBm LO input at 406 MHz.³

The mixer inputs and outputs were at 435 MHz and 29 MHz. The 29 MHz port uses a diplexer to provide a wideband 50 Ω termination. The 435 MHz port feeds a 3-pole helical filter with a 3 dB 20 MHz bandwidth. Two 3-pole filters are used in order to provide sufficient attenuation of the image frequency when a 21.4 MHz IF is used with narrow-band crystal filters.

¹Notes appear on page 39.

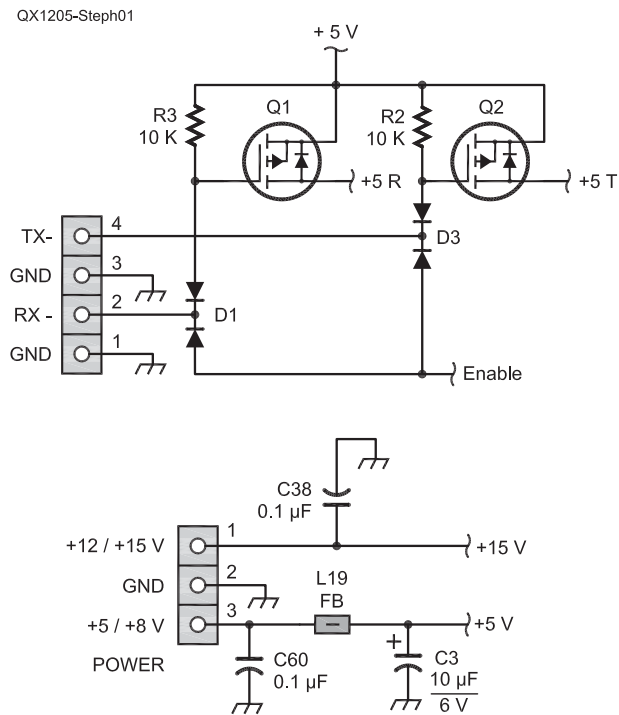


Figure 1 — This schematic shows the power switching scheme used for the mixer boards.

There are also two MMIC amplifiers with an SOT-89 footprint on each board — one for transmit and one for receive. One RFMD (RF Microdevices — formerly from Sirenza Microdevices) SGC-6389 (receive) and one SGC-6489 (transmit) silicon-germanium amplifier are used on each board. Two PE4259 CMOS silicon on sapphire SPDT

switches from Peregrine Semiconductor control the RF signal path. The MMIC power is switched by standard P-channel FETs, as shown in Figure 1. Grounding the TX or RX inputs controls T/R switching. Figure 2 shows the schematic diagram of the test circuit boards, with the MMIC amplifiers and RF switching. The individual test

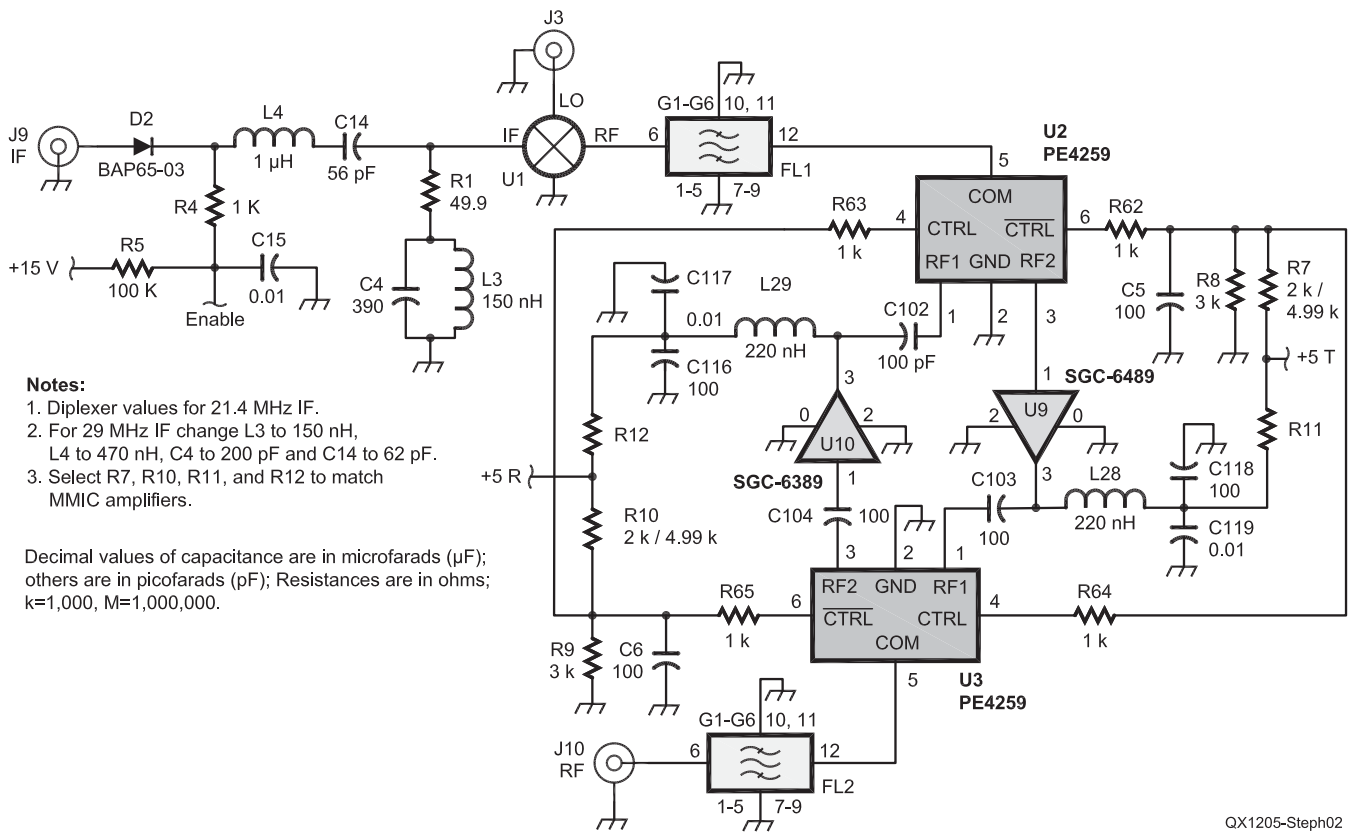
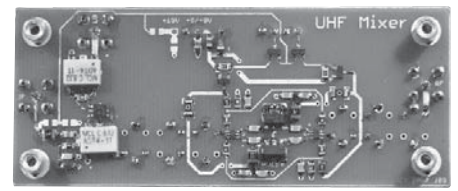
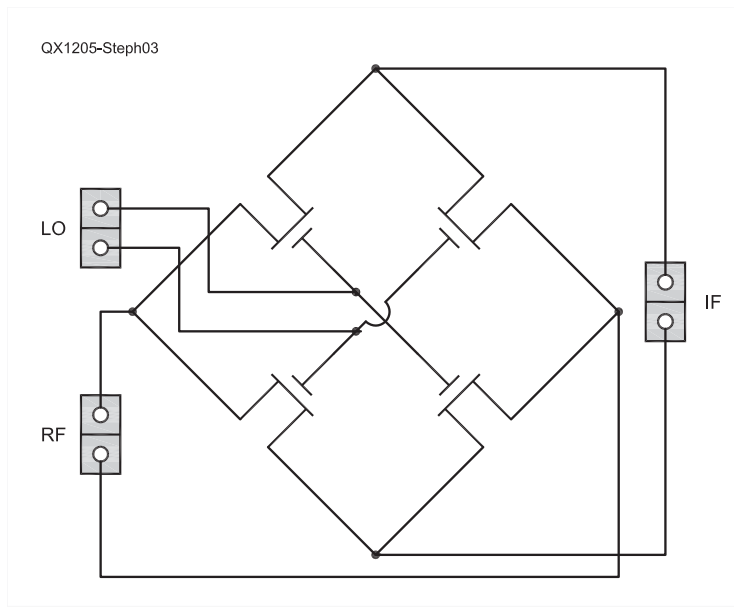
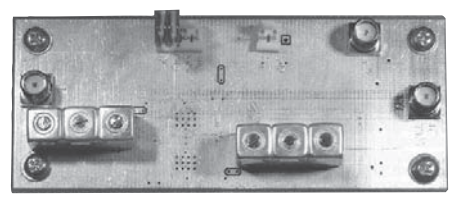


Figure 2 — Here is the mixer board schematic diagram, with RF switching. The various individual test mixers are connected where the mixer symbol is shown.



(A)



(B)

Figure 3 — The FET mixers use a Peregrine Semiconductor PE4140 CMOS silicon on sapphire IC. This schematic is a diagram of that IC.

Figure 4 — Here is the dual FET mixer circuit board.

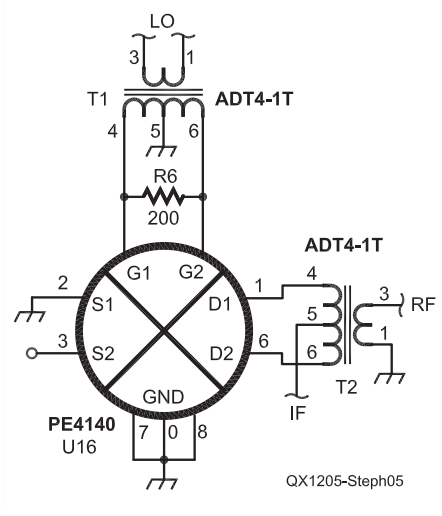


Figure 5 — This schematic diagram shows the dual FET Mixer circuit.

mixers are inserted where mixer U1 is shown on the schematic of Figure 2.

In these tests, the PIN diode switch was not needed so D2 was bypassed and R4, R5, C15 and C38 were not installed. Therefore, the +15 volt supply was not used. The FETs used in the first two mixers are contained in a CMOS silicon on sapphire integrated circuit from Peregrine Semiconductor, as shown in Figure 3. The sources are connected to the RF port and the drains to the IF port.

Hewlett-Packard 8640B and Rhode and Schwarz SM300 signals generators were used to generate test signals that were combined in a Mini-Circuits ZFSC-2-1. IMD was measured on an Rhode and Schwarz FS300 spectrum analyzer. Transmit IMD_3 is measured at the PCB RF output with two -3 dB signals at 28.5 MHz and 29.5 MHz on the mixer IF port. Receive IMD_3 is measured at the PCB IF output with two -22 dBm signals at 434.5 MHz and 435.5 MHz on the RF input to the PCB.

Dual FET Mixer

The dual FET mixer, shown in Figures 4 and 5, contains two wideband transformers. T1 drives the gate-to-source junctions of the two FETs and T2 is in the drain circuit. The RF port is the primary winding of T2. The FETs are connected to either side of the secondary winding and the IF port is connected to the center tap of the secondary. The two FETs with their sources connected to ground are used as switches and the other two are unused. Switching on one FET or the other reverses the phase of the signal passing through the mixer. The impedance of the signal path is 50Ω and the resistance of the

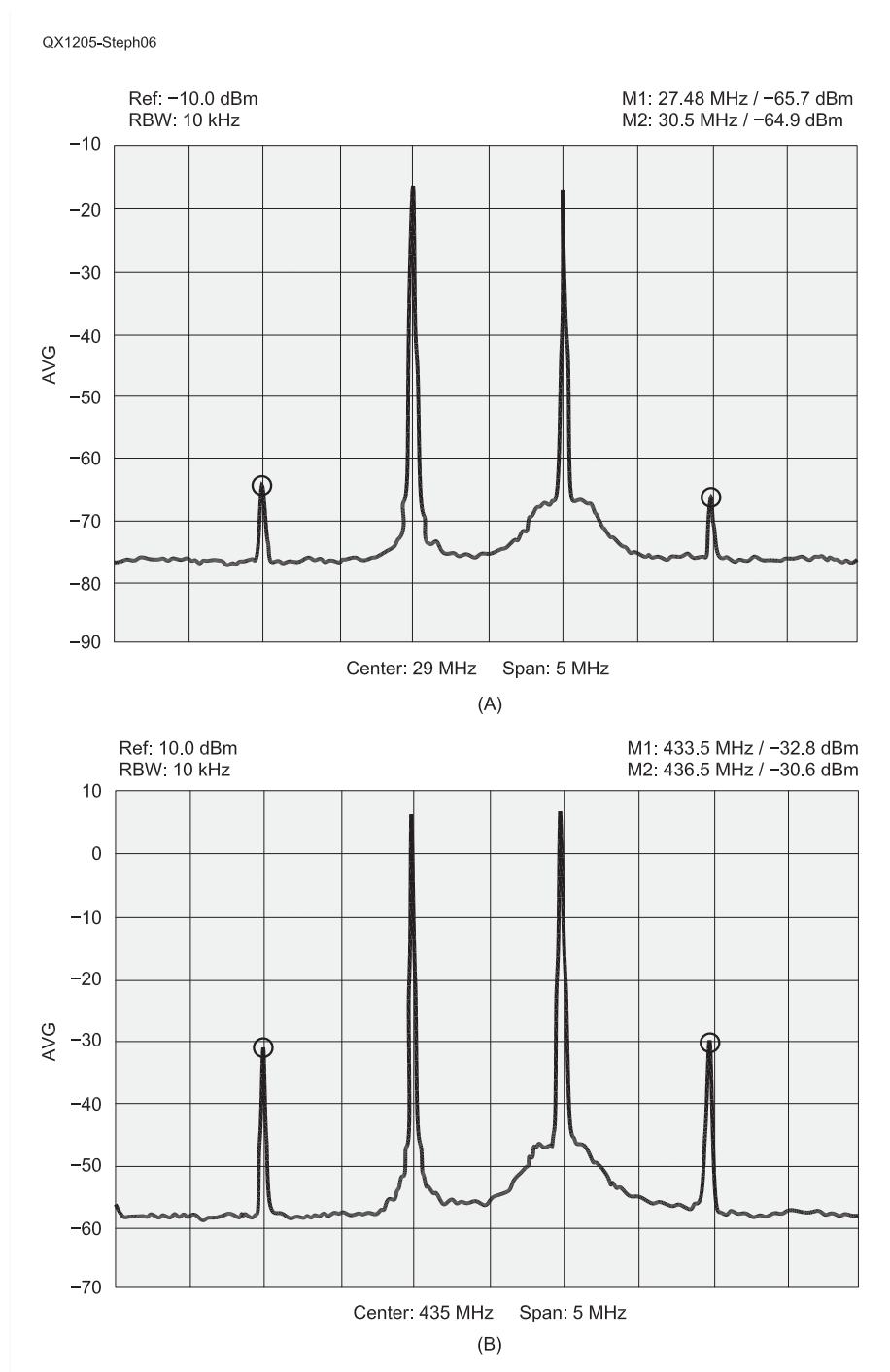


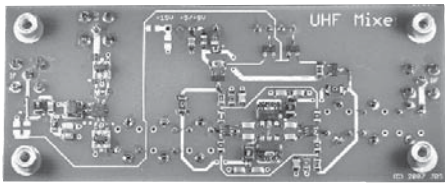
Figure 6 — The dual FET receive mixer IMD_3 is shown on the top and the transmit mixer IMD_3 is on the bottom.

conducting FET is about 8Ω . Grounding the FET sources should minimize modulation of the conductance of the FETs by the IF or RF signals and minimize IMD. Figure 6 shows the results of the measurements made on this mixer.

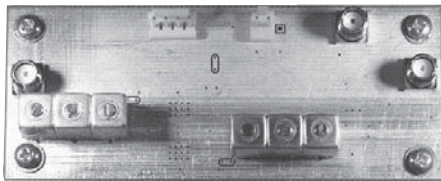
Quad FET Mixer

The quadruple FET mixer, shown in

Figures 7 and 8, contains two transmission line transformers for the LO and RF ports and one traditional transformer for the IF port. Depending on LO polarity, the upper left and lower right or the upper right and lower left FETs in U16 conduct. Half of the time, D1 is connected to S1 and D2 is connected to S2 and the other half of the time D1 is connected to S2 and D2 is connected to S1. This reverses the phase of the signal



(A)



(B)

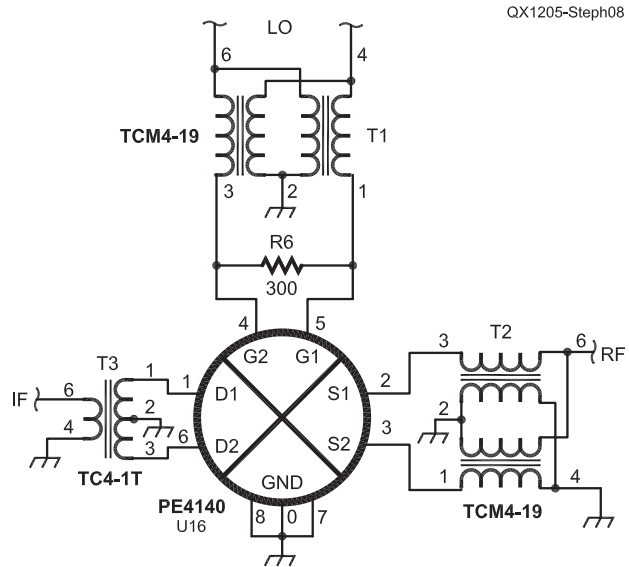
Figure 7 — This photo shows the quad FET mixer circuit board.

passing through the mixer as the dual FET mixer does. The impedance of the signal path is $200\ \Omega$ and the resistance of the two FETs is $16\ \Omega$ so the ratio is halved and IMD should decrease. The sources are not grounded, however, so the LO voltage between the gate and source could be reduced. Figure 9 shows the results of the measurements on this mixer.

Diode Mixer

The diode mixer, shown in Figures 10 and 11, is a package device from Mini-Circuits. The data sheet specifies a typical input intercept of $+29\ \text{dBm}$ for the 100 to 1500 MHz frequency range with resistive loads. The LO

current passes through half of the diodes on positive peaks causing them to conduct and the other half of the diodes during negative peaks causing them to conduct. This reverses the phase of the RF to IF path. The LO voltage is present on the diodes, however, so it must be balanced out in the architecture of the mixer. Thus, diode mixers must be double-balanced. Figure 12 shows the results of the measurements for transmitting and receiving.



QX1205-Steph08

Figure 8 — Here is the quad FET mixer schematic diagram.

Conclusion

Table 1 shows the gain and input intercepts for transmitting and receiving, and the estimated mixer input intercept while receiving. We want low receive gain because there will be an LNA near the antenna. Typically, the helical filters each contribute about 2.5 dB of loss and the RF switches each contribute about 0.4 dB of loss. The transmit and receive amplifiers contribute about 22.7 and

QX1205-Steph09

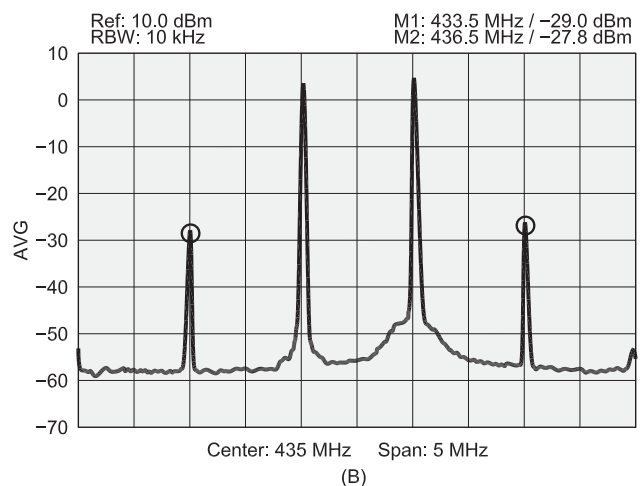
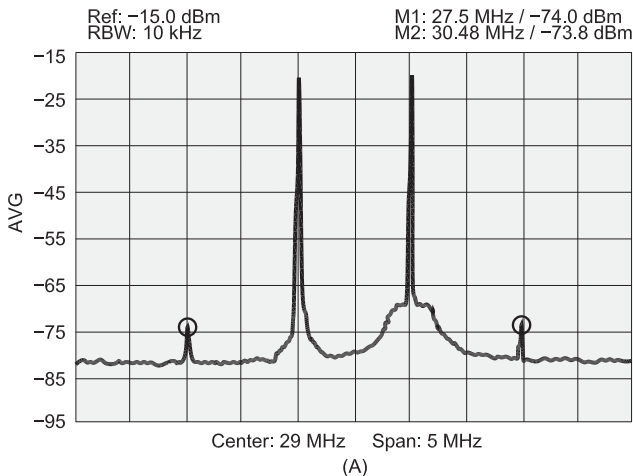
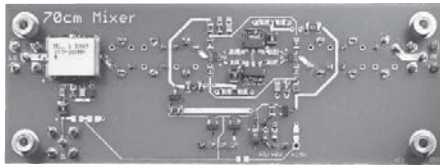
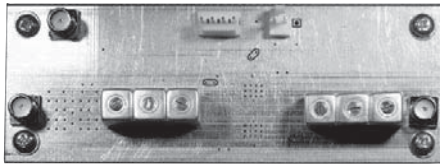


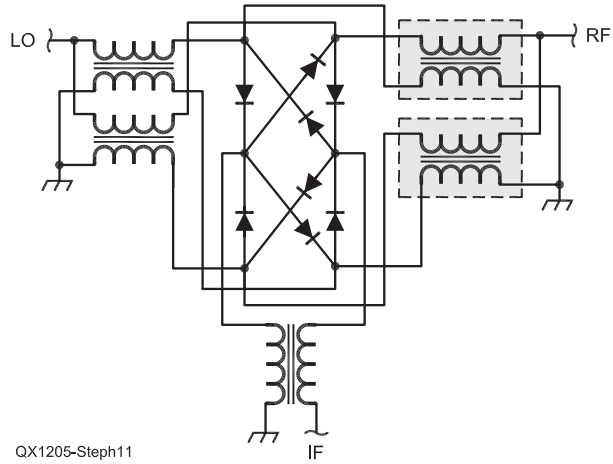
Figure 9 — The quad FET mixer receive IMD3 is shown on the left and the transmit mixer IMD3 is shown on the right.



(A)



(B)



QX1205-Steph11

Figure 10 — Here is a photo of the diode mixer circuit board.

Figure 11 — This is the SYM-30DHW diode mixer schematic diagram.

QX1205-Steph12

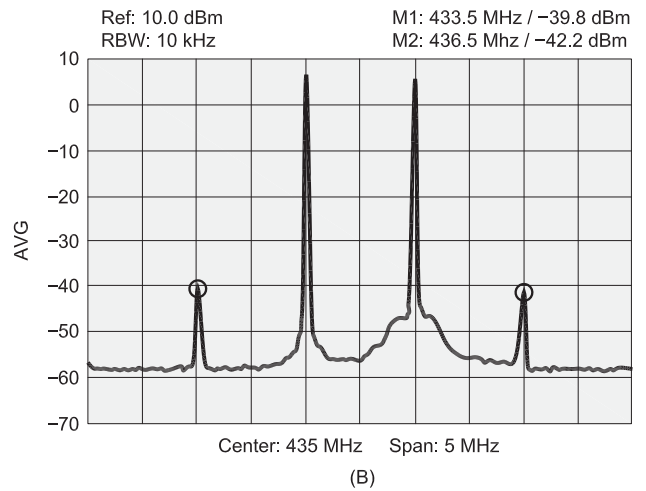
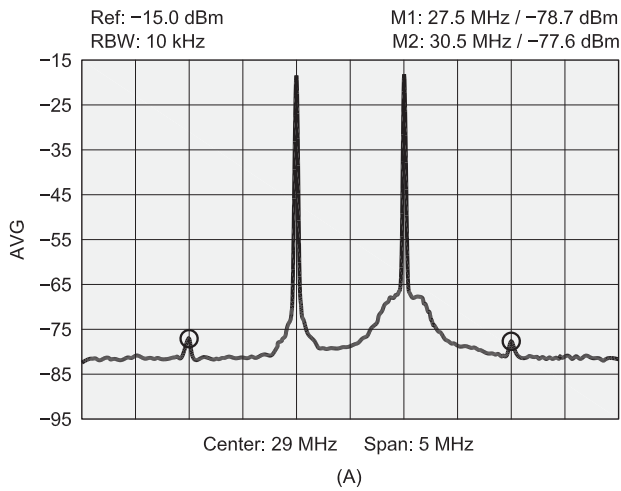


Figure 12 — The diode mixer receive IMD3 is on the left and on the right is the transmit mixer IMD3.

Table 1
Mixer Third-Order Intercept Points

Mixer Type	Transmit Gain (dB)	Receive Gain (dB)	Transmit IIP ₃ (dBm)	Receive IIP ₃ (dBm)	Mixer IIP ₃ (dBm)
Dual FET	8.60	4.95	+15.65	+2.12	+13.92
Quad FET	7.50	2.90	+13.45	+5.40	+17.25
Diode	8.95	4.80	+20.50	+8.50	+20.30

17.6 dB of gain. Thus, we can estimate the input intercept of the mixers when receiving.

The IMD measurements for the FET mixers were surprising, because they were not equal for transmit and receive, and the diode mixer provided the highest third-order intercept point in both cases. There are two possible reasons that the diode mixer outperforms the FET mixers. The on-resistance of the diodes could be lower and/or the switching time of the diodes could be faster. FET mixers at HF have been shown to degrade significantly as the frequency is increased from 3.5 MHz to 30 MHz, so the process would continue through the VHF and UHF ranges. This is consistent with slow switching times. There are broadband FET resistive mixers with higher intercepts at 435 MHz but these use 8 FETs and a +23 dBm LO, which would make for faster switching and lower

on-resistance.

It may be possible to improve FET mixer performance at UHF with narrow-band designs. The LO and IF transformers could be tuned in a way to minimize coupling through the drain-to-gate capacitance of the FETs. Diode mixers, however, seem to work better in simple broadband designs at high frequencies.

John Stephensen, KD6OZH, became interested in radio at age 11, when his grandfather bought him a crystal radio kit. During the 1960s, he built several HF receivers using vacuum tubes and other parts procured from discarded black-and-white TV sets. After attending the University of California, he and two friends founded PolyMorphic Systems — a supplier of personal computer kits, and later manufactured computers — in 1975. In 1985, he was cofounder of Retix, a networking hard-

ware supplier. John earned his Amateur Radio license in 1991, and has been active on bands from 7 MHz to 24 GHz, with interests including HF and microwave DXing and contesting. He has also been active on packet, satellites and on the HF bands using several digital modes. John has always designed and built his own Amateur Radio gear, some of which has been described in QEX. John is an ARRL Member.

Notes

¹John B. Stephensen, KD6OZH, "A Soft Processor for Digital Signal Processing," Winter 2009 TAPR Packet Status Register.

²John B. Stephensen, KD6OZH, "An FPGA-Based Transceiver Module," 2010 TAPR/ARRL Digital Communications Conference Proceedings.

³John B. Stephensen, KD6OZH, "A stable Low-Noise VFO for VHF-UHF Transceivers and Transverters," as yet unpublished.

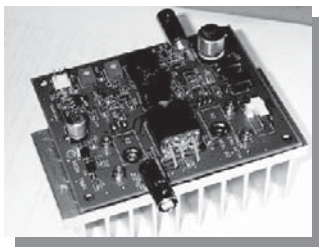
QEX



HPSDR is an open source hardware and software project intended to be a "next generation" Software Defined Radio (SDR). It is being designed and developed by a group of enthusiasts with representation from interested experimenters worldwide. The group hosts a web page, e-mail reflector, and a comprehensive Wiki. Visit www.openhpsdr.org for more information.

TAPR is a non-profit amateur radio organization that develops new communications technology, provides useful/affordable hardware, and promotes the advancement of the amateur art through publications, meetings, and standards. Membership includes an e-subscription to the *TAPR Packet Status Register* quarterly newsletter, which provides up-to-date news and user/technical information. Annual membership costs \$25 worldwide. Visit www.tapr.org for more information.

NEW!



PENNYWHISTLE
20W HF/6M POWER AMPLIFIER KIT

TAPR is proud to support the HPSDR project. TAPR offers five HPSDR kits and three fully assembled HPSDR boards. The assembled boards use SMT and are manufactured in quantity by machine. They are individually tested by TAPR volunteers to keep costs as low as possible. A completely assembled and tested board from TAPR costs about the same as what a kit of parts and a bare board would cost in single unit quantities.

HPSDR Kits and Boards

- **ATLAS** Backplane kit
- **LPU** Power supply kit
- **MAGISTER** USB 2.0 interface
- **JANUS** A/D - D/A converter
- **MERCURY** Direct sampling receiver
- **PENNYWHISTLE** 20W HF/6M PA kit
- **EXCALIBUR** Frequency reference kit
- **PANDORA** HPSDR enclosure



TAPR

PO BOX 852754 • Richardson, Texas • 75085-2754
Office: (972) 671-8277 • e-mail: taproffice@tapr.org
Internet: www.tapr.org • Non-Profit Research and Development Corporation

SDR: Simplified

Filter Design Program

Wes Hayward, W7ZOI, Rick Campbell, KK7B, and Bob Larkin, W7PUA, present a short description of DSP techniques and filtering in *Experimental Methods in RF Design*.¹ One of the best items included with the book is a BASIC program (written by Bob Larkin, W7PUA) on the CD, that will calculate the coefficients for a finite impulse response (FIR) filter. It is a very well written program, but not terribly useful in a modern world without *QBasic* or *GWBasic* programs on our computers. Luckily, I still have a version of BASIC that came with *MS-DOS 3.0* for the original IBM PC back in the 80s that I used to verify my port of the program to C.

One of the programs in the `5x12_Mack_SDR.zip` file for this installment is the program that I have written that implements the BASIC code in C.² The present incarnation is designed to create a C source file with the FIR filter coefficients and related information. The logic of the program is entirely Bob's, but even Bob used code from another source. In making sure I had the new program correct, I verified the Bessel calculation with the source Bob used from the second edition of *Numerical Recipes in C*.³ This is a fantastic book that you can read in its entirety on the web. To paraphrase Newton, "we see farther because we stand on the shoulders of giants."

The Gibbs Phenomenon

The program starts with a rectangular shaped ideal filter. Figure 1 shows such a low pass filter with a 1000 Hz cutoff and a 8000 Hz sample rate. The coefficients of an FIR filter are generated by calculating the Fourier transform of the filter frequency response to determine the impulse response in the time domain. For all but the simplest filter shapes, the Fourier transform can get pretty messy. It turns out that the Fourier transform and impulse response for the low pass, high pass, and band pass response is the same rather simple equation with different parameters based on the cutoff frequencies. In essence, all three filter types are variations of a rectangular pulse shape.

Let's choose to create a filter with

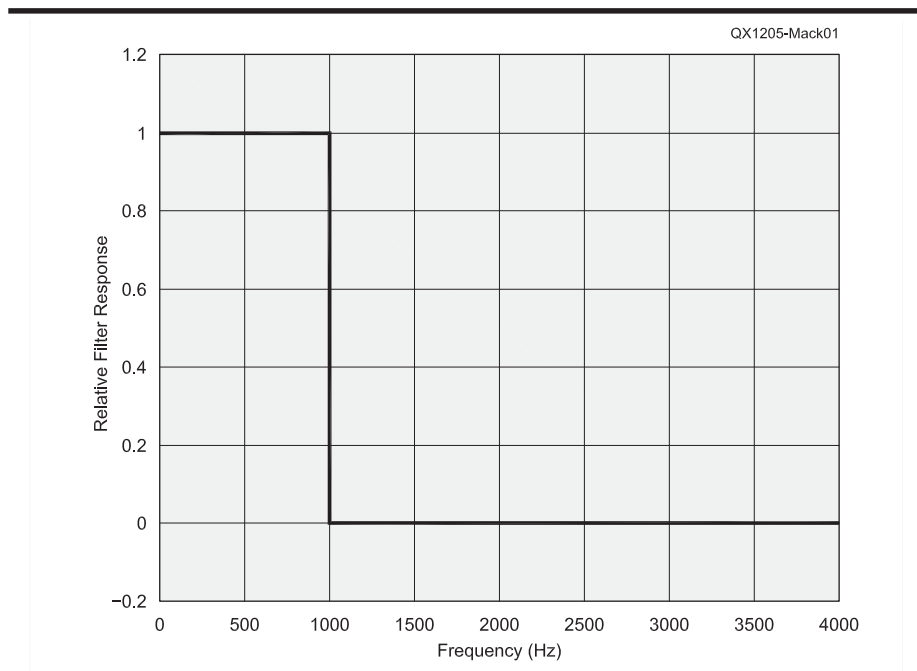


Figure 1 — This graph shows the ideal filter response of a 1000 Hz low pass filter with 8000 Hz sample rate.

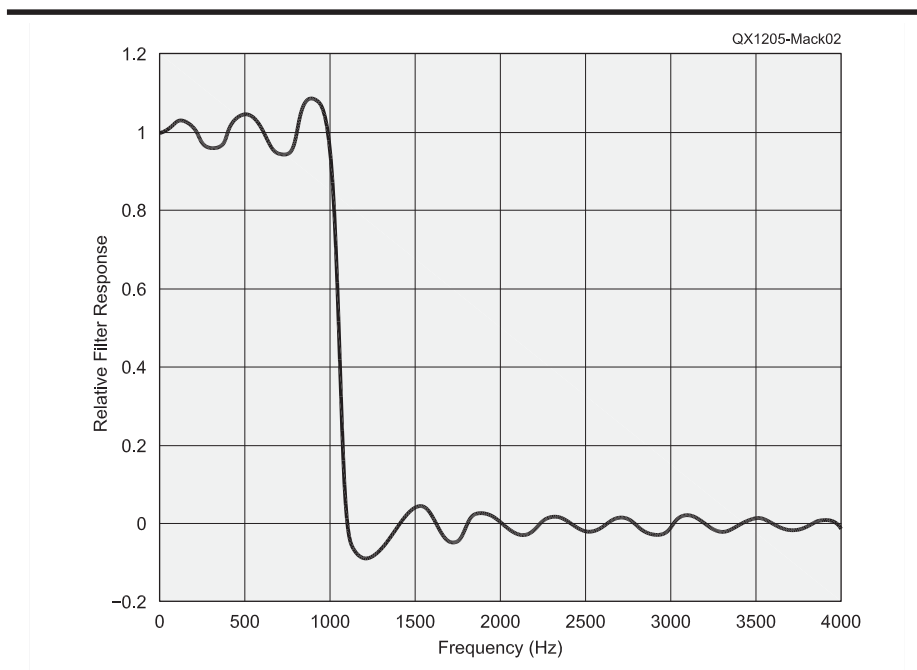
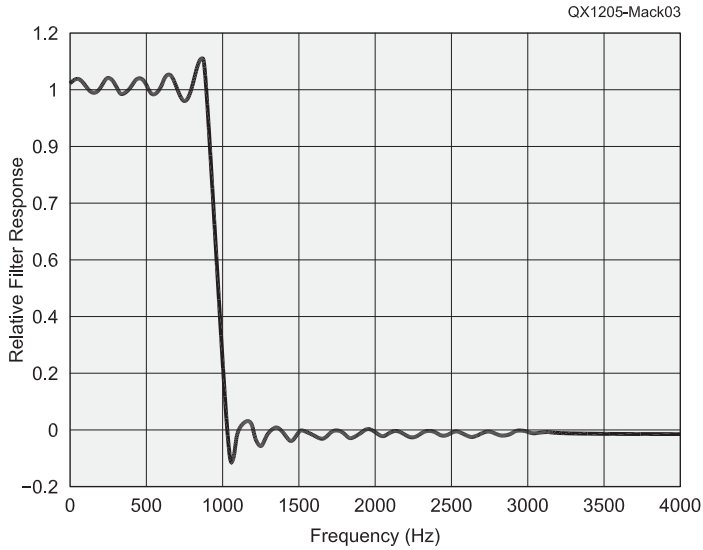
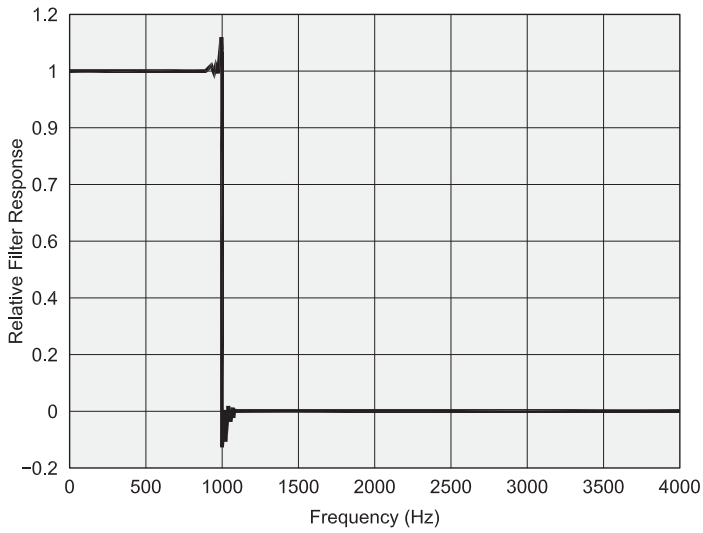


Figure 2 — Here is the actual frequency response of an "ideal" FIR filter with 1000 Hz cutoff, 8000 Hz sample rate and 20 coefficients. The filter response is shown with linear scaling rather than the magnitude in dB.

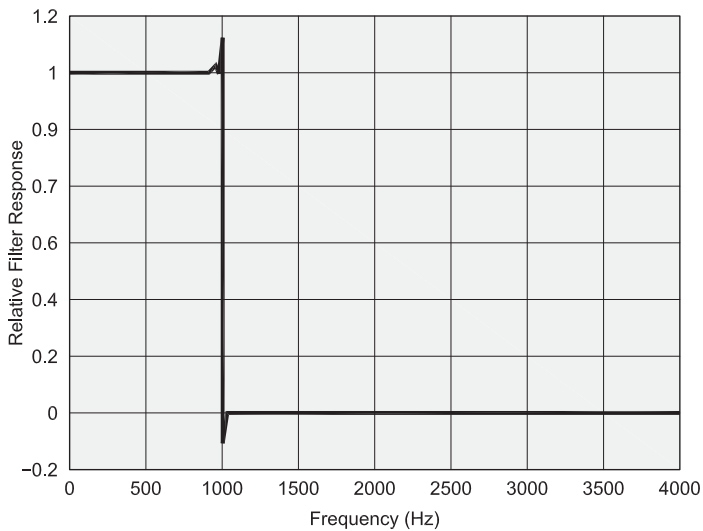
¹Notes appear on page 44.



(A)



(B)



(C)

Figure 3 — Part A shows an “ideal” low pass filter with 40 coefficients. Part B shows the same filter, but with 200 coefficients. Part C shows the same filter, but with 1000 coefficients. You can see that each filter has the characteristic 8.9% overshoot and undershoot.

from
MILLIWATTS to KILOWATTSSM
More Watts per DollarSM



Taylor
TUBES

**Quality
Transmitting
& Audio Tubes**

- COMMUNICATIONS
- BROADCAST
- INDUSTRY
- AMATEUR



Immediate Shipment from Stock

3CPX800A7	3CX15000A7	4CX5000A	813
3CPX5000A7	3CX20000A7	4CX7500A	833A
3CW20000A7	4CX250B	4CX10000A	833C
3CX100A5	4CX250BC	4CX10000D	845
3CX400A7	4CX250BT	4CX15000A	866-SS
3CX400U7	4CX250FG	4X150A	872A-SS
3CX800A7	4CX250R	YC-130	5867A
3CX1200A7	4CX350A	YU-106	5868
3CX1200D7	4CX350F	YU-108	6146B
3CX1200Z7	4CX400A	YU-148	7092
3CX1500A7	4CX800A	YU-157	3-500ZG
3CX2500A3	4CX1000A	572B	4-400A
3CX2500F3	4CX1500A	807	M328/TH328
3CX3000A7	4CX1500B	810	M338/TH338
3CX6000A7	4CX3000A	811A	M347/TH347
3CX10000A7	4CX3500A	812A	M382

— TOO MANY TO LIST ALL —



ORDERS ONLY:

800-RF-PARTS • 800-737-2787

Se Habla Español • We Export

TECH HELP / ORDER / INFO: 760-744-0700

FAX: 760-744-1943 or 888-744-1943



An Address to Remember:

www.rfparts.com

E-mail:

rfp@rfparts.com



RF PARTS
COMPANY

20 coefficients. The resulting filter response looks something like Figure 2. You see that the pass band has ripples every 200 Hz and the stop band has ripples also spaced every 200 Hz. The ripples don't look very big when plotted on a linear scale. They are pretty serious when you plot them as dB, however. These ripples are called the Gibbs Phenomenon (first discovered in 1848 and named for J. Willard Gibbs who described the phenomenon in detail in 1899). The short description of the phenomenon is that any discontinuity in one domain causes an infinite series in the other domain. In the case of our filter, the sharp discontinuity at 1000 Hz in the frequency domain requires an infinite number of coefficients in the time domain to implement that frequency spectrum. Since we cannot implement our filter in the time domain with an infinite number of coefficients, the 20 coefficients create 20 discrete bins each 200 Hz wide (4000 Hz / 20). If we had chosen a 40 coefficient filter, the size of the ripples in the pass band and stop band would be smaller in both width (now only 100 Hz wide) and height because the sum of the series is closer to convergence. The longer filter is a closer approximation to the original function. Figure 3 shows how increasing numbers of coefficients increase the slope of the transition but that even very large numbers of coefficients will not eliminate the issues right at the edge of the transition region. Gibbs found that an FIR filter will have 8.9 % maximum ripple for the first ripple on either side of the transition, regardless of the number of filter coefficients.

The Kaiser Window

Gibbs observed that as a function becomes smoother, the coefficients of the transform near the center become much larger and coefficients further away quickly tend toward zero. There are two ways to force the frequency response to have fewer ripples and approach a smooth shape. The first is to design a filter that is not ideal, has sloped shoulders, and a gradual transition from pass band to stop band. The problem with this approach is that it requires using the Fourier Transform to calculate the coefficients and the results are unique for each filter. The second way is to start with an ideal response, with its simple calculations, and then force the coefficients to have a shape that has significant central coefficients but with the coefficients near the edges rapidly approaching zero. This process is called windowing. There are many functions that can be multiplied against the ideal filter coefficients to achieve varying amounts of pass band or stop band ripple reduction or both. The transition rate from pass band to stop band is also affected. Each window method has its own set of advantages and disadvantages. As with most other situations in engineering, you can affect stop band or pass band or transition rate: pick two!

The C program uses a Kaiser window that

Table 1 — Frequency Register Values for the Allowed Sample Rates

Rate	R	J	D	P	MADC & NDAC	DOSR & AOSR	PLL Frequency
8000	1	1	792	2	2	128	10.752
16000	1	1	792	1	2	128	21.504
24000	1	3	584	1	2	128	43.008
48000	1	7	1680	1	2	128	86.016
96000	1	7	1680	1	1	128	86.016
192000	1	7	1680	1	1	64	86.016

Listing 1 — The code for the main signal processing loop.

```

while (1)
{
    /* Read 16-bit left channel Data */
    EZDSP5535_I2S_readLeft(&data1);
    /* Read 16-bit right channel Data */
    EZDSP5535_I2S_readRight(&data2);
    // perform the IF filtering
    error = fir(&data1, coefficients, &data1,
               delay_buffer, 1,
               number_of_coefficients);
    //Do the demodulation
    switch (modulation_type)
    {
        case AM: // square law detector
            demod_sample *= demod_sample;
            break;
        case FM:
            demod_sample = demod_FM(data1);
            break;
        case CW:
            demod_sample = demod_CW(data1);
            break;
        case LSB:
            demod_sample = demod_LSB(data1);
            break;
        case USB:
            demod_sample = demod_USB(data1);
            break;
    }
    // perform the baseband filtering
    error = fir(&demod_sample, baseband_coefficients,
               &demod_sample, demod_delay_buffer,
               1, number_of_baseband_coefficients);
    /* Write 16-bit left channel Data */
    EZDSP5535_I2S_writeLeft(data1);
    /* Write 16-bit right channel Data */
    EZDSP5535_I2S_writeRight(data2);
    // If any key has been hit in the debugger, we exit
    if (_kbhit())
    {
        break;
    }
}

```

applies a Bessel function to the coefficients to set a desired amount of stop band attenuation close to the pass band in exchange for a more gradual transition band and a flat pass band. The Kaiser window is named after J. F. Kaiser, who decided to use some very obscure (even for mathematicians) and dif-

ficult to calculate functions called prolate spheroidal functions. Kaiser windows are probably some of the best for controlling the depth of the first side lobe while still giving a rapid transition. Fortunately, Bob Larkin handled the nasty math in his original program.

More TI Software Resources

TI gives away a package called DSPLIB that can be used for any of their DSP families. Go to www.ti.com/lit/ug/spru422j/spru422j.pdf to download the Programmer's Reference. Then go to www.ti.com/tool/sprc100 to download the zip file containing the library and its source code. You need to place the header file dsplib.h in the `ccsv4\tools\compiler\include` directory. Place all of the library files in the `ccsv4\tools\compiler\lib` directory. You will need the source files because the library is compiled in the small memory model and the other libraries are in large memory model. For this program, you need `fir.asm` in your project directory.

We are interested in the function "fir." You will find the reference information on page 4-46 of the reference manual. The function takes six arguments. The first argument is the address of the array of input samples. The second is the address of the array of filter coefficients. The next one is the address of the output buffer, which can also be the address of the input buffer for computation in-place. The fourth argument is the address of the delay buffer, which holds all of the history of the filter. This buffer is equal in size to the number of coefficients plus one more that holds the array index of the oldest entry. The C language does not include the size of an array as part of the array storage. That means we have to keep track of the size as another piece of data. The "fir" function uses the fifth argument to hold the size of the input array and the sixth is the size of the filter coefficient array. All of the arguments are 16 bit signed or unsigned numbers.

Figure 4 shows the concept of an FIR filter. In fact, this structure applies to any FIR operation where "filter" can encompass any manipulation such as a Hilbert transform (90° phase shift with no amplitude change). The figure shows a trivial example where the delay line (a shift register when implemented in hardware) starts with all registers holding zero. It goes through the first six sample periods showing the data in the delay line and the calculations that occur. The data samples are (-1, -2, -1, 2, 5, 10) and the six coefficients are (-1, 2, 6, 6, 2, -1).

The code for this experiment uses the `fir()` function in its single element mode. The data word is applied to all of the delay elements and the total is added together to produce a single output word. The intermediate history is held in the `delay_buffer` array that is declared inside our automatically created data file. The documentation calls for the array to be initialized to all zeros, but that occurs automatically as part of the C startup when `delay_buffer` is copied into memory.

The Bare Metal Filter and Receiver Program

The last step in making a radio with a band pass filter is to port the filter coefficient

calculation into our receiver so that we can tune the filter to any signal within the pass band. The biggest risk in moving the FIR filter coefficient task into our DSP is running out of program memory. The FIR coefficient calculation uses floating point and numerous math library functions that consume quite a lot of program memory.

In addition to calculating the coefficients, we need to set the PLL to achieve the design sample rate. We saw in the Mar/Apr issue that we need to calculate both an integer and fractional value to set the sample rate. Here is the equation:

$$PLL_FREQ = \frac{PLLCLK \times (R \times J.D)}{P}$$

The PLLCLK value is 12 MHz [Remember from the last issue that the dot between the J and the D is the notation for the multiplication factor. If R = 1, P = 1, J = 7 and D = 1680, then the expression (R × J.D) = (1 × 7.1680). — Ed.] Fortunately, the data sheet gives the values for 12 MHz MCLK to generate 48 kHz and 44.1 kHz so we only have to do the calculations for the other allowed sample rates. Table 1 captures the register values for the sample rates.

The result at this point is the output of our tunable IF filter. The next step is to convert the IF signal to a baseband signal. The output of the conversion to baseband always contains extra signals that we do not want in our output. The last DSP step is to filter out those signals so we are left with our audio. The baseband filter is a short length (20 coefficients) low pass filter to eliminate frequencies that are far removed from audio. The last step is a call to read the console for input that will halt the signal processing and return to the tuning input dialog. Since the interface is a "teletype terminal," it is not what one would want in a real radio, but it works for our experiments. The console input must be a non-blocking call so that the program will continue DSP operations if there was no terminal activity.

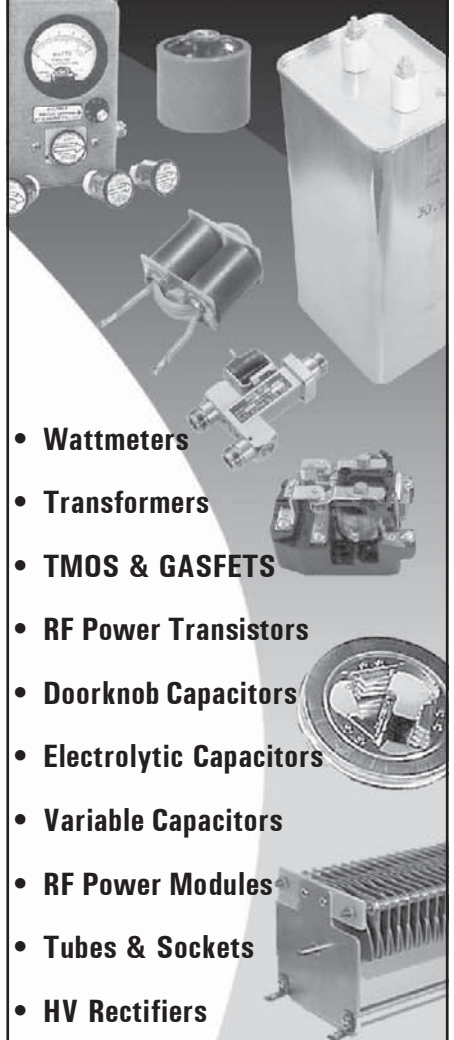
Listing 1 contains the main logic for the DSP loop. The switch statement selects the type of signal to be demodulated. At this point, I have only implemented the AM demodulator. The other modulation types require that a function is implemented, but they all return without performing any action.

Filter Response Program

Gnu Octave has a function (`freqz`) that is supposed to allow you to plot the frequency of either an Infinite Impulse Response (IIR) or FIR filter. The interface is not especially easy to use, however. The zip file for this installment also includes a frequency response calculator. The output of the program is a set of X-Y points in a text file that you can import into *Gnu Octave*, *Gnuplot*, or a spreadsheet such as *Excel*, so that you can see the plot. Plotting in *Gnuplot* is especially

From
MILLIWATTS
to **KILOWATTS**

More Watts per Dollar



- Wattmeters
- Transformers
- TMOS & GASFETS
- RF Power Transistors
- Doorknob Capacitors
- Electrolytic Capacitors
- Variable Capacitors
- RF Power Modules
- Tubes & Sockets
- HV Rectifiers



ORDERS ONLY:

800-RF-PARTS • 800-737-2787

Se Habla Español • We Export

TECH HELP / ORDER / INFO: 760-744-0700

FAX: 760-744-1943 or 888-744-1943

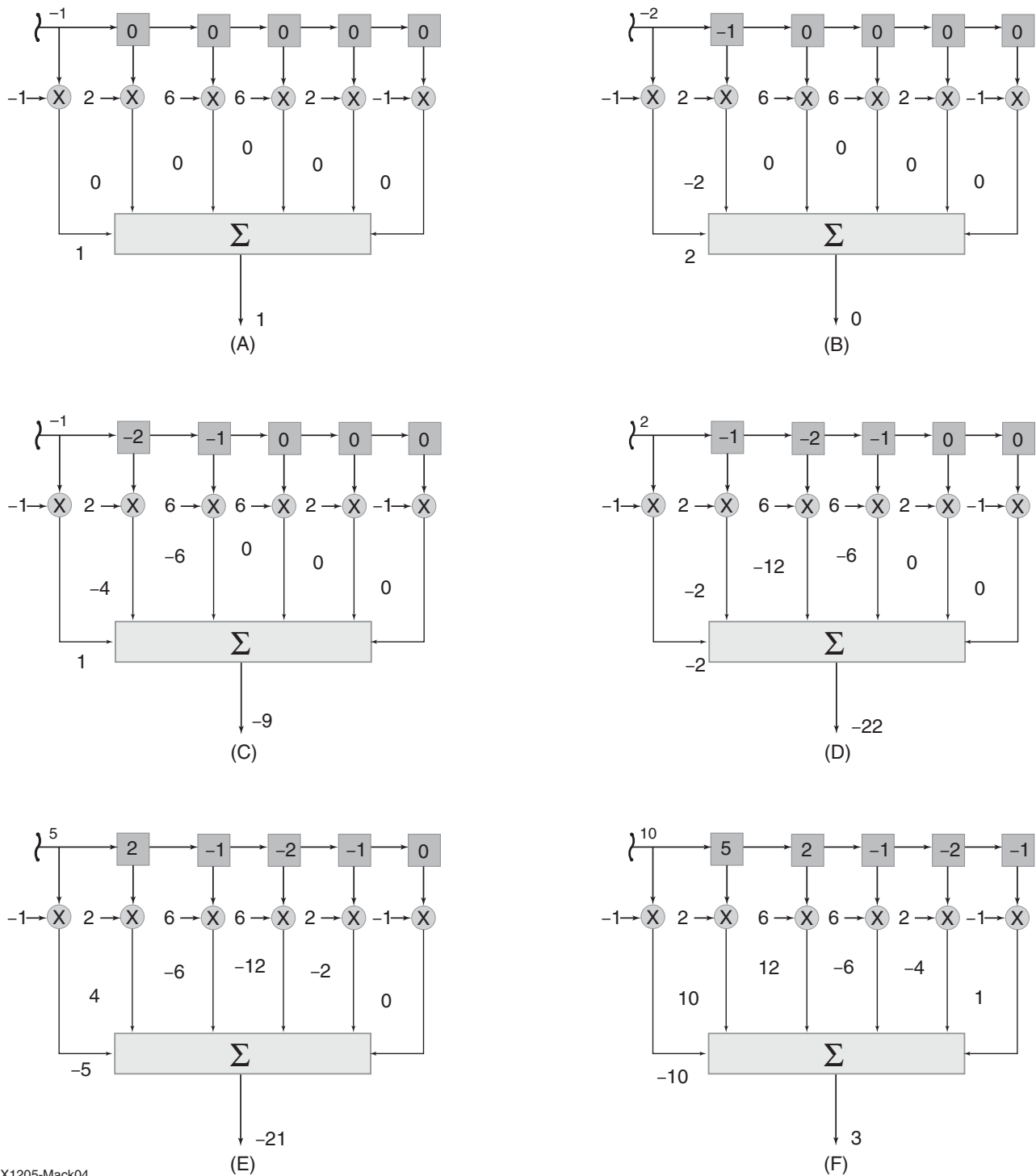


An Address to Remember:
www.rfparts.com

E-mail:

rfp@rfparts.com





QX1205-Mack04

Figure 4 — Here is a graphical description of an FIR filter implementation. The sequence shows how the first 6 samples enter the delay line, and gives the first 6 output samples.

easy, since you can run a script and simply repeat the last command to plot the new data. While we are experimenting with various types of filters and windows, the ability to see the response is very useful. It is especially useful to zoom the plot to just a portion of the total frequency range of the system.

Notes

¹Hayward, Campbell, Larkin, *Experimental Methods in RF Design*, The American Radio Relay League, 2003.

²The software files described in this Column are available for download from the ARRL

QEX files website. Go to www.arrl.org/qex-files and look for the file **5x10_Mack_SDR.zip**.

³Press, Teukolsky, Vetterling, Flannery, *Numerical Recipes in C*, Cambridge University Press, 1992.



Letters to the Editor

A New Horizontal Polarized High Gain Omni-Directional Antenna (Nov/Dec 2011)

Hi Larry,

I enjoyed the article "A New Horizontally Polarized High Gain Omni-Directional Antenna" by Tom Apel, K5TRA, in the Nov/Dec 2011, issue of QEX, on pages 3-9. The article jogged my obsession with three-phase power and reminded me of an antenna I saw in a text book decades ago.

That antenna was a microwave example of an omnidirectional tripole antenna built of three dipoles at 120° orientations around a circle, using three-phase feed points tapped off at 120° intervals around TM(1,1) circular waveguide. It appears in Electronic Designers' Handbook, by Landee, Davis, Albrecht, published by McGraw-Hill, 1957, page 21-37 and page 20-37.

This suggested to me a tripole antenna built of three quarter-wavelength whip antennas as follows. I haven't tried this yet, but I can't resist sharing the idea to find out who has already tried it.

The basic tripole comprises three quarter-wave whips pointing radially outward from a center point to form a planar Y. The inner ends of the whips form the feed point. Unlike most feed points, the tripole feed point has three terminals, and is fed with three-phase power through a three-phase transmission line. Three-phase open-wire transmission lines are common at 50 and 60 Hz, but are rare at radio frequencies.

Three coaxial lines can be used, with each center conductor driving one terminal of the feed point. The three shields are tied together at the feed point, and are not connected to anything else. From the point of view of each single coax, one whip is driven, and the other two are used as ground radials for that coax. The tripole forms a rotating dipole in the plane of the Y, so the axis of rotation is perpendicular to the plane of the Y.

Unbalance in the feed signals leads to simultaneous counter-rotating dipoles, called positive sequence and negative sequence in the three-phase literature.

In the horizontal plane, a single horizontal tripole is horizontally polarized and omnidirectional. Along the vertical axis, a single horizontal tripole emits circularly-polarized radiation.

Stacked tripoles can be used to increase horizontal omnidirectional gain similarly to the antennas discussed in Tom's article.

Tripole Yagi for Circular Polarization

Helices and crossed Yagis are well-known directional antennas for circular polarization. (See "Microwavelengths: Circular Polarization," by Paul Wade, W1GHZ, QST, Oct 2011, pp 98-99).

A crossed Yagi is two Yagis crossed on the same boom, driven 90° out of phase. At each element location on the boom, there are four half elements sticking out in four directions to make a cross.

A tripole Yagi replaces each cross of four half-elements with three half elements 120° apart. The driven element is a tripole as described above.

— 73, Peter Traneus Anderson, KC1HR, 42 River St, Andover, MA, 01810;
traneus@verizon.net

Hi Peter,

Thanks for letting us know that you enjoyed the article by Tom Apel, K5TRA. Your description of a tripole Yagi does sound interesting. I wonder if any readers have tried such an antenna, and what experiences they may have to share.

— 73, Larry Wolfgang, WR1B, QEX Editor;
lwolfgang@arrl.org

2012 Appalachian Trail Ham Radio Survey

The goal of this survey is to determine ham radio coverage all along the Appalachian Trail and develop a list of useable repeaters, VOIP links and APRS tracking/texting reliability for hikers with HT's along the trail. Ham hikers are asked to schedule a 1 or 2 day local hike while carrying an APRS HT and GPS, so that their track and coverage will be captured by the <http://aprs.fi> web page.

The survey hikes will begin in Georgia in mid March, Tennessee/North Carolina in early April, Virginia in April and early May, then Maryland, Pennsylvania and New York in late May. After a month break, the survey will resume in Connecticut in July, and on to Maine by the end of August. The timing is designed to coincide with the north-bound trek of the hundreds of thru-hikers that attempt the 2175 mile hike each year. In this way, ham radio can also serve in a support role for any emergency assistance for these hikers.

If you are interested in helping with the survey, see the plan on <http://aprs.org/at.html> and contact me.

— 73, Bob Bruninga, WB4APR, 115 Old Farm Ct, Glen Burnie, MD, 21060;
wb4apr@amsat.org.

Hi Bob,

I am sorry we weren't able to get this note into QEX in time for the southern part of the survey, but I hope some of our northeast readers will be able to hike sections of the AT and add their data to your results.

— 73, Larry Wolfgang, WR1B

NEW!
The ABCs of Software Defined Radio
Why Your Next Radio Will Be SDR
SDR Made Easy!
Martin Ewins, AAG

Amateur Radio operators are finding themselves incorporating Software Defined Radio—the latest big step in radio communications—into their operational activities. From low-end QRP rigs to the most powerful radios, they're all using SDR technology.

The ABC's of Software Defined Radio is an introductory guide to SDR and Digital Signal Processing (DSP) technologies. Written in a friendly style, it offers a straightforward look inside SDR and provides a foundation for those who want to understand the subject on a more fundamental level. As you read, you'll discover the basic principles of SDR, advantages to SDR technology, and ways to utilize it in Amateur Radio operations ...all with a minimum of mathematics!

Contents:

- It's a New World!
- The Meaning of "Digital"
- Real-World Software Defined Radio
- Computers and Software for SDR
- Using SDR
- Coming to a Shack Near You
- ...and more!

The ABCs of Software Defined Radio

ARRL Order No. 6320
Special ARRL Member Price!
Only \$19.95* (regular \$22.95)
*plus shipping and handling

ARRL The national association for **AMATEUR RADIO®**

SHOP DIRECT or call for a dealer near you.
ONLINE WWW.ARRL.ORG/SHOP
ORDER TOLL-FREE 888/277-5289 (US)

Upcoming Conferences

2012 Annual Conference, Society of Amateur Radio Astronomers

June 24 – 27, 2012
National Radio
Astronomy Observatory
Green Bank, WV

The Society of Amateur Radio Astronomers (SARA) will hold its 2012 Annual Meeting and Technical Conference June 24 through June 27, 2012, at the National Radio Astronomy Observatory (NRAO), Green Bank WV. Papers will be presented on radio astronomy hardware, software, education, research strategies, and philosophy.

Advance Registration Deadline:

Because SARA Conferences require quite a bit of advance planning, early registration is encouraged. To register for the 2012 SARA Conference, your remittance in full must be received by our Treasurer (not simply postmarked) not later than 31 May, 2012. All registrations received after that date, or walk-in registrations, will be assessed an additional 15% late registration fee. SARA Treasurer, Melinda Lord, 2189 Redwood Ave, Washington, IA 52353; treasurer@radio-astronomy.org. There is also a link for PayPal registration.

For more information go to www.radio-astronomy.org.

46th Annual Central States VHF Society Conference

July 26–28, 2012
Clarion Hotel and
Convention Center
525 33rd Avenue, SW
Cedar Rapids, IA, 52404

The Central States VHF Society, Inc (CSVHFS) invites you to attend the 46th annual conference in Cedar Rapids, IA, July 26–28, 2012. The Planning Committee has a fun-filled, educational event in store for you! The on-line registration form is now active.

Call for Papers

The Central States VHF Society is soliciting papers, presentations, and poster displays for the 46th annual conference. All aspects of weak-signal work on Amateur Radio bands of 50 MHz and above are sought.

The papers will be published in the *Conference Proceedings*, which will be available at the conference. You do not have to attend the conference nor present the paper to have it published in the *Proceedings*. Posters describing your project will be displayed during the 2-day conference.

Presentations and Posters at the conference may be technical or non-technical but will cover the full breadth of amateur weak signal VHF/UHF activities. The presentations generally vary from 15 to 45 minutes, covering the highlights with details in the *Proceedings* paper. Topics of Interest include:

- VHF/UHF Antennas
- Propagation Modes – such as Meteor Scatter, Sporadic E, Aurora, & Troposcatter
- Equipment Design & Construction – such as pre-amps, transverters, power amplifiers, and related accessories
- EME (Moon Bounce)
- Rover Stations — design, construction, and operation.
- Digital Modes
- Digital Signal Processing & Software Defined Radios
- Operating — including Contesting, DXpeditions, and Awards

If you would like to contribute a paper, presentation, or poster, please contact Rod Blocksome, K0DAS, CSVHF Conference Program Chairman *as soon as possible* with the title and a short description. You can reach Rod at k0das@arrl.net or 690 Eastview Dr, Robins, Iowa 52328. Author Guidelines and other details are available at the Society website: www.csvhfs.org.

Submissions Deadlines:

Proceedings – June 15, 2012
Presentations – July 26, 2012
Posters – July 26, 2012

The 31st Annual ARRL and TAPR Digital Communications Conference

September 21-23, 2012
Sheraton Gateway
Hotel Atlanta Airport
1900 Sullivan Road
Atlanta, Georgia 30337
www.sheraton.com/atlantaairport

Mark your calendar now and start making plans to attend the premier technical conference of the year, the 31st Annual ARRL and TAPR Digital Communications Conference to be held September 21-23, 2012, in Atlanta, GA. The conference location is the Sheraton Gateway Hotel Atlanta Airport, Atlanta, GA.

We recommended that you book your room prior to arriving. TAPR has reserved a block of rooms at the special DCC room rate of \$95.00 single/double. This special rate is good until 5:00 PM EDT, August 29, 2012. After that you will pay the regular room rate. To book your room, use the link on the TAPR website under Conferences (www.tapr.org/dcc.htm) or call the hotel directly (Reservations: 1-800-325-3535) and mention the group code ARRL and TAPR Digital Communications Conference when making reservations. Be sure to book your rooms early!

The ARRL and TAPR Digital Communications Conference is an international forum for radio amateurs to meet, publish their work, and present new ideas and techniques. Presenters and attendees will have the opportunity to exchange ideas and learn about recent hardware and software advances, theories, experimental results, and practical applications.

Topics include, but are not limited to: Software defined radio (SDR), digital voice (D-Star, P25, WinDRM, FDMDV, G4GUO), digital satellite communications, Global Position System (GPS), precision timing, Automatic Packet Reporting System® (APRS), short messaging (a mode of APRS), Digital Signal Processing (DSP), HF digital modes, Internet interoperability with Amateur Radio networks, spread spectrum, IEEE 802.11 and other Part 15 license-exempt systems adaptable for Amateur Radio, using TCP/IP networking over Amateur Radio, mesh and peer to peer wireless networking, emergency and Homeland Defense backup digital communications, using Linux in Amateur Radio, updates on AX.25 and other wireless networking protocols and any topics that advance the Amateur Radio art.

This is a three-Day Conference (Friday, Saturday, Sunday). Technical sessions will be presented all day Friday and Saturday. In addition there will be introductory sessions on various topics on Saturday.

Join others at the conference for a Friday evening social get together. A Saturday evening banquet features an invited speaker and concludes with award presentations and prize drawings.

The ever-popular Sunday Seminar will feature Tom Rondeau, KB3UKZ, teaching


"Exploring GNU Radio: From Filters to Digital Demodulators." This is an in-depth four-hour presentation, where attendees learn from the experts. Check the TAPR website for more information: www.tapr.org.

Call for Papers

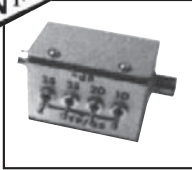
Technical papers are solicited for presentation and publication in the Digital Communications Conference Proceedings. Annual conference proceedings are published by the ARRL. Presentation at the conference is not required for publication. Submission of papers are due by 31 July 2012 and should be submitted to: Maty Weinberg, ARRL, 225 Main Street, Newington, CT 06111, or via the Internet to maty@arrl.org. There are full details and specifications about how to format and submit your paper for publication on the TAPR website.




NATIONAL RF, INC.




VECTOR-FINDER
Handheld VHF direction finder. Uses any FM xcvr. Audible & LED display
VF-142Q, 130-300 MHz \$239.95
VF-142QM, 130-500 MHz \$289.95



ATTENUATOR
Switchable, T-Pad Attenuator, 100 dB max - 10 dB min BNC connectors
AT-100, \$89.95



**TYPE NLF-2
LOW FREQUENCY ACTIVE ANTENNA AND AMPLIFIER**
A Hot, Active, Noise Reducing Antenna System that will sit on your desk and copy 2200, 1700, and 600 through 160 Meter Radio Signals!
Type NLF-2 System: \$369.95



DIAL SCALES
The perfect finishing touch for your homebrew projects. 1/4-inch shaft couplings.
NPD-1, 3 1/2" x 2 3/4", 7:1 drive \$34.95
NPD-2, 5 1/8" x 3 5/8", 8:1 drive \$44.95
NPD-3, 5 1/8" x 3 5/8", 6:1 drive \$49.95

NATIONAL RF, INC
7969 ENGINEER ROAD, #102
SAN DIEGO, CA 92111

858.565.1319 FAX 858.571.5909
www.NationalRF.com

We Design And Manufacture To Meet Your Requirements
*Prototype or Production Quantities

800-522-2253

This Number May Not Save Your Life...

But it could make it a lot easier! Especially when it comes to ordering non-standard connectors.

RF/MICROWAVE CONNECTORS, CABLES AND ASSEMBLIES

- Specials our specialty. Virtually any SMA, N, TNC, HN, LC, RP, BNC, SMB, or SMC delivered in 2-4 weeks.
- Cross reference library to all major manufacturers.
- Experts in supplying "hard to get" RF connectors.
- Our adapters can satisfy virtually any combination of requirements between series.
- Extensive inventory of passive RF/Microwave components including attenuators, terminations and dividers.
- No minimum order.

NEMAL

Cable & Connectors for the Electronics Industry

NEMAL ELECTRONICS INTERNATIONAL, INC.
12240 N.E. 14TH AVENUE
NORTH MIAMI, FL 33161
TEL: 305-899-0900 • FAX: 305-895-8178
E-MAIL: INFO@NEMAL.COM
BRASIL: (011) 5535-2368
URL: WWW.NEMAL.COM


Array Solutions

Your Source for Outstanding Radio Products

Top-ranked Measurement Equipment from Array Solutions

Announcing the NEW: PowerAIM 120
Vector Impedance Analyzer for Broadcast Engineers


- Patented, unique technology offers the broadcast engineer the full capabilities of a single port network analyzer
- Small, lightweight, software-driven instrument
- Easy to carry on airlines and in the field.
- Very simple to set up and use.
- Safe measurements in RF-dense broadcast environments.
- Time Domain Reflectometer (TDR) Functions.



NEW!

PowerMaster II

- New Larger, Sharp & Fast LCD Display
- Reduced Energy consumption
- USB and RS-232 interface built-in
- New - Both 3kW and 10kW couplers on one display - switched
- Hi / Lo Power Level Monitoring
- Supports 2 like couplers simultaneously (3kW & 3kW, 3kW & V/UHF, 10kW & 10kW)
- SWR Threshold Protection (with amp PTT bypass)




NEW!

Single and Dual Rack Mount available
New "Power Master Basic" Software FREE!

Vector Network Analyzer Model VNA 2180

Measures impedance magnitude, phase and transmission parameters for antennas, filters, and discrete components - using one or two ports.


- Frequency range is 5kHz to 180MHz.
- Data plots include: impedance, SWR, return loss, S11 and S21.
- Plots can be saved for before and after comparisons.
- Dual Smith charts with zoom and rotation.
- Time Domain Reflectometer (TDR) Functions.
- New - 6 port VNA multiplexer for measuring directive arrays including Phase/Magnitude vector scope software.



NEW!

AIM uhf Analyzer

- Frequency range from 5 kHz to 1 GHz.
- Data plots include SWR, RL, R + X, series and parallel, magnitude, phase, and more.
- Dual Smith charts with rotation and 20 markers.
- Plots and calibration files can be saved and used anytime in CVS and dynamic formats.
- AIM 4170C is still in production covering 5kHz to 180 MHz.
- Time Domain Reflectometer (TDR) Functions.



Other Quality Products from Array Solutions...

<p>ACOM Sales and Service for Amplifiers and Accessories</p>	<p>Phillystran, Inc. Official Worldwide Phillystran Distributor</p>	<p>RigExpert Analyzers and Interfaces</p>	<p>Prosisel Rotators Strongest Rotators on the Market</p>	<p>OptiBeam Antennas German Engineering means High Performance</p>	<p>Hoff® Surge Arrestors & Antenna Switches</p>
---	--	--	--	---	--

www.arrayolutions.com

Sunnyvale, Texas USA
Phone 214-954-7140
sales@arrayolutions.com
Fax 214-954-7142

Array Solutions analyzers are used by amateur, commercial, and professional broadcast engineers. See our web site for other products and additional details on these analyzers.

Out of the Box

A New Microstrip Filter Technique

About 6 years ago, I started seeing articles in trade journals that described a new element for microstripline filters. This element is called a defected ground structure (DGS). I have never seen an article in an Amateur Radio journal describing this new circuit element.

A fundamental part of a microstrip is a large continuous ground plane under the “center conductor” in order for the impedance to be consistent and to work as a transmission line. If one makes a cutout in the ground plane immediately under the transmission line, the hole in the ground plane will force the ground current to flow a longer distance than the current in the transmission line. The result of the altered ground current is a response that is equivalent to a parallel resonant circuit. The response is that shown in Figure 1. Figure 2 shows a basic slot and some representative dumbbell shapes used in DGS circuits. The fundamental part of the defected ground structure is the narrow resonant slot that is placed directly under the transmission line. The only way to design and use a workable DGS element is to model the system in a 3D simulator such as *Sonnet Lite*. The different shapes are used to implement elements with different frequencies and Q values. I have not found a useful description of the relative merits of the various shapes.

Notice that all of the DGS elements have a narrow slot under the transmission line. A DGS element will radiate significantly more than a normal microstrip because the gap acts exactly like a slot antenna. The radiation requires that you build a prototype in order to be certain of the real response. It is usually not practical to fully model the effects of the radiation or the absorbers you may need to put in the enclosure to control the radiated energy. I found an article in my search that put the operation of a defected ground structure in perspective.¹ The DGS in that article is a structure that looks just like an interdigital filter with no input or output. The interdigital structure and its use is shown in the structure on the right in Figure 3, with detail of the bottom copper shown in Figure 4. Essentially, the interdigital structure couples energy into the ground at either end and only takes energy from the transmission line at the “filter” resonant frequency. A slot antenna type DGS works in a similar fashion. The slot radiates some of the energy passing above it but only where the “antenna” is resonant. It is that resonant absorption of energy that accounts for the transmission zero in the frequency response.

The interdigital structures of Figure 3 were hard for me to visualize at first because my eye tends to focus on the light areas rather than the dark areas. The meander lines in the left and center parts of Figure 3 are a variation of the interdigital structure. They get their name from the meandering look of the empty areas. You can clearly see the interdigital filter aspect

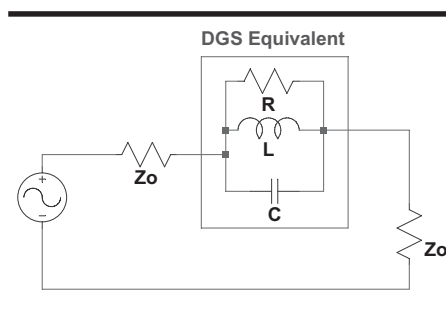


Figure 1 — The electronic lumped equivalent for a defected ground structure (DGS) element.

in Figure 4, however, if you force your eyes to focus on the six metal resonators instead of the seven “white” spaces. The white areas represent etched copper while the shaded areas are copper remaining on the board.

The *Sonnet Lite* program can be used to evaluate DGS filters. You can download the program for free if you agree to license it and allow the program to report back usage.² There is a 20 minute tutorial on the site that will show you how to create a microstrip filter. I haven’t finished the tutorial or the “homework” yet due to other commitments, but it is on my schedule for next month. What I have seen so far is very helpful for doing your first filter project. I also checked out the knowledge base. I am just starting the process, but from what I can see of the tutorial system on their web site, the folks at Sonnet Software really know how to support their customers. [Sonnet Software is owned by Dr. James Rautio, AJ3K — Ed.] I spent a little time going through the tutorial structure on line. It is huge! It is also well written and easy to follow. I suspect that learning 3D electromagnetic modeling is going to be similar to my journey learning 3D solid modeling with *SolidWorks*. There are a lot of concepts unique to this subject and it will take a while to learn anything more than the basics.

Sonnet Suites is the full professional version of *Sonnet Lite*. It is a full wave 3D planar EM simulator. *Sonnet Suites* will solve for the EM waves and modes in 3D and compute the cross coupling between all sub-sectioned elements in all 3 dimensions. More importantly, however, *Sonnet Suites* solves for arbitrary currents in the XY plane, only. It will calculate current in the strict Z direction through vias, but it assumes an even distribution through its length or the substrate thickness. Full 3D modeling requires the purchase of another full professional program, *CST Studio Suite*, also available from Sonnet Software.

As far as I know, *Sonnet Lite* is the only reasonably priced 3D modeling program (you can’t beat free). There has not been any coverage of that topic in the Amateur Radio

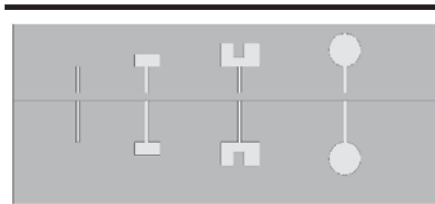


Figure 2 — These patterns show various DGS elements. Part A shows a simple slot DGS element, Part B shows a rectangular dumbbell, Part C shows an H dumbbell and Part D shows a circular dumbbell. Each shape has its own advantages with respect to frequency, size, and Q .

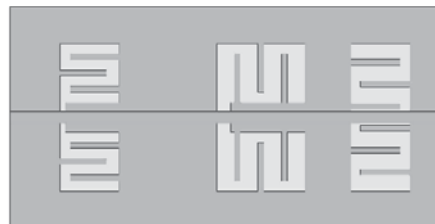


Figure 3 — Three representative Meander Lines showing the microstrip transmission line above the DGS element.



Figure 4 — The interdigital filter DGS element showing only the bottom copper pattern.

press. A friend here in Austin, Texas is also learning 3D modeling. As we develop useful information, we will pass it along here.

Notes

¹Balalem, Ali, Machac, and Omar, Quasi-Elliptic Microstrip Low-Pass Filters Using an Interdigital DGS slot: web.elmag.org/lib/exe/fetch.php/wiki:user:machac:texty:dgs.pdf.

²The Sonnet Software website describes the Sonnet Software products. You can download the free *Sonnet Lite* program here, as well: www.sonnetsoftware.com/products/lite.

ARRL Field Day is June 23-24, 2012

Get Active, Get Outdoors and Get on the Air!

Show off your support for ARRL Field Day!

Official Field Day pocket t-shirts, hats, participation pins, and more—are a great way to recognize your involvement in this annual operating event. **Clubs, order early!** Collect orders from members, and place a single order—pay only \$12.50 shipping for orders over \$50, while supplies last.

Now Shipping!

- **Field Day Pocket T-Shirt**
Sand pocket t-shirt featuring the 2012 Field Day logo above the pocket. ARRL diamond and "Ham Radio" silkscreened on top back. ARRL Order No. 1098..... **Only \$14.95**
- **Field Day Hat**
Texas orange cap embroidered with "Field Day". One size fits most. ARRL Order No. 2301..... **Only \$9.95**
- **Field Day Pin**
Official 2012 Field Day Pin. Size 1-1/8" x 7/8". ARRL Order No. 3357..... **Only \$5.00**
- **GOTA Pin**
Don't forget GOTA pins for your Field Day newcomers. Size 1" x 1". ARRL Order No. 8911..... **Only \$5.00**
- **Field Day Poster** (pack of 25)
Encourage participation in ARRL Field Day. A great recruitment tool! ARRL Order No. 4840..... **Only \$5.95**
- **Field Day Logbook**
Log sheets, dupe sheets, VHO Operating Tips, WAS map and more. ARRL Order No. 4500..... **Only \$7.95**
- **The ARRL Field Day Handbook**
A collection of tools and resources for Field Day FUN! ARRL Order No. 0885..... **Only \$19.95**



Back of
Shirt


HAM RADIO
www.arrl.org

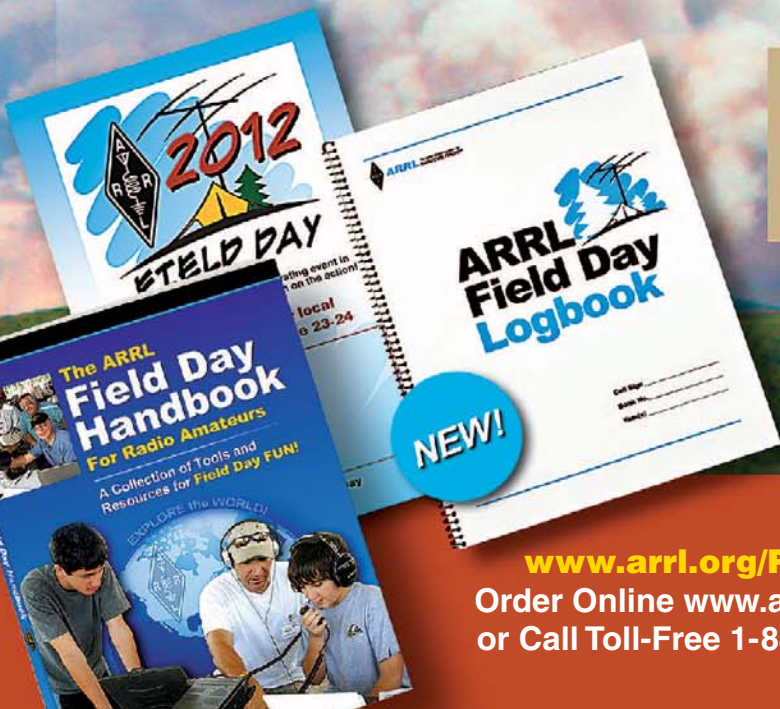
**NEW
Pocket
Tee!**



NEW!

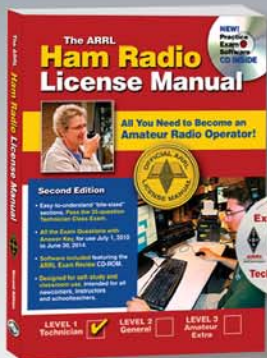
www.arrl.org/FieldDay

Order Online www.arrl.org/shop
or Call Toll-Free 1-888-277-5289

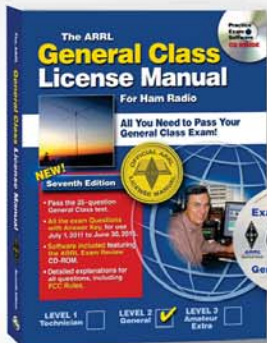


ARRL License Manuals

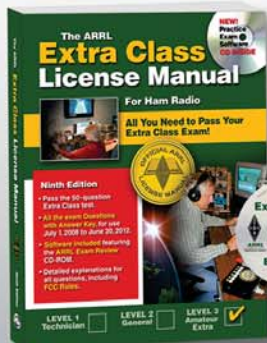
Now Including Practice Exam Software!



Level
1



Level
2



Level
3

ARRL's popular license manuals just got even better! Each book now includes the ARRL Exam Review CD-ROM. Use the software with your book to review the study material. Take randomly-generated practice exams using questions from the actual examination question pool. Additional features allow you to print sample exams...as many as you like. ARRL Exam Review tracks your progress, giving you the feedback you need to fine-tune your studies. **You won't have any surprises on exam day!**

Get your **FIRST** ham radio license!

The ARRL Ham Radio License Manual—**Second Edition**
Let ARRL guide you as you get started in Amateur Radio—as you select your equipment, set-up your first station and make your first radio contact.

- **Easy-to-understand “bite-sized” sections.** Pass the 35-question Technician Class exam.
- **Includes the latest question pool with answer key,** for use through June 30, 2014.
- **Software** included featuring the **ARRL Exam Review** CD-ROM.
- **Designed for self-study and classroom use.** Intended for all newcomers, instructors and schoolteachers.

Upgrade and enjoy more frequency privileges!

The ARRL General Class License Manual—**Seventh Edition**
Upgrade to General and experience the thrill of worldwide communications!

- Pass the 35-question General Class exam.
- **All the Exam Questions with Answer Key,** for use through June 30, 2015.
- **Software** included featuring the **ARRL Exam Review** CD-ROM.
- Detailed explanations for all questions, including **FCC rules.**

Achieve the highest level of Amateur Radio licensing!

The ARRL Extra Class License Manual—**Tenth Edition**
Complete the journey to the top and enjoy all the operating privileges that come with earning your Amateur Extra Class license.

- Pass the 50-question Extra Class exam.
- **All the Exam Questions with Answer Key,** for use July 1, 2012 to June 30, 2016.
- **Software** included featuring the **ARRL Exam Review** CD-ROM.
- Detailed explanations for all questions, including **FCC rules.**

Book and CD-ROM
Only \$29.95*/ea.
Order Today!

*Shipping and Handling charges apply. Sales Tax is required for orders shipped to CT, VA, and Canada. Prices and product availability are subject to change without notice.



ARRL The national association for
AMATEUR RADIO®

225 Main Street, Newington, CT 06111-1494 USA

SHOP DIRECT or call for a dealer near you.

ONLINE WWW.ARRL.ORG/SHOP

ORDER TOLL-FREE 888/277-5289 (US)

QEX 5/2012

Study
Anywhere!

